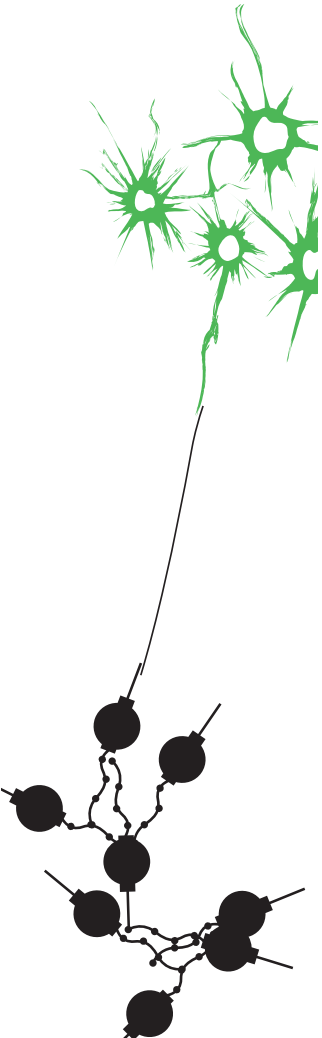

ROBOTICS AND MECHATRONICS

DEVELOPING A PATH PLANNING ALGORITHM TO ENHANCE THE PERFORMANCE OF A SOFT ROBOTIC ENDOSCOPE

J.W. (Jornt) Lageveen

MSC ASSIGNMENT

Committee:
prof. dr. ir. G.J.M. Krijnen
dr. ir. M. Abayazid
dr. ir. H. Naghibi Beidokhti
dr. C. Brune

October, 2019

044RaM2019
Robotics and Mechatronics
EEMathCS
University of Twente
P.O. Box 217
7500 AE Enschede
The Netherlands

UNIVERSITY OF TWENTE. | TECHMED CENTRE UNIVERSITY OF TWENTE. | DIGITAL SOCIETY INSTITUTE

Summary

Current interest in Minimal Invasive Surgery (MIS) and Natural Orifice Transluminal Endoscopic Surgery (NOTES) applications stimulates the development of surgical robotics applications. However, a current limitation of the technology at hand is the lack off flexible tools that are able to manipulate during surgical operation, due to their lack off stiffness capabilities. This provides a potential barrier for further improvements. A possible solution for this problem can be found inspired by nature, in the shape of soft robotics. Soft robotics has potential to combine flexible and stiff properties, making it possible to follow complex trajectories where high flexibility is needed, as well as being able to use stiff properties to for example properly exert the necessary amount of force during operation.

In this study, the control of a multi-module endoscope was investigated by means of using path planning. The research goal included the development of a path planning algorithm that would increase the safety of operation, while taking into account the physical limitations of the soft robotic endoscope. Objectives were to avoid collisions and to stay away from the boundaries of the insertion environment as much as possible. Other factors that were considered are operating speed and the amount of inserted pressure.
Due to the limited bending performance of the previous design, a new design was chosen and fabricated. The new module was made of EcoFlex 0030 and implemented outer sheathing. Knowledge has been obtained regarding the bending capabilities of the endoscopic modules, together with the pressure-bending relation of every respective module, which were analysed during characterization experiments. A model describing the bending behaviour of the endoscopic modules has been defined, which has been tuned using the knowledge obtained from characterization. This model, together with the endoscope module dimensions and characteristics found, formed a basis for the development of the path planning algorithms. A Path Planner algorithm was developed that would define a path through the environment. This algorithm was based on a variation of Rapidly-Exploring Random Trees (RRT*), which builds a path tree based on randomly sampled points. Using the kinematic model approximation of the soft endoscopic modules, the endoscope was simulated to follow the created path, of which the bending angle response has been documented.
The resulting angles were converted into pressures by using the defined pressure-bending relation of the endoscopic modules inside the assembly. Due to the hysteresis behaviour of the soft robotic endoscope modules, combined with the stick-slip effect of the platform on which the experiments were conducted, this pressure-bending relation was rather difficult to predict. Eventually, the average of the hysteresis curve of the modules was used to convert the angles to pressures, which would be inserted in the path planning experiment. To verify the performance of the path planned endoscope, the performance was compared to manual insertion of the endoscope.

Due to the open loop nature of the path planned control of the soft robotic endoscope inside the two selected scenarios, combined with several factors which affected the eventual performance such as stick-slip phenomena, hysteresis behaviour, and inaccuracies in mapping pressures to bending responses, it was difficult to perform the insertion inside the environments using path planning. Manual experiments provided a solid claim for the need of an alternative for manual control, but without proper control feedback it is difficult to realize the desired path planned behaviour.

This study has laid the first stones in the path that is yet to be discovered regarding the control of multi-module soft robotic endoscopes. Several aspects were treated throughout the process, leading to more knowledge regarding the steps that have to be taken towards proper control of the endoscope, as well as the numerous challenges that lie ahead. The current infrastructure

built from this research not only could serve as a means to evaluate current soft robotic endoscope designs, but can also be utilized as a tool to develop these designs. All in all, this study gives useful insights for future soft robotic applications.

Acknowledgements

This work would not have been possible without the support of the following people, both for my work and for me personally.

I would like to thank my daily supervisors Momen Abayazid and Hamid Naghibi, for their guidance and support throughout the study. Thank you for all the lessons and fruitful discussions. Furthermore, I would like to thank Yoeko Mak, who has fulfilled many roles throughout my study, both as mentor and teacher as well as fellow student and friend. Thank you for always being there when I needed help. I would like to thank my fellow colleagues from the office as well, for all the good times and for all the good suggestions throughout the process. The team always supported me You made the graduation process bearable for me and I will always cherish the moments together. A big thanks to Geert Folkertsma, Marcel Welleweerd and Vincent Groenhuis, for thinking with me during the most crucial moments. Without them, several important steps would not be developed as far as they are now. Furthermore, I would like to thank Teun van der Molen, Alexander Dijkshoorn, Jeroen van Dorp, Jan Lenssen and Yoeko Mak, as friends at work who gave their time to think with me and bringing me further up the road. A special thanks to Jan Lenssen, as he has been my mentor throughout the fabrication and design process, and has built an infrastructure on which lots of us could continue their work upon.

Furthermore, there are countless people behind the scenes that were just as important for the process, as they kept me standing and supported me in every phase and mental state along the way. Therefore, I would like to thank my family. They always has been the most supportive persons and even though they might not always get the topics I am working on, they would still always be there to provide help. Thank you for all the love and support, throughout all stages of my life. I could not have been more fortunate. Although my family was a big support throughout my thesis, the biggest support throughout this thesis has been my girlfriend, who basically had suffered the most from my work. She found a broken man coming home late more times than I could count, listened to me, motivated me and polished me up again. Thank you very much for being in my life and for making it so enjoyable. Furthermore, I have to thank the fraternity GTD, for bringing so much joy to these desperate times. Next to that, a big thanks to my old board mates, who always were there for me. Especially Dave Vogel, who always was ready to help. A big thanks to my house, who understood my situation and spared me in times where I had come home very late a little too often. Sorry for that. Furthermore, thanks to the 'Koffiebois', for forcing me to have a normal life and let me have an enjoyable break every once in a while.

Next to that, I would like to thank the technicians, who helped me and thought with me during many steps in development, with special thanks to Sander Smits and Henny Kuipers. I would like to thank Jolanda Boelema-Kaufmann for her endless care and support throughout the year, bringing me relief in stressful moments.

A big thank you to all the participants of my study, who sacrificed their time to perform my experiments. A big thanks to all the people that sat down with me and posed critical questions regarding my work. Thank you to all the people that were there and supported me, but I forgot to mention previously.

Contents

1 Introduction **1**
1.1 Soft Robotics . . . 1
1.2 Path Planning . . . 2
1.3 Research Goal . . . 3
1.4 Contribution . . . 4

2 Theoretical Background **5**
2.1 Soft Pneumatic Endoscope Modules . . . 5
2.2 Rapidly Exploring Random Trees . . . 6

3 Study Approach **10**
3.1 Assumptions . . . 10
3.2 System Overview . . . 10

4 Design and Characterization Procedure **13**
4.1 Module Design Choice . . . 13
4.2 Bending Characterization Single Modules . . . 15
4.3 Characterization of Endoscope Modules in Environment . . . 16
4.4 Angle to Pressure Conversion . . . 20
4.5 Discussion . . . 22
4.6 Conclusion . . . 25

5 Kinematic Model: Bending Module **27**
5.1 Constant Curvature Model . . . 27
5.2 Integrating Modified Model . . . 28
5.3 Comparison Models and Physical Module . . . 29
5.4 Discussion . . . 29
5.5 Conclusion . . . 31

6 Path Planning Algorithms **32**
6.1 Path Planner . . . 32
6.2 Endoscope Kinematic Planner . . . 36
6.3 Path Planned Endoscopic Pressures . . . 45
6.4 Comparison Weighted Centerline Error . . . 46
6.5 Discussion . . . 48
6.6 Conclusion . . . 49

7 Evaluation of Path Planner Performance **51**

7.1 Manual Insertion Experiment . . . 51
7.2 Path Planned experiment . . . 53
7.3 Results Evaluation of Path Planner Performance . . . 54
7.4 Discussion . . . 58
7.5 Conclusion . . . 62

8 Discussion **63**

9 Conclusion **65**

10 Future Recommendations **67**
10.1 Current Behaviour Mismatch . . . 67
10.2 Algorithm . . . 67
10.3 Imaging Connection . . . 67
10.4 Module Design . . . 67
10.5 Actuation . . . 68
10.6 Interaction . . . 68
10.7 Medical Knowledge . . . 69

Bibliography **70**

Appendix A: Literature review **75**
A.1 Abstract . . . 75
A.2 Introduction . . . 75
A.3 Conventional Path Planning Algorithms . . . 75
A.4 Trajectory planning algorithms . . . 78
A.5 Novel Path Planning Approaches . . . 78
A.6 Alternative methods for autonomous motion . . . 79
A.7 Virtual Endoscopic Path Planning . . . 80
A.8 Potential for Endoscopic Operations . . . 81
A.9 Discussion . . . 82
A.10 Conclusion . . . 82

Appendix B: Commercial Endoscopes **83**

Appendix C: Fabrication process **85**
C.1 Design description . . . 85
C.2 Manufacturing the chambers . . . 85
C.3 Pouring the first layer: EcoFlex 0030 . . . 86
C.4 Adding the top layer: DragonSkin 10 . . . 88
C.5 Suggestions for future fabrication . . . 89

Appendix D: Data Analysis Characterization - Single Module **90**

Appendix E: Data Analysis Characterization in Quaternions - Endoscope Modules **95**

E.1 The Principle of Defining Bending Angle 95

E.2 Post-Processing Angle Data 95

Appendix F: Hysteresis Results for Inner Sheath Design **97**

F.1 Results 97

F.2 Discussion 97

F.3 Conclusion 98

Appendix G: Malfunction and Maintenance **99**

Appendix H: Extensive Information Developed RRT* **101**

Appendix I: Image Processing of the Experiment Data **104**

I.1 Procedure 104

I.2 Discussion 106

Appendix J: Results Questionnaire **108**

J.1 Elaboration on Results 108

1 Introduction

An important area of interest in current surgical operations is the field of Minimally Invasive Surgery (MIS) (Vitiello et al., 2013). This type of surgery started to develop in the 1960s and is currently a widely used term in the medical field. MIS procedures have several benefits, such as scar reduction and decreased recovery time (Gomes, 2011). One of the aspects that enabled the development of MIS is the field of surgical robotics. With the increase in popularity of MIS technology, improvements of the current technology were requested, after which developments in the area of surgical robotics followed. (Gomes, 2011)

Examples of MIS operations are laparoscopic surgery and Natural Orifice Transluminal Endoscopic Surgery (NOTES) (Vitiello et al., 2013)(Gomes, 2011). Laparoscopic surgery (Garry, 2006) is a technique that is able to substitute a large incision by making use of multiple small incisions. Using multiple small tools and with the help of proper vision of the inside, this technique aims to reduce trauma. NOTES (Voermans et al., 2007) is an endoscopic type of surgery that focuses on surgery performed using only the natural orifices to enter the human body, such as the mouth and anus. A great benefit of this technique is that no incision has to be made at all to be able to perform surgery.(Voermans et al., 2007)

As technologies are being developed, their limitations also emerge. For both techniques, it is mentioned that current operation has limited flexibility (Vitiello et al., 2013)(Cianchetti, 2013). It has been stated that there is a need for so-called flexible robotics that are able to meet the demands of Flexible Access Surgery (FAS), which implies operating through openings that are not optimally aligned and are complex to manoeuvre through (Vitiello et al., 2013). Other articles also address the performance problem when dealing with rigidity in instruments used (Vyas et al., 2011). In this case, this is focused on laparo-endoscopic single-site surgery (LESS) and NOTES. The authors also mention the need for flexible systems to reduce this problem (Vyas et al., 2011). However, a problem that occurs with flexible structures is that they lack the possibility of exerting proper force upon the environment (Loeve et al., 2010), which limits their functioning during operation.

A new and interesting development that might overcome the dilemma between flexible and rigid endoscopes is the development of soft robotics. The area of soft robotics (Trivedi et al., 2008) has shown characteristics that overcome mobility limitations. Stiffness methods can be implemented into the soft material, creating a combination of rigidity and flexibility (Gifari, 2018). This is why soft robotics could be considered a good candidate in further development of this field of MIS applications.

1.1 Soft Robotics

Soft robotics is an upcoming technological development, inspired by natural phenomena such as the physical properties of animals (Trivedi et al., 2008)(Kim et al., 2013). Examples of animals (Kim et al., 2013) possessing soft structures that inspired robotic devices are worms, octopuses and caterpillars.

Benefits of the implementation of soft robotics (Kim et al., 2013) are, among others, a more safe interaction with the environment. An example of this is the contact with human tissue during surgery. Additionally, an article mentioned that the soft components would be cheaper compared to the conventional technology. (Kim et al., 2013) Furthermore, it has been mentioned that the use of soft material could serve as a substitute for metal parts, making it possible to operate the system in MRI environments. (Fraś et al., 2015)

An important aspect of soft robotics is the ability to regulate and change the stiffness of the material (Fraś et al., 2015). The flexible properties are interesting when considering following

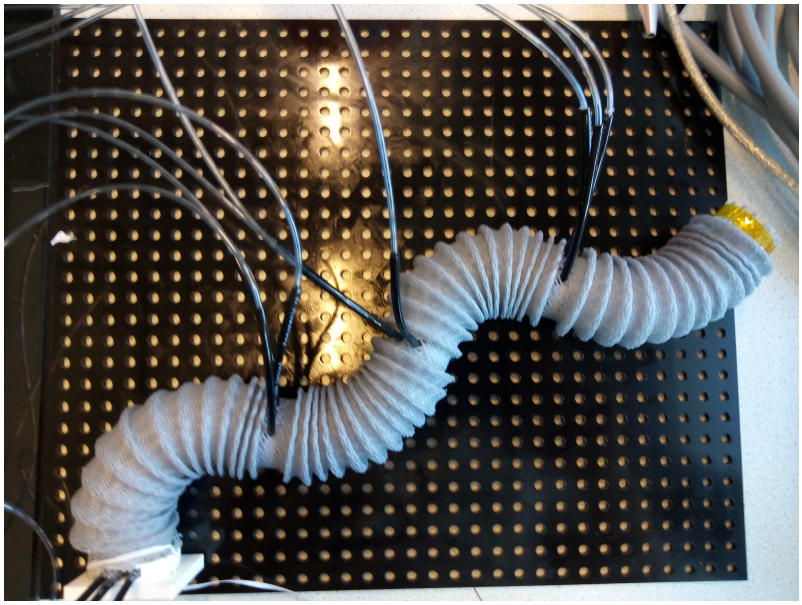

Figure 1.1: Representation of the soft robotic endoscope from the current study, which behaves rather similar to a tentacle of the octopus.

a certain trajectory through the environment, while the possibility of gaining rigid properties enables the operator to exert a higher amount of force during interaction with the environment when manipulating. (Fraś et al., 2015)

Soft robotics can be implemented in various scenarios, of which the medical field (Kim et al., 2013) is one. It has been mentioned that, due to less chance of trauma when operating, the soft robotic technology could be suitable for MIS applications. Other applications for soft robotics mentioned are, for example, research and rescue operations, as well as cases where they can be assisting humans. (Kim et al., 2013)
As this area of soft robotics could provide promising steps to improve MIS performance, the research group of Robotics & Mechatronics at the University of Twente started a project to explore the possibilities of soft robotic technology (Gifari, 2018)(Lenssen, 2019). The currently made design has been inspired by a soft robotic application called the STIFF-FLOP (STI, 2015). This system is inspired by the physical functioning of the arms of an octopus (STI, 2015). The resemblance can be seen in the current endoscope as well, indicated in Figure 1.1. The soft robot is named MOLLUSC, which stands for Multi-LeveL Stiffness Controllable robot (Gifari, 2018). Another iteration followed the development of the MOLLUSC (Lenssen, 2019), although stiffening properties were left out, and the main focus was aimed at scaling the module design down. Next to the design aspect, attention was paid to the kinematic representation of the endoscope module behaviour (Lenssen, 2019) (Jansen, 2018).

1.2 Path Planning

As the soft robotic endoscope is being developed, it is essential to think about ways to control and steer the endoscope for application purposes. When regarding endoscopic operations, the target is often not close to the insertion site, which results in the endoscope having to cover a certain distance through a passage consisting of hard or deformable tissues. With commercial flexible endoscopes only having a controllable tip, this would make it rather difficult to avoid any interactions. The combination of modules into a soft robotic endoscope would enable to have full control over the whole endoscope structure.

In order to minimize the invasiveness during any endoscopic operation, the path from the insertion site to the target needs to be determined in a way that the target is reached with a reas-

onable speed, with the least dissection required and the least risk of damage to the tissues around the endoscope. One of the important criteria for the path that should be taken into account is the safety of the patient. The created path should avoid the risk of damaging tissue as much as possible. Another measure that has to be taken into account regarding safety is the amount of bending that is performed by the endoscope. Reducing the amount of bending results in a reduced use of pressure, which decreases the risk of damaging the endoscope and potentially harming the patient. Other criteria that have to be taken into account are the speed and stability of the endoscopic operation. Operating the endoscope should occur at reasonable speed. The current soft robotic endoscope design might suffer from speed limitations during operation, due to the fact that multiple modules have to be actuated accordingly. This should be taken into account as well.

A path planning algorithm will be developed, which takes into account safety measures regarding pressure, maximum bending, and position in the environment, as well as general constraints of the soft robotic endoscope.

1.3 Research Goal

This research focusses on the development of a path planning algorithm specified for our soft robotic endoscope, to optimize reaching the target area, while considering safety and physical boundaries of the soft robotic endoscope. The main research question can be stated as follows:

How can a path planning algorithm be developed for soft robotic endoscopes, taking into account safety and the physical boundaries of the system?

Potential sub-questions are:

1. Which path planning algorithm would suit the steering of a soft robotic endoscope?
2. What bending characteristics can be found regarding the endoscope module performance?
3. In what way can the path planning algorithm(s) be coupled to the actual bending characteristics of the endoscope modules?
4. Which approaches can be used in combination with the path planning algorithm to make a safe path that can be followed by the soft robotic endoscope?
5. What setup can used to be able to experimentally test the developed path planning algorithm?
6. How would the path planning algorithm perform compared to manual operation in terms of safety and speed?

The field of endoscopic MIS and NOTES is used as target application. To specify our case in more detail, colonoscopy is chosen as test case. The choice of this application is made based on the current size of our endoscope design, as this is an operation which would be deemed most possible to use. However, this study can also be of use when considering other endoscope applications, when regarding this type of soft robotic endoscope.

In the following chapter, the background of soft robotics and the use of different path planning methods will be given. Chapter 3 will give a broad overview of the assumptions made throughout this study, together with a layout of the following chapters that represent the process. Chapter 4 will cover the design and characterization of the endoscopic modules, whereas Chapter 5 will describe the used kinematic model to define module bending behaviour. In Chapter 6, the developed path planning algorithms are introduced. Chapter 7 will address the methods used for the final experiments, together with the corresponding results. Chapters 8

and 9 will address the discussion and conclusions regarding this research. Finally, recommendations for future research are given.

1.4 Contribution

This study will provide new insights in the use of path planning for soft robotic endoscope actuation. To the author's knowledge, using path planning to control a soft robotic endoscope has not yet been researched before, although steps are made in the area of combining path planning with continuum robotic endoscopes (Gao et al., 2019) (Chen et al., 2014).
Furthermore, this study will shine light on the behaviour of multiple connected modules during operation, something which has not yet been extensively studied in the area of soft robotic endoscopes. Moreover, contributions to the design, as well as defining the hysteresis behaviour are contributions which add to the knowledge regarding future soft robotic endoscope applications.

2 Theoretical Background

This chapter will briefly describe the basic working principle of the soft pneumatic endoscope modules. Furthermore, this chapter will give background information regarding the path planning algorithm chosen for this study, together with some of the mentioned benefits found in literature and applications related to the current research. A more general description of path planning is mentioned in the Appendix (Chapter A). The chapter also concerns sub-question 1.

2.1 Soft Pneumatic Endoscope Modules

Soft Pneumatic Actuation has been under study at the Robotics and Mechatronics group for quite a while, as it has promising features for future applications. One application was the simulation of the movement of the liver using soft pneumatic actuators (van Dorp, 2019). In this study, to focus was on developing a setup that could mimic respiratory motion and, if possible, an inclusion of the heartbeat as well. Other studies use the soft pneumatic actuation integrated in orthoses, to stimulate correct positioning. A rather big branch in Soft Robotics research focusses on the development of a soft robotic endoscope, of which the design has been under study by Gifari(Gifari, 2018) and Lenssen (Lenssen, 2019).

2.1.1 Bending Principle

The main principle of the pneumatic endoscope module is bending through expansion of the actuated chambers, which is described well by the work of Naghibi et al. (Naghibi et al., 2019) and can be seen in Figure 2.1.

Applying pressure to the chambers causes the chambers to expand, resulting in a bending of the module towards the opposite direction of the chamber. Multiple chambers in one module can be actuated together, forming a resultant bending or, when complete bending cancellation occurs, lengthening of the modules. It is desired to limit the expansion of the chambers in radial direction as much as possible, as this limits bending performance. Therefore, several sheathing techniques have been treated. The material used for these modules is often a com-

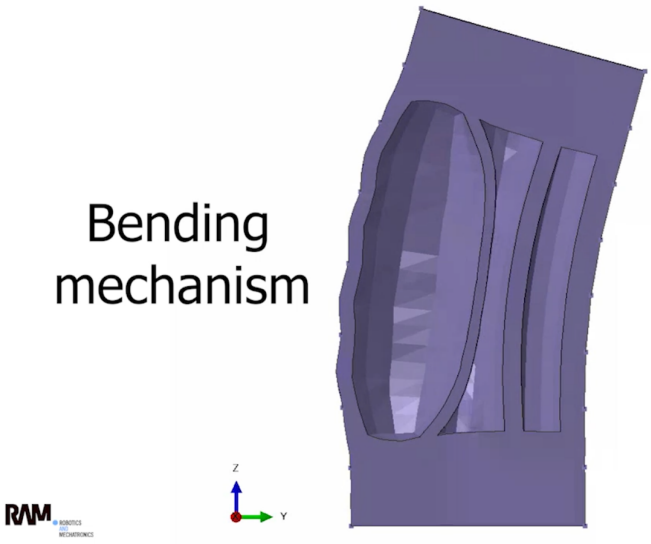

Figure 2.1: Internal structure of the soft pneumatic endoscope module, showing the bending motion by means of chamber expansion, from the work of Naghibi et al. (Naghibi et al., 2019).

bination of EcoFlex 0050 and Dragon Skin 10, both silicone materials that can be utilized in for example the fabrication of face masks (Smooth-On, -). Due to a combination of high tensile strength (around 2.17 MPa (Smooth-On, -)) and high compliance, the material is suitable for this bending application.

2.1.2 Previous Studies

Gifari (Gifari, 2018) worked on the characterization and stiffening of a soft robotic endoscope module, based on the work of the STIFF-FLOP (STI, 2015). The study was focussed on one module that was made from EcoFlex 0050, having a cover of Dragon Skin 10. The module was surrounded by an outer sheath, made from computer cable housing, which was manipulated to facilitate proper bending. The same computer cable housing has been used in other studies (van Dorp, 2019) to facilitate pneumatic actuators, as they properly constrain expansion in radial direction. The design had four chambers, placed with equal spacing from each other. Gifari focussed as well on the integration of vacuum chambers in combination with pressure chambers, to facilitate stiffening (Gifari, 2018). A hole was made in the middle of the module, so potential tools such as a camera could be inserted.

Lenssen (Lenssen, 2019) developed the newest version of the soft robotic endoscope modules. The main focus of the study was the scalability of the endoscopic modules. The modules were made out of EcoFlex 0050 with an additional layer of Dragon Skin 10 and had the dimensions of 50 mm in height and 25 mm in diameter. The design of such a module consisted of three chambers, surrounded by wiring to restrict the chamber from expanding in the radial direction, instead of using an outer sheath. Lenssen also created a central tube for the tooling, but left the stiffening mechanism out of the design. From his work, it was concluded that increasing the number of chambers to four would not increase the number of degrees of freedom, compared to three chambers. Furthermore, it was mentioned that using three chambers would reduce the number of tubing and potential control infrastructure. (Lenssen, 2019)

This study will continue based on the work of Lenssen (Lenssen, 2019). However, the technique of surrounding the chambers by means of wire severely limited bending capabilities, stressing the need for an alternative design with more bending.

2.2 Rapidly Exploring Random Trees

This section treats the background theory behind the Rapidly-Exploring Random Trees (RRT) algorithm, which will be used throughout the study. The following sections contain a description of the algorithm, the working principle, several applications making use of the algorithm, and some of the modifications of the algorithm found in literature.

2.2.1 Description

RRT is a path planning algorithm which can be classified under Sampling Based Planners (SBP) (Noreen et al., 2016a). SBP algorithms work by means of creating randomly sampled points in order to grow and propagate. The earliest mentioning of the RRT algorithm was by LaValle in 1998 (LaValle, 1998). He proposed this algorithm as an alternative to Probabilistic Roadmaps (PRM) for situations in which non-holonomic constraints occur.

Several benefits of the algorithm are mentioned by LaValle, which are addressed by other sources as well (Yang et al., 2014) (Abayazid et al., 2014)(Noreen et al., 2016b) (Noreen et al., 2016a)(LaValle and Kuffner Jr, 2001). One of the advantages LaValle mentions (LaValle, 1998) is the tendency of the algorithm to bias growth towards unexplored regions. This is very efficient, as the environment is being explored rather fast (Yang et al., 2014). The phenomenon can be captured in a term called Voronoi bias, which stands for the characteristic of RRT algorithms to grow the planner tree towards regions that have not yet been covered by the algorithm, leading to fast visiting of new places. (Yang et al., 2014)

The RRT has shown to be rather fast in computation (Abayazid et al., 2014), making it suitable for on-line path planning approaches where the path has to be updated throughout the trajectory.

Next to being able to cover an environment in a brief amount of time, it is also mentioned that RRT can take into account dynamic environments (Noreen et al., 2016b) and non-holonomic constraints (Noreen et al., 2016b)(LaValle, 1998). The article of Noreen et al. (Noreen et al., 2016b) mentions the benefits of SBP, such as low computation cost and good performance for higher dimensional and complex problems.

Next to that, Noreen et al. (Noreen et al., 2016a) indicated the characteristic of SBP algorithms to be probabilistic complete, which is also mentioned about RRT algorithms by LaValle (LaValle, 1998), under general conditions. This implies that, if there exists a path solution, the algorithm will eventually find it, given infinite time (LaValle and Kuffner Jr, 2001).

Furthermore, the RRT algorithm is promoted as being a relatively simple algorithm, which can easily be integrated into other planning systems (LaValle, 1998). Next to that, a beneficial aspect that was stated is the ease of use, as it does not need any additional control or steering to move towards the target. This makes for a rather stand-alone algorithm. (LaValle, 1998)

The work of Elbanhawi et al. (Elbanhawi and Simic, 2014) describes many phenomena considering RRT and variations on the algorithm.

2.2.2 Procedure

Several variations on the RRT algorithm exist, ranging from forward search to backwards search and even bidirectional growth of the trees (LaValle, 2006). An example of bi-directional growth can be found in the article by LaValle et al. (LaValle and Kuffner Jr, 2001), depicting a simulation of the path planning algorithm.

Furthermore, several varieties of RRT exist in terms of the moment the algorithm finishes its computation. Some algorithms stop as soon as one branch of the grown tree reaches from the initial starting point up to the target. Others have a predefined number of iterations that have to be completed, after which the best possible path is selected.

Regarding the general form, which has been proposed by LaValle (LaValle, 1998), the steps of the algorithm can be described in the following manner. Each iteration, a random point is sampled. Based on the distance of this point compared to the other point in the tree, the nearest tree point selected. From this point, a feasible input is chosen, which minimizes the distance between the two points. Before connecting, a check is performed to verify no collision occurs during connection. Then, the new point is added to the tree. Besides storing the coordinates of this new point, the input necessary to reach this point is also stored. (LaValle, 1998)

In case the random point is still rather far from the current tree, it is custom to limit the possible motion towards that point. In other words, when the random point lies outside the predefined step size, a new and feasible point will be generated in the direction of the tree target point. The aspect of this new edge generation is nicely depicted in the work of Blanco et al. (Blanco et al., 2015), where RRT is used to develop a path for the application of the driving of autonomous cars. A similar illustration of this is given in Figure 2.2. Here, when the point is outside the specified region, a new point will be created on the edge of this region. When the point is created inside the region, this point can directly be selected as the new point. If there is no collision-free path possible between the new point and the tree, the option of connecting a new edge is discarded. In this case, it can be seen that steps taken by Blanco et al. (Blanco et al., 2015) are defined as splines, concerning the bent nature of the step. Three scenarios are depicted in the article; random point outside region, random point within region, and collision path.(Blanco et al., 2015)

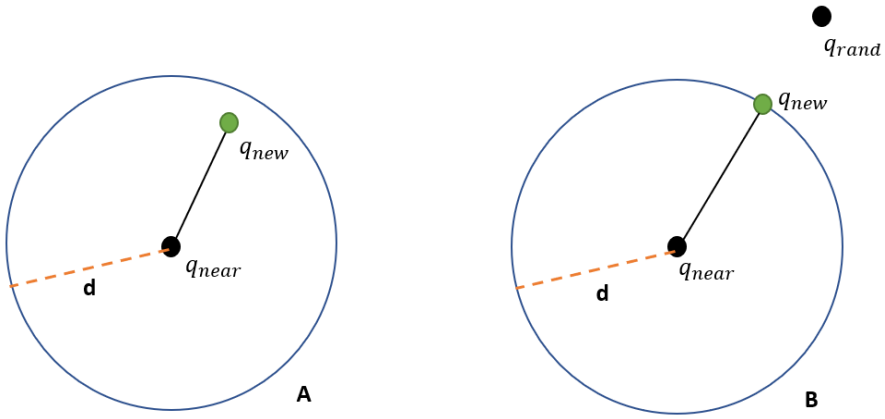

Figure 2.2: Two of the scenarios that can occur after choosing the closest point in the tree with respect to the randomly sampled point. **A)** Point found inside specified boundary region, direct connection can be made. **B)** Randomly sampled point found outside of specified region from the selected point of the tree, causing a new point to be created on the path towards the random point, on boundary of the point. Image inspired by the representation in the article of Blanco et al. (Blanco et al., 2015).

2.2.3 Applications

The application direction of the RRT algorithm is rather broad, although one of the main applications seems to be that of (autonomous) vehicles. Examples can be found in (Blanco et al., 2015) (Kuwata et al., 2008)(Liu, 2017) (Han et al., 2011) (Katrakazas et al., 2015). Furthermore, Liu addresses the autonomous control of Unmanned Aerial Vehicles (UAV's) (Liu, 2017).

The use of the RRT algorithm as a path planner has not yet been utilized for endoscopic procedures to the writers knowledge. However, the principle can be found in the area of needle steering (Xu et al., 2008) (Patil and Alterovitz, 2010) (Abayazid et al., 2014).
The work of Xu et al. (Xu et al., 2008) focusses on the development of a path planner than could plan a path for the steerable needle throughout an environment containing obstacles. The article mentions the difficulty that arises with the bevel tip design of the needle, bringing forth non-holonomic constraints. It also stated the potential for RRT algorithms to cope with non-holonomic constraints. (Xu et al., 2008)
Patil et al. (Patil and Alterovitz, 2010) developed an RRT algorithm that could produce results with a high speed for a steerable needle inside an environment containing obstacles, which makes it suitable for potential future on-line path planning applications. It would then be possible to control the needle throughout the environment based on imaging techniques, such as MRI. (Patil and Alterovitz, 2010) The study by Abayazid et al. (Abayazid et al., 2014) uses RRT as a method to quickly develop paths throughout the trajectory of the bevel-tip needle. It enables the combination of ultrasound images with the path planner. This allows for compensation of movements by the target, the obstacles, or both. (Abayazid et al., 2014)

The study of Park et al.(Park et al., 2015) used the RRT algorithm to develop motion trajectories for the robot arm holding the endoscopic tool for a Da Vinci surgical robot.

2.2.4 Modifications to the algorithm

Aside from several benefits, the implementation of RRT suffers from some drawbacks as well. Examples of drawbacks are a sub-optimal solution (Noreen et al., 2016a) and a uniform expansion method without targeted direction (Wang et al., 2012). Next to these aspects, computing a big and complex tree can be a heavy load in terms of computation. Performance will go down when the environments tend to become more complex (Wang et al., 2012). Processing time is affected by this. Furthermore, it has been mentioned that RRT planners can have difficulties

with narrow passages (Rilk et al., 2009). To tackle these limitations and to improve upon the stated conditions, several modifications can be applied.

As the sampling of random points is one of the reasons why limitations occur within this algorithm, several methods are proposed to increase sampling efficiency. The article of Patil et al. (Patil and Alterovitz, 2010) makes use of a reachability guided sampling heuristic, which only takes into account random points that are computed within range of the current tree. Another successful way to reduce the number of samples is to reject all the random samples that are positioned in the obstacle regions, as also is mentioned by Noreen et al. (Noreen et al., 2016b). These two methods reduce the amount of computation to only the most relevant cases.

To reach the target earlier, one can choose to define a target region instead of a stand-alone target coordinate, which would speed up the process. The so-called goal region was also found in the article by Alterovitz et al. (Alterovitz et al., 2011). Another approach is implemented by Patil et al. (Patil and Alterovitz, 2010), which mentions the use of a goal bias towards the target region. This goal bias supports the growth of the tree towards the target.

RRT* is a version of RRT which takes into account potential nearest neighbours that have a lower distance cost compared to the originally computed path (Noreen et al., 2016b). This algorithm is very comparable to RRT, but the additional nearest neighbour cost computation makes the eventual result more optimal in terms of distance cost.

Rapidly-Exploring Roadmaps (RRM) (Alterovitz et al., 2011) has some similarities with RRT*, but differ in the fact that the refinement will not occur uniformly but rather directed towards the computed goal path. In other words, the RRM algorithm only refines when the path is connected with the goal, saving computation effort on refinement compared to RRT*. (Alterovitz et al., 2011) The RRM method works using an ω-value, which indicates the relation between exploring and refining. This refinement option is able to reach an optimal solution when time goes to infinity. The algorithm was tested upon a moving point robot and a concentric tube robot for medical purposes (Alterovitz et al., 2011).

Other work (Falatehan, 2012) mentioned the RG-RRT algorithm, or the Reachability Guided RRT, which possesses a section that checks whether a randomly generated sample can be reached by a section of the tree. Not-reachable samples will be discarded. The standard RRT algorithm gets less efficient when regarding rather complex environments, since fewer points are found suitable for use and more points will eventually be initialized, asking for more computational power. This alternative algorithm can reduce the amount of computation by simply reducing the number of potential options. (Falatehan, 2012)

Noreen et al. (Noreen et al., 2016a) address the differences of RRT and RRT* with respect to yet another variation; RRT*-Smart, which incorporates sampling that is biased towards a defined beacon region as well as utilizing a biasing ratio that can be used for a smarter exploration of the environment. (Noreen et al., 2016a)

2.2.5 Application to this study

The RRT algorithm possesses several benefits that can be of use for the application of path planning in combination with the soft robotic endoscope. For one, the algorithm is suitable for handling holonomic and non-holonomic constraints, which also can be found when controlling the soft robotic endoscope. Furthermore, the planning algorithm is said to be rather fast, making it suitable for potential future use as an on-line path planner, when eventually sensing is combined with the control of the endoscope. Next to that, it has been mentioned that RRT is suitable for use in dynamic environments, which would be a useful potential to have considering operating inside the human body implies a dynamic environment.

3 Study Approach

In earlier chapters, the outline of this study has been presented, as well as some theoretical background on the material that will be implemented during this study. This chapter will discuss the main assumptions made during research, together with an overview of the different stages treated throughout this study, as well as the relation between the different stages.

3.1 Assumptions

This study deals with several simplifications and assumptions made throughout the process. Although the eventual target application will be based on operation in a 3D space, the initial focus of this study is only considering a 2D environment, which simplifies both planning and actuation.
Next to that, the current study deals with a static environment as a start, implying that the surroundings remain the same, while keeping in mind that this assumption does not hold with respect to the physical scenario. The human body is rather dynamic, possessing deformable tissues and suffering from the effects of gravity, breathing and beating of the heart, which all contribute to movement of the organs. This makes for many factors to consider. However, for the sake of simplification, the initial work will consider a static environment.
Furthermore, as the focus of this study is mainly on the working principle of the algorithms and the use of the physical endoscope in combination with this software, the accurate representation of the used environment is currently deemed of less importance. The used environments are abstract representations of bending scenarios that might occur during operation, but do not resemble a realistic scenario in such.
In general, the RRT-algorithm has the ability to provide an efficient resulting path for environments in the human body that could have complicated branching structures, which normally would make it difficult to define a path. Although the more complex scenarios would shine more light upon the benefits of using RRT, the main objective was to define the contribution to steering the soft robotic endoscope, which is why more complicated branching has been left out for now.

3.2 System Overview

The steps taken throughout this study to get from a specified environment towards the eventual pressures are represented in the Figure 3.1. The big phases throughout the study can be divided into design and characterization, modelling, path planning implementation, angle to pressure conversion, and eventually the final experiments to compare path planning with manual insertion. These are depicted with letters in Figure 3.1, in order of occurrence throughout the report.

It should be mentioned that the process contained iteration, as for example a modification of the model leads to changes in the algorithms as well. A distinction between the previous model and the modified model will be elaborated upon in the chapter concerning the model (Chapter 5) and the chapter describing the algorithm (Chapter 6). The following section shortly describes the process throughout the report (with exception of Stage D, which is included in the design and characterization chapter, Chapter 4).

3.2.1 Layout of Procedure

Based on the limited bending performance of the previous design of Lenssen, it was decided to develop a new design to stimulate module bending. Various design alternatives were developed, constructed and tested, to find a more suitable module design capable of more bending. This occurs in Stage A1. The resulting module design (Step 1) has been characterized

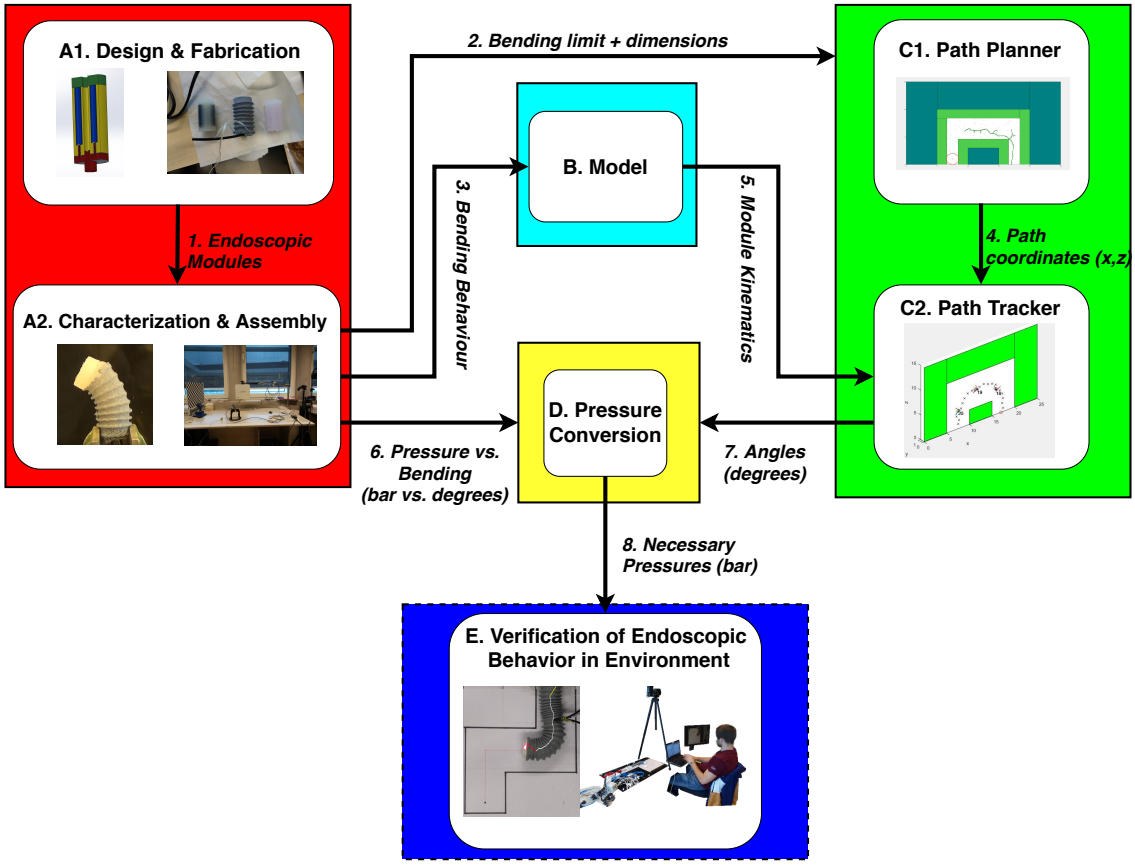

Figure 3.1: A schematic representation of the sections that are treated throughout this study. Here it can be seen that hardware and software are combined to develop a complete system, which will be tested in a later phase.

and assembled into a soft robotic endoscope. This happens in Stage A2. After assembly, the modules were characterized in the used environment, to define their behaviour under circumstances. The findings regarding bending limitations and endoscope module dimensions were used as criteria for the development of the path planner algorithms (Step 2), whereas the bending behaviour found aided in the development of the kinematic model (Step 3). More on this in Chapter 4.

The model (Stage B) used the kinematic representation of the module considering the constant curvature assumption, which was found in earlier work (Jansen, 2018) based on Webster lll (Webster III and Jones, 2010). By means of experiencing module bending during characterization, a modified model has been developed (Step 3). The model serves as a basis for the kinematic representation of the 'Path Tracker, or 'Endoscope Kinematic Planner' (Stage C2). Elaboration follows in Chapter 5.

The path planning algorithms make use of this knowledge (Step 2) to define an endoscope simulated response for a given setting. The Path Planner (C1), uses the RRT-algorithm to develop a path inside the pre-defined environment. The coordinates of the path are passed on (Step 4) to the Endoscope Kinematic Planner from Stage C2. The Endoscope Kinematic Planner, or 'Path Tracker', simulates the endoscope behaviour using the defined module kinematics (Step 5), after which a resulting angle profile is given for all used modules throughout the simulation (Step 7). Chapter 6 will treat this in more detail.

Combining the angle profiles (Step 7) with the defined pressure-bending behaviour (Step 6), Stage D translates the angles into desired pressure responses per module, based on fitting

the characterization. The resulting pressure profiles (Step 8) are used as a basis for the path planned endoscope, which can be compared to the manual insertion performance in Stage E. In Chapter 7, the methods for these experiments will be elaborated upon, together with the corresponding results.

4 Design and Characterization Procedure

In this chapter, the design choice and methods for characterization of the soft endoscopic modules is described, together with the corresponding results. This corresponds to Stage A1 and A2, described in Figure 3.1 (Chapter 3). To improve bending conditions, a new module design is chosen, after which characterization was performed. A distinction is made regarding bending characterization for a single module with respect to the bending characterization of the assembled endoscopic modules inside the environment. Finally, the approaches for converting desired angles into required pressures for each module are treated (Stage D).

This Chapter provides the answers to sub-question 2 and a part of sub-question 3.

4.1 Module Design Choice

Initially, it was attempted to implement the module design of Lenssen (Lenssen, 2019). However, one problem arose from the functional characteristics of the new design; the bending was very limited. The modules did not show bending above 30 degrees. As can be seen from Table 1 in Chapter B of the Appendix, commercial flexible endoscopes reach up to far higher bending angles. Furthermore, initial simulations pointed out that for an angle below 40 degrees, the endoscope would not be able to go through the simulated environment properly. Therefore, additional modules designs were manufactured and tested to improve the bending properties towards more commercial standards. The subsections below describe the design alternatives, experimental approach and eventual design choice.

4.1.1 Module Design Alternatives

New modules were made that are similar to the recent design of Lenssen (Lenssen, 2019), but including three extra 5 mm air holes. A hole is placed between every chamber, with the intent to improve the overall bending performance of the module. It was assumed that the reduction of material would reduce the effort necessary to bend the module in the desired direction.

Furthermore, some alternative designs were considered. At the moment, the design for the module incorporates the material EcoFlex 0050 (Smooth-On, -). To increase the flexibility of the module design, it was thought of to swap the main material for EcoFlex 0030, which is a more flexible type of silicone. The small coating inside, which is surrounding the chamber, is still made of EcoFlex 0050 for these design alternatives. This is to enhance the strength of the module chambers. Next to the idea of having an inner sheath containing the chambers, the alternative of using an outer sheath around the module was considered. The outer sheath contains the module as a whole, which initially gives more space for the chambers inside the modules to expand. All modules are coated with a layer of Dragon Skin 10 on top. Dragon Skin 10 is rather stiff compared to the Ecoflex silicone. It is placed on top to improve the strength.

These four alternatives were tested and the influence of adding three air holes was investigated. A more detailed description of the fabrication process can be found in Chapter C of the Appendix.

4.1.2 Bending Characterisation

To analyse the bending characteristics of the various modules that were demonstrated before, an experiment was performed using a Festo 2-bar pressure regulator (VEAB-L-26-D2-Q4-V1-1R1) (Festo, 2018) and a MATLAB application, initially developed by Lenssen (Lenssen, 2019). All chambers of the modules were tested separately, while the other chambers remained at atmospheric pressure. Pressure was increased from 0 bar up to 1 bar, often with steps taken of 0.1 bar. When ballooning would occur, the experiment would be stopped, as this could result in

eventually breaking the module. The measurements were repeated three times, except for the ones of EcoFlex 0030. The reason for this was the occurrence of rupture of two chambers in an earlier test. All experiments were recorded using a video camera. The module type, chamber number, round and applied pressure were registered on video. From the recordings, images were taken to analyse the orientation for every applied pressure step. This has been mainly performed using the software tool ImageJ (ImageJ, -). From this and from visual inspection, the bending performance could be deduced.

4.1.3 Module Design Choice

During examination of the performance of several design alternatives, it was found that the use of outer sheath modules consisting of EcoFlex 0030 material would lead to the most bending up to a certain pressure. From experiencing the performance, it was also examined that the additional holes did not give any extra bending performance.

Therefore, the further design focus of the endoscopic modules was on the outer sheath model with EcoFlex 0030 as main material. The holes are also added. From the bending performance it was found that the new module design could only handle pressure up to around half of the 1 bar mentioned earlier. This is taken into account during future characterization.

4.1.4 Module Connector Piece

To eventually connect the modules together without having too many loose wires around, the connector piece design of Lenssen (Lenssen, 2019) was altered to fit the application. This meant that all the pressure inputs of the connector were aligned on the same place, such that the pressure tubes could stay out of the way of the endoscope bending (this was present in an older version of the design of Lenssen, but is not used in his application). Rubber rings were designed on the inside of the connector inlet, such that the pressure tubes could easily be fixated to the connector piece without further glueing or attaching. This would simplify removal of the outer sheath and the pressure tubes, without too much hustle.

The design of the connector piece can be seen in Figure 4.1. The pressure inputs are on the same side, making it possible to separate the pressure tubes from the bending plane. The dark connector cylinders are inserted in the pressure chambers. The pressure tubes are pushed in the three holes on the side. Rubber rings inside of the holes keep the tubes in place.

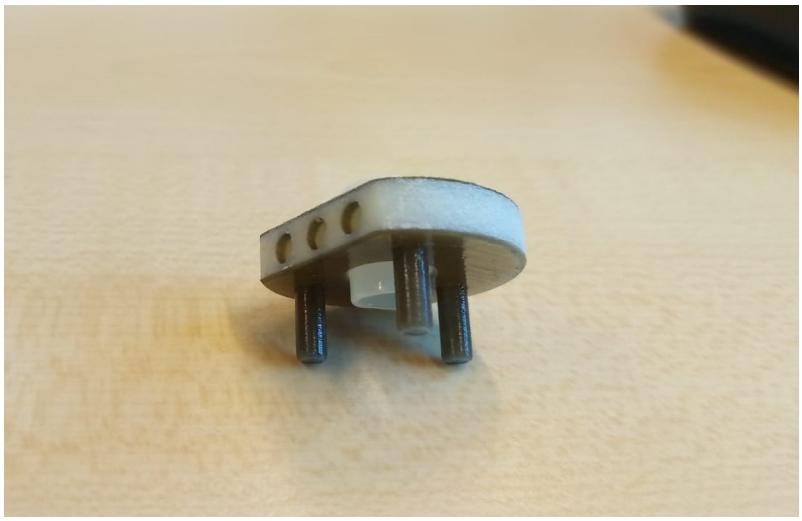

Figure 4.1: Representation of a connector piece design with which the modules will be connected together. Modification of the design of Jan Lenssen (Lenssen, 2019).

4.2 Bending Characterization Single Modules

To gain more insights in the bending behaviour and repeatability of the new design, more modules were fabricated and experiments were held to further characterize the EcoFlex 0030 modules. Initially, experiments were performed with single modules, in upright position. All modules were tested with the same external sheath, such that the characteristics were mainly focussed on the module itself and were not that reliant on the position and structure of the external sheath. The Aurora EM Tracker was used to define the bending performance. The same pressure regulators are used compared to the previous bending experiment.

In total, four modules were tested, which all had special connectors that were attached. Due to plastic deformation occurring in the sheathing, the same side was used for every experiment to not limit bending performance.

The main sequence for applying pressure starts at 0 bar, going in steps of 0.1 bar until 0.2 bar is reached. The reasons for this step size is because in the initial stage of the bending not a lot of bending can be seen. After 0.2 bar, the actual bending starts. After that, steps of 0.05 bar are performed up to a pressure of 0.55 bar. This limit is taken because after 0.55 bar the modules seem to expand rather than bend, making it less interesting in terms of bending and potentially more susceptible to damage. The respective modules were bent three times before actual measurements were performed, to detect defects and 'warm up' the module.

Every chamber was tested five times. Every time the limit of 0.55 bar was reached, the pressure was brought back to 0 bar directly.

4.2.1 Bending Results

Regarding the bending of the four EcoFlex 0030 modules with outer sheath, the following results were found. In Figure 4.2, an example is given of the bending performance from the three different chambers of one module. The behaviour could be considered rather similar, although the maximum deviation would almost approach 20 degrees in bending performance. Figure 4.3 shows the average pressure-bending response of four modules, containing average results of multiple rounds for every chamber inside the module. Here, it can also be deduced that the overall response of the modules is deemed rather similar.

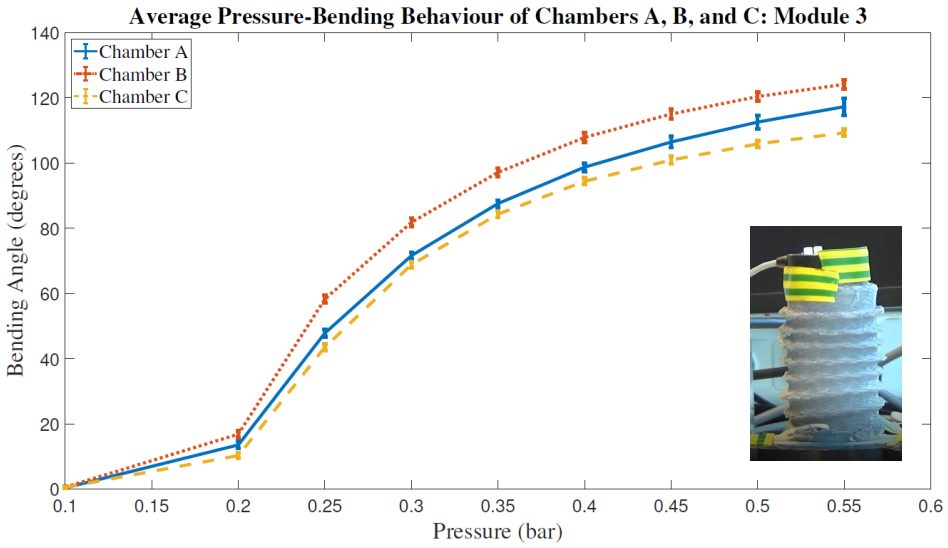

Figure 4.2: Average results for every chamber of a single module in upright position (Module 3), together with the corresponding standard deviation. The average has been conducted over five cycles. The module setup is presented on the right.

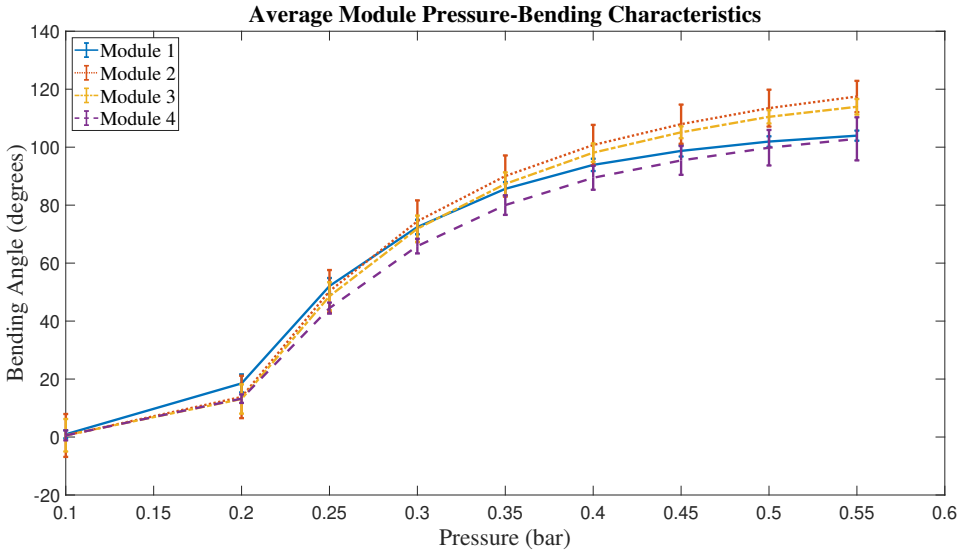

Figure 4.3: Average bending performance of all modules, without additional load and in upright position. The average is taken over all chambers, for five cycles per chamber.

Elaboration upon data processing for these plots can be found in Chapter D in the Appendix.

4.3 Characterization of Endoscope Modules in Environment

To ensure that the endoscopic output pressures of the system take into account the physical characteristics of the module together with the influence of the environment upon endoscope performance, the endoscope modules had to be characterized in the environment. In this way, the effects of friction, gravitational load, load of other modules upon bending module and reaction forces of for example the pressure tubes can be related to the endoscope performance. It must be mentioned that an exact mapping of performance into a single characterization would be rather impossible, as so many factors have an influence on the position and every orientation of the endoscope would result in a different characterization.

For now, the experiment is kept rather basic. Every module is be actuated in a sinusoidal fashion, ranging from -0.55 bar up to 0.55 bar. The first module (bottom module) is fixed to the environment using a 3D printed connector piece. The EM Tracker sensor is placed on the level of the tip of the actuation module, which often resulted in a fixation of the sensor to the pressure tubes of the next module. At the tip, the sensor would be placed inside a 3D printed casing, which would be connected to the endoscope tip. This ensured fixed position of the sensor, as well as keeping the external sheathing in place. During this experiment, the modules below the actuated module are set to 0.1 bar of pressure on one side. This would increase the stiffness of the module, creating a more stable platform for the modules to bend on. This was in order to extract the behaviour that would be closer to a scenario during operation (during operation probably all modules will be pressurized), as well as to make a proper comparison with the fixed bottom module. Due to time constraints, it was assumed that pressurizing the modules above the actuated module would not have a big effect upon the bending performance of the actuated module, although it is imaginable that pressurizing the other modules as well would result in an improved bending.

The experiment was executed by means of actuating the endoscope manually using the newly-built MATLAB application, in combination with running the EM Tracker software. The EM Tracker program was set to take a sample every second, starting with a start-up time of four seconds to prepare the MATLAB application. Every ten seconds displayed by the EM Tracker software, the pressure concerning the actuated module was increased or decreased by a step

of 0.05 bar. Four solenoid valves have been connected (MHE2-M1H-3/2G-QS-4-K) to facilitate switching between chambers (Festo, 2013). Four of the same pressure regulators compared to the previous experiment have been used to control the pressures. The experiment finished after three rounds of swinging to the left and to the right. A display of a section of the actuated pressures can be seen in Figure 4.4. Every time the zero bar is reached, the solenoid valves will switch in order to let the opposite chamber(s) be pressurized, making the endoscope module bend in opposite direction. The setup with the Aurora EM tracker can be seen in Figure 4.5, where the sensor is connected to the tip. Data is mainly processed in ways described in Chapter D and Chapter E of the Appendix.

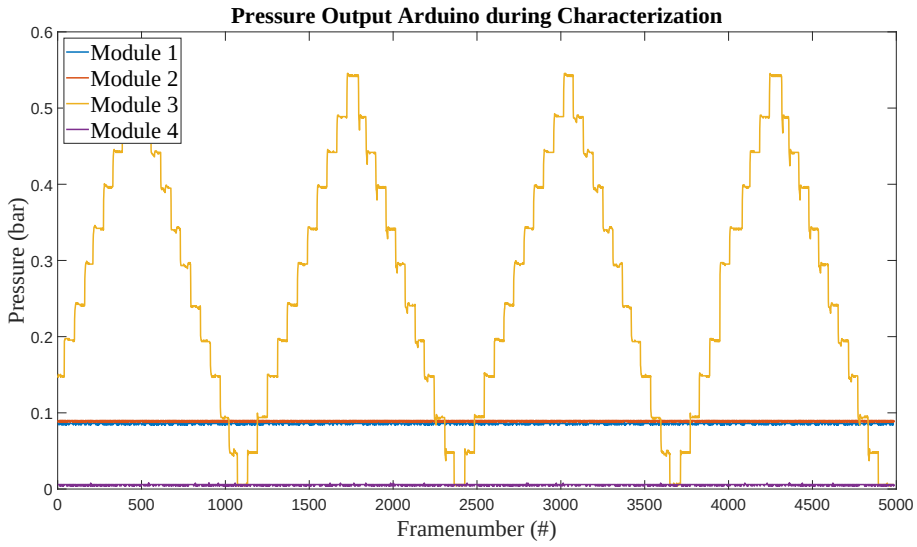

Figure 4.4: Section of the pressure output for characterization of the third module during bending characterization in assembly.

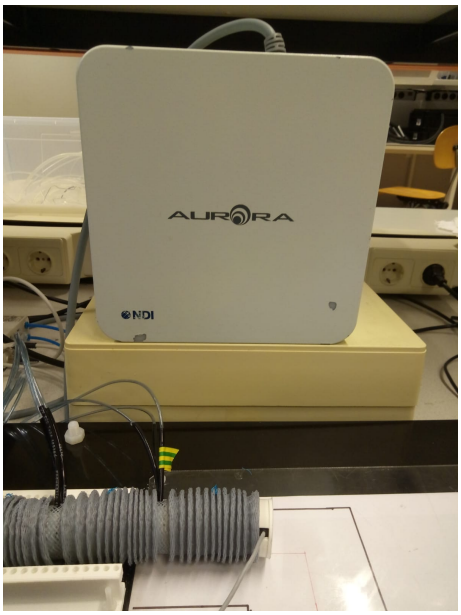

Figure 4.5: Endoscope setup used for the final characterization of the separate modules. The position of the module is being tracked by means of the Aurora EM track system. The same environment is used for the final experiments, although initial characterization used an older version.

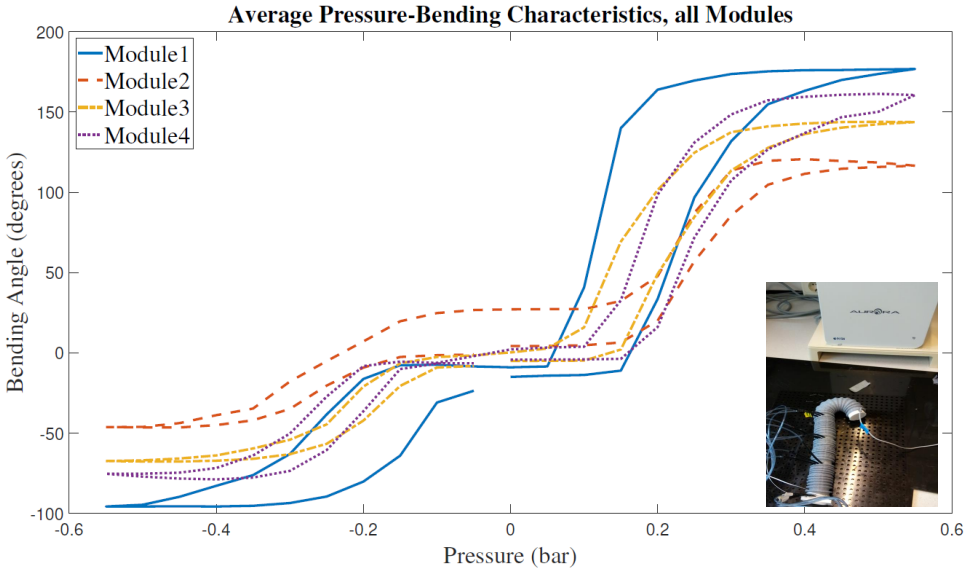

Figure 4.6: Average pressure-bending characteristics of all the modules, executed in assembly on a test platform. On the right, the corresponding test platform can be seen. The plots are average responses over three cycles.

4.3.1 Results Characterization Endoscope Modules in Environment

The behaviour of every module in response to the pressure approach similar to what can be seen in Figure 4.4 has been recorded using the EM Tracker disk sensor. Since the pressure for every time step of the tracker is known, a pressure-bending curve could be deducted.

The average response of the modules inside the endoscope can be seen in Figure 4.6. Here it is visible that similar pressures do not lead to similar orientations. The bending profiles seem to be dependent on historical behaviour, which will be further referred to as hysteresis behaviour. To approximate the behaviour of every endoscope module, the average of the cycles will be taken to eventually get to one hysteresis curve.

Several deductions can be made from Figure 4.6. First of all, it seems that bending performance when pressurizing two chambers results in less bending compared to bending with one chamber actuated. Furthermore, it is possible to detect three zones: the 'dead zone', the 'expansion zone' and the 'saturation zone'. The dead zone shows limited bending response for the initial pressures. After this, the bending performance sharply increases, which is followed by a saturation behaviour. Here, the further module expansion is contained. The average maximum bending performance at 0.55 bar varied from 116.6 degrees for Module 2 to 176.8 degrees for Module 1, for bending towards the right. The standard deviations from the average were found to be small, being on average around 4 degrees. Only the second module had an average standard deviation of around 15 degrees.

4.3.2 Hysteresis Behaviour

This hysteresis effect was assumed to be mainly due to the contact of the endoscope with the surface, which sometimes increases the difficulty of moving the endoscope back. Therefore, other alternative methods of holding the endoscope might be considered that reduce the contact with the surface. Potential solutions for this could be hanging the endoscope in a vertical position, as well as using the endoscope in water.
To examine the effects of friction upon the hysteresis behaviour, a setup was constructed in

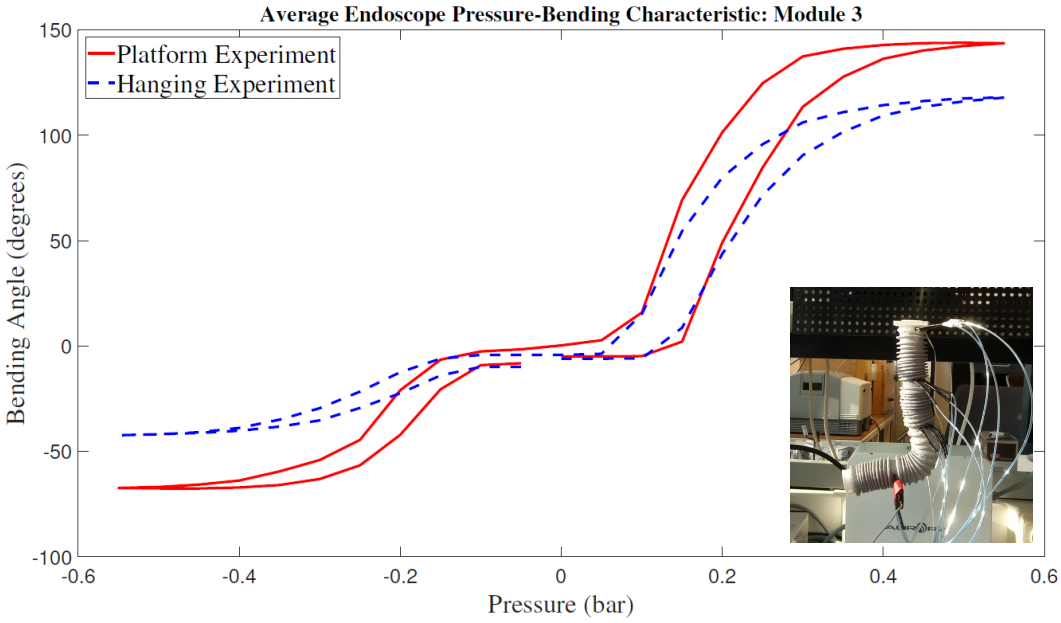

Figure 4.7: Endoscope bending performance of Module 3, considering movement on the platform with respect to movement while in hanging orientation. Negative pressures correspond to bending towards the left. The response is an average taken over three cycles.

which the endoscope was hung upside down. In Figure 4.7, a comparison is being made between an endoscope module bending on the platform, with respect to the bending performance of the same module while hanging the module upside down. Friction with respect to the platform was avoiding in this way. The results of the figure are an average response of the bending module, with respect to three cycles. The results show that the effect of hysteresis is still present.

Chapter F of the Appendix presents an experiment with a two-module inner sheath endoscope, based on the previous module design of Lenssen (Lenssen, 2019). The resulting plot is showing that also there hysteresis behaviour could be found.

4.3.3 Characterization Later Stage

Over time, the endoscope has been used very frequently, causing some of the modules to rupture. To ensure the endoscope would be in a proper state, a new endoscope has been formed using newly fabricated modules.

Due to several modules that broke down during characterization, the pressure was limited to maximum 0.4 bar for both directions. Pressure is being adjusted in the same fashion; steps of 0.05 bar with pauses of ten seconds in between.

As the hysteresis behaviour made it very complicated to grasp the exact performance of the endoscope module while bending, it was attempted to come up with an algorithm that would take into account the bending history of the module while bending. To be more precise, it was thought of to develop a collection of hysteresis curves based on an increased bending pressure, which would potentially grasp the approximate bending behaviour of a module after reduction of pressure. An example of the complex 3D hysteresis characterization can be found in Figure 4.8.

Furthermore, a switch from using the quaternions to the use of Euler angles was performed. Initially, all characterization experiments using the Aurora EM Tracker were outputting bending

angles based on quaternions. The implementation was such that the resulting angles were that of the resultant bending plane. Since the bending behaviour of the endoscopic modules was not always in line with the 2D-plane of the environment platform, the use of this approach might result in a characterization that would deviate from actual performance on that plain. Therefore, for the final characterization experiments, the angles are expressed in Euler angles, preserving the response in line with the platform plane. This has been integrated in Figure 4.8.

4.4 Angle to Pressure Conversion

This section covers Stage D mentioned earlier in Chapter 3. Based on previously derived functions concerning the bending characterization of the endoscopic modules (Stage A2), the pressure values per module for each step can be derived. This is realized using the defined angles from the Endoscope Kinematic Planner of Stage C2. Several approaches were thought of to transform the generated angles into pressure outputs for the soft robotic endoscope. Main approaches that were attempted are:

- Segmented curve fit
- Non-linear regression fit
- 3D mapping
- Average hysteresis fit

All approaches had their drawbacks and benefits. The main drawbacks found were related to computation complexity and implementation difficulties. The attempted approaches are treated below.

Fitting outer hysteresis curve

The fitting of the hysteresis curve throughout this study has been approached using several practices, as has been mentioned before. One of the approaches was to fit the outer curve using several fits together. The hysteresis curve would be divided into eight segments, for which all polynomial functions could be defined. This would be a quite intensive approach, as every curve had to be divided and several fits had to be made. However, a reduction of segments would lead to a worse fit compared to what was done before. Furthermore, the algorithm should take into account when a switch should be made towards another part of the hysteresis curve.

Non-linear regression fit

Another approach was the use of non-linear regression model for computation. With the use of the MATLAB function fitnlm, it was attempted to define specified functions for the upper and lower half of the hysteresis curve. The following base function was used, for which the parameters were searched by the algorithm:

$$F(x) = b_1 + b_2 x + b_3 \sin(b_4 x + b_5) + b_6 \sin(b_7 x + b_8) \tag{4.1}$$

This, together with a set of pre-defined values, was used to create a fit across the present curves. However, during the use of the functions to represent the curve lines, it was found that the eventual pressure response after conversion was rather oscillating. After plotting the function, it was assumed that the oscillations came forth out of error in the fitting function. Therefore, the fits based on this method were skipped, and focus was put on alternative methods.

3D Mapping

As mentioned before, a complex structure was attempted using multiple hysteresis plots with different limits, to get a better grasp of the bending behaviour. In Figure 4.8, the bending re-

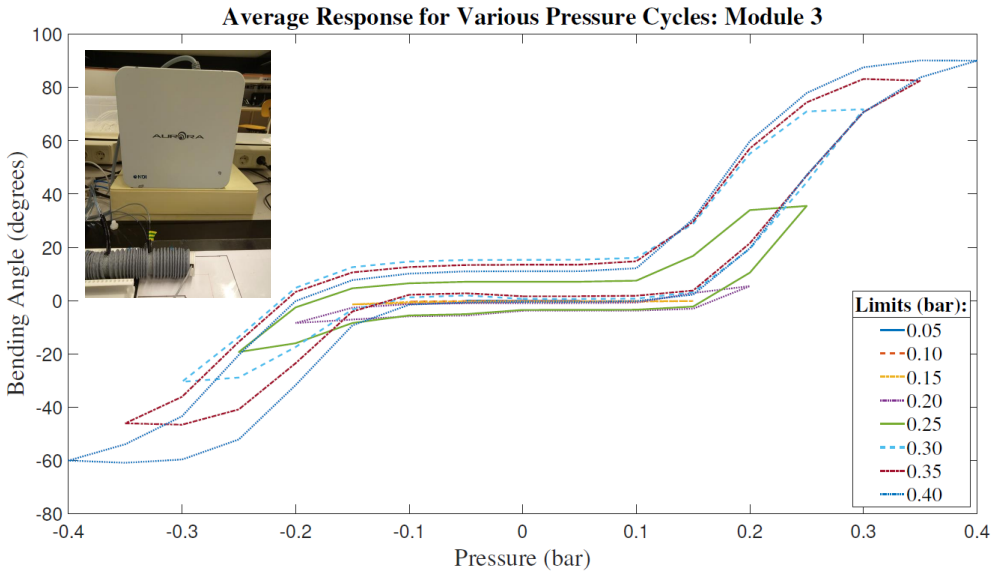

Figure 4.8: The representation of the pressure-bending response of Module 3, for several ranges of pressure inputs. This time, the bending response is derived from the use of Euler angles, which are focussing on the in-plane response. In the left corner, the utilized setup is depicted. The plots are averaged over three cycles.

sponse was shown, described in Euler angles. Every pressure cycle is repeated three times, after which a pressure cycle is taken with a higher pressure limit. From the figure, it can be seen that the ends of the extremes of every curve do not seem to align properly for a lot of cases. This could simply be due to a decomposition of the resulting bending angle, which makes the connections not fit. However, when different hysteresis curves already separate before reaching there specified limit, it would become very difficult to retrieve on which curve corresponds to the current behaviour.

This, in combination with a limited amount of time, has lead to the decision to further simplify the characterization approach. Since following the outside of the curve also gave some difficulties in computation, it has been chosen to continue with the use of the middle line of the most outer hysteresis curve, which does not show angle reduction at the tip. This would result in rather simple computation, of which the offset error is inevitable.

Fitting the middle line

After trying several alternatives, the relatively simple fit of the centerline was deemed most convenient, although this would introduce a certain standard deviation from the actual behaviour. The process of finding the average line was performed by means of averaging the angle per pressure step, after which the line was computed. The result of this can be seen in Figure 4.9, where the middle line is computed next to the fit of this middle line.

Actually, it would be more desired to find the average pressure necessary for a certain degree of bending, since that is the target approach. However, since the pressure was the current independent variable, this middle line based on the average bending angle would be found in an easier way. The alternative would be fitting both sides of the hysteresis curve and applying a range of degrees to determine the average pressure.

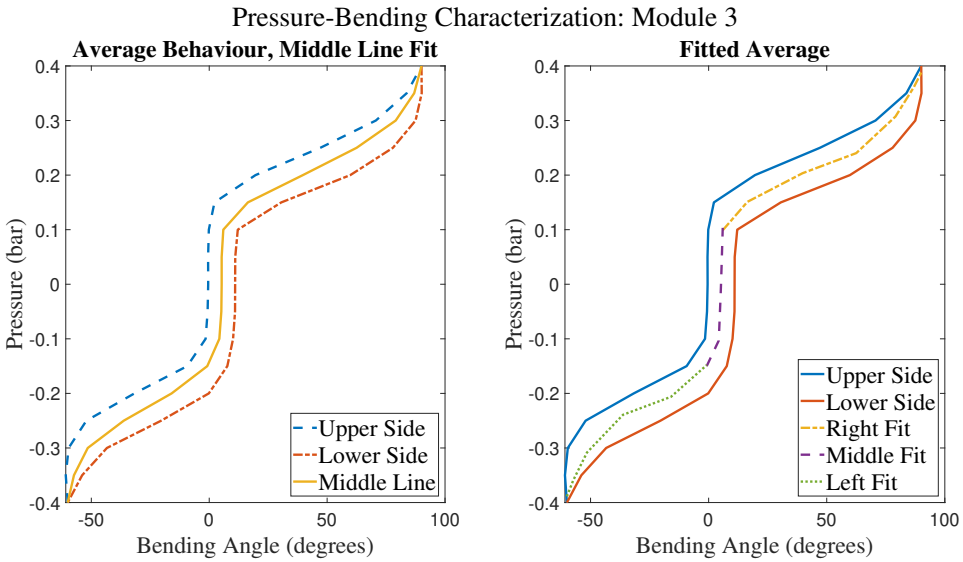

Figure 4.9: On the left, the fit of the middle line from the hysteresis plot is depicted, which is divided into three segments and fitted using 3rd order polynomials, as can be seen on the right.

As can be seen in the second image of Figure 4.9, the middle line is divided into three segments, each fitted with a polynomial of the third degree. These resulting functions are used to transform angles into pressure, bounded by angle limits.

4.5 Discussion

4.5.1 Module Fabrication

During the fabrication process, it was observed that several aspects of module fabrication could be questioned or improved upon. These aspects can have an impact upon the performance of the endoscope as a whole, or the connection between the separate modules for example. Furthermore, several steps were taken in the fabrication process that could maybe be simplified or adjusted in order to improve results. The core points are mentioned below. Malfunction and maintenance are discussed in Chapter G of the Appendix.

Regarding the design in general, it might be reconsidered to use a four-chamber module design again, as this simplifies 2D control in terms of behaviour. Furthermore, the whole outer sheath currently is covering all four modules, which might influence and restrain bending behaviour. Modular modules that could easily be inserted and ejected would be preferable for the ease of assembly. Furthermore, since the sheathing might be causing unpredicted behaviour and is difficult to make uniform, an alternative sheathing method might be desired. Besides that, the weight applied on the endoscope by the pressure tubes has also an effect upon bending performance. The extra weight makes the endoscope have to carry a higher load, as well as affects the orientation of the endoscope modules sideways (see Figure 4.11). Potential ways to reduce this process is by guiding the tubes through the inside of the endoscope or by creating a type of tubing guide to keep the tubes in place during operation. However, both options might cause limitations in terms of bending.

4.5.2 Individual Module Characterization

During the characterization experiments of the endoscope modules, several aspects can be pointed out that can have an influence upon the performance and thus the experimental results. These aspects mainly are related to the way of placement of the modules.

Due to improper placement and constraining of the outer sheath, ballooning could occur, causing potential damage and undesired bending. Furthermore, due to the sheathing not being uniform (fabrication, plastic deformation), this could affect bending performance. Although it was attempted to always orient the sheath in the same way with respect to the actuated chamber, this might not always have been the same, resulting in a difference in bending performance.

Next to the problems connected to the outer sheath, there could also be a difference in positioning of the sensor itself. The EM tracker sensor that is placed on the top of the module is connected to the module via a connector piece, which is kept in place using tape. During bending, the shape of the module changes, making the connection between sensor and module tip also to potentially differ. Due to wear in the tape performance and difference in the repositioning of the tape and sensor after each chamber, this also effects the position of the sensor eventually. Furthermore, the inner tube of the modules often swells up during bending, which could push the sensor up. The results are influenced by the fact that the sensor is not completely connected properly. An example of this can be seen in Figure 4.10, showing a loose connection between sensor and module.

Next to that, the sensor in combination with the connector piece actually adds weight to the whole structure, affecting the eventual bending of the module. The extra weight is assumed to increase bending performance in the current single module experiment. In the assembled case, effect of the additional weight would be smaller due to the influence of the weight of other modules, but could still slightly alter the motion behaviour.

Furthermore, the fixation of the module to the stage and the containment of the sheath using wire has to be taken into account. To counteract the effects of the sheath moving up, the sheath was fastened with wires. This might interfere with bending performance.

Additionally, leakage between the connector piece and the module, due to an improper connection, could result in decreased effective pressure to the modules. This might cause the phenomenon seen in Figure 4.5, where the pressures do not exactly meet 0.1 bar. The modules are checked on significant leakage before experimenting, by means of inspecting on sound.

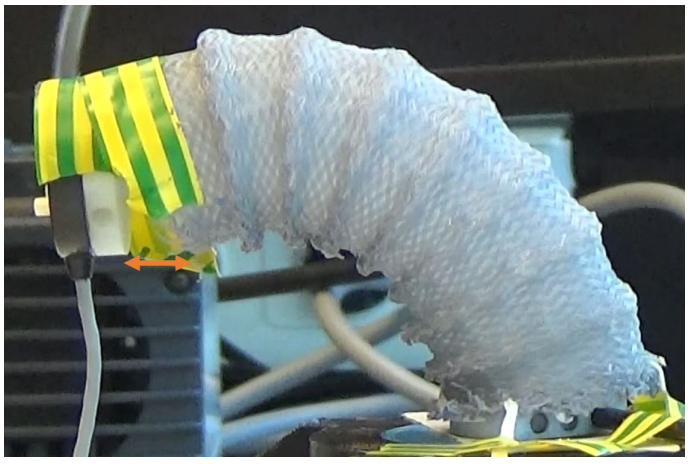

Figure 4.10: An example showing a failing connection between the sensor and the bending module, leading to an affected result in terms of pressure-bending characteristic. The orange arrow indicates the gap.

4.5.3 Endoscope Characterization

One of the major factors that was difficult to grasp is the effect of the bending of other modules upon the bending performance of the respective module. As the outer sheath was covering the whole endoscope, movement of one module could cause differences in position of the outer sheath with respect to the other modules, creating new conditions. Motion of other modules could also alter the interactions with the surface, causing different stick-slip situations. Furthermore, the bending of one module might be further enhanced due to the movement of another module, as this movement might help to overcome friction.
The difference in module bending performance of Figure 4.3 compared to Figure 4.6 is assumed to be due to a difference in external sheaths. The initial experiments were performed with a tight outer sleeve, whereas the endoscope contains a much looser outer sheath covering all modules. This might reduce bending restriction of the module. Furthermore, some modules had to be replaced after being damaged.

Several remarks can be made regarding the characterization procedure, beside earlier mentioned aspects such as sensor placement. Although the bending angle deviation within a standard pressure loop seems small, more repetitions are necessary to create a more accurate representation of the bending behaviour.
Furthermore, the steps currently taken inside the characterization experiments are rather big, making it more difficult to estimate intermediate behaviour. The work of Antonio Lanciano shows an approach in which an Arduino script is used instead of manually filling in the values. His pressure-bending relationships are much smoother, making it an ideal approach for future investigation of the pressure-bending relation.
Currently, only cycles going from bending towards the right to bending towards the left are considered. It is assumed that the cycle will influence bending behaviour, but to what extent is yet unclear. If open loop control is really desired, all scenarios should be taken into account, making for a rather tedious process. Furthermore, the switching of the solenoid valves during change of bending direction could trap some of the remaining air inside the chamber, which affects bending performance. Therefore, it is preferable for future use to not consider using solenoid valves, but instead use more pressure regulators.

From the results of the hysteresis plots it becomes clear that the effect of two-chamber bending seems to result in less bending compared to one-chamber bending. A possible reason for this is the aspect of the chambers having to share the same volume inside the outer sheath, limiting their expansion possibilities. The results are in line with the results found in the study of Naghibi et al. (Naghibi et al., 2019). The article shows an increase in bending capacity for single chamber bending compared to dual chamber bending in both simulation and experiment. Although the used design in their work utilizes four pressure chambers and contains some other design differences, the phenomenon occurring there might be similar to the situation fo this study. However, the difference in bending performance for this current study are much bigger compared to their findings (Naghibi et al., 2019).
The occurrence of the three different stages within the hysteresis behaviour of the modules could be related to the consistency of the module. For the initial pressure values, the expansion of the module chambers seems not yet to be limited by the outer sheath, causing the limited bending. This might also be due to overcoming stick-slip limitations. The saturation at the highest pressure values might be due to full constraint of the module expansion by the outer sheath.

Several experiments were performed to define the cause of the hysteresis behaviour. The hanging experiment showed that without influence of friction, hysteresis could still be found. From the results of the characterization of the modules with inner sheath design it became clear that hysteresis behaviour was also present. Therefore, one could assume that hysteresis behaviour can also be potentially attributed to the Ecoflex material itself, which is in accord-

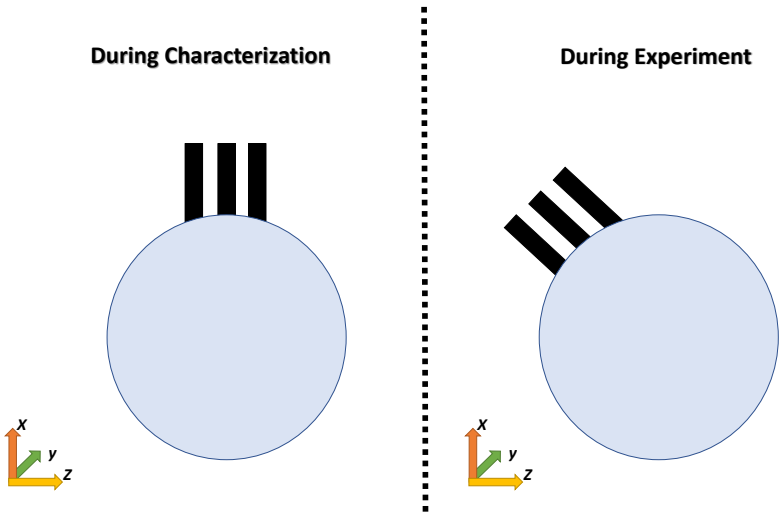

Figure 4.11: Cross section of the endoscopic module with pressure tubes, depicting a potential scenario causing orientation difference between characterization and experiment. This could lead to mismatches in the pressure-bending relation.

ance with literature (Ahmad et al., 2019). However, since both designs have sheathing, either inside or outside, there could still be an influence based on sheathing only.

4.5.4 Angle to Pressure Conversion

It was attempted to develop a 3D hysteresis map, based on the results of Figure 4.8, to use for accurate characterization. However, it was found in the figure that multiple hysteresis plots did not align in terms of corresponding bending angle from the set pressure value. This might be due to decomposition of bending angles along the EM Tracker plane, as Euler angles were used. Due to the mismatch and lack of time, only the outer plot per module was used for the eventual experiments.

Due to a mismatch between the orientation during characterization and actual experiment, the pressure-bending relation when using Euler angles might flaw in defining the necessary pressures. An illustration of this problem is given in Figure 4.11.

Considering the hysteresis behaviour, the difference between potential angles for the same pressure can be rather big. Choosing the average line of the hysteresis plot therefore results in certain error with respect to the actual behaviour. Due to the non-linear behaviour of the pressure-bending relation, this can make the difference between bending and not bending, making it very difficult to rely upon.

4.6 Conclusion

Based on experience with examining various designs, the design incorporating the EcoFlex 0030 material, together with the use of an outer sheathing, eventually resulted in the highest bending angle based on similar module length. This module design is incorporated in the eventual endoscope.

The bending performance of a number of EcoFlex 0030 modules has been tested in free upright position and resulted in finding a rather similar behaviour for all modules, as well as for the chambers of each module. The average bending performance at 0.55 bar was found to be around 107 degrees (106.8 ± 9.0).

The resulting response from the assembled endoscopic modules inside the old environment showed hysteresis behaviour, when using a different pressure profile and including bending

towards opposite direction. Average response extremes at 0.55 bar varied from 116.6 degrees for Module 2 to 176.8 degrees for Module 1, for bending towards the right. Two chamber bending, which equals bending to the left in this case, was found to reach a less high bending compared to one chamber bending.

Based on the hanging endoscope experiment, it has been found that the hysteresis behaviour does not solely exist due to the effects of friction. The hysteresis behaviour was found in both the outer sheath model and the inner sheath model.

Regarding the 3D representation, the decomposed angle when using Euler angles causes discrepancies in the bending response per pressure value, making this method difficult to use as a reference for bending performance. A fit of the middle line of the hysteresis plots of the four modules is used as a means to convert future desired angles into pressure outputs for the eventual path planned endoscope.

5 Kinematic Model: Bending Module

To be able to define the angles necessary to move through the specified environment, a model is required describing the endoscope module bending behaviour. This chapter covers the modelling of the endoscopic modules, which is used in the algorithms to approximate the simulated endoscope response in Stage C2. The chapter treats Stage B from Figure 3.1 of Chapter 3. A distinction is made between the initially used Constant Curvature Model and the Modified Model, which was developed after assessing the bending behaviour of the respective endoscopic modules. This chapter answers part of sub-question 3.

5.1 Constant Curvature Model

The bending behaviour of the soft robotic endoscope module was initially approximated by a Constant Curvature Model, described by Webster et al. (Webster III and Jones, 2010), who divided the motion of the module into a rotation around the z-axis, accompanied with a bending over the y-axis. Equation 5.1 demonstrates this phenomenon, which actually describes the behaviour of a bending beam in 3D.

$$\mathbf{H} = \begin{bmatrix} \mathbf{R}_z(\phi) & 0 \\ 0 & 1 \end{bmatrix} \begin{bmatrix} \mathbf{R}_y(\theta) & \mathbf{p} \\ 0 & 1 \end{bmatrix} \tag{5.1}$$

where $\mathbf{R}_z(\phi)$ describes the rotation around the z-axis as a function of the rotation angle ϕ (rad), $\mathbf{R}_y(\theta)$ describes the bending of the beam around the y-axis as a function of θ (rad), and $\mathbf{p}$ describes the current position of the tip position with respect to the module base. The position of the tip of the module could be described by $\mathbf{p} = [r(1-\cos(\theta)), 0, r\sin(\theta)]^T$, with r is the radius of curvature (cm). Figure 5.1 gives a representation of the bending beam, with radius of curvature r (cm), bending angle around y-axis θ (rad), length l (cm) and z-rotation ϕ (rad). After writing out the matrices from Equation 5.1 and performing the multiplication, the resulting matrix looks like Equation 5.2. Here, the notation $\mathbf{H}_i^{i-1}$ is used to clarify that this homogeneous matrix corresponds to the relative position with respect to the previous module.

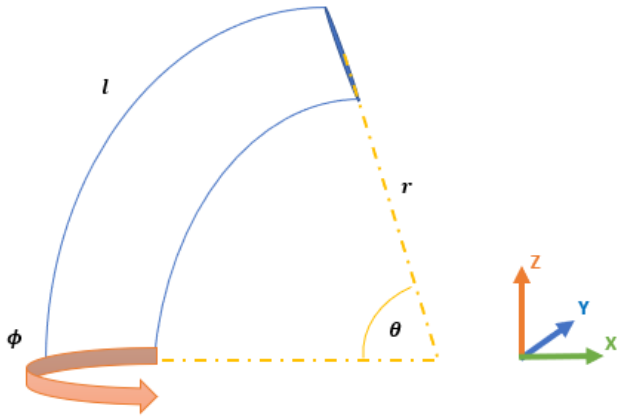

Figure 5.1: Representation of the bending beam model, in which rotation around the z-axis is shown together with the bending over the y-axis. Image based on the related figure in the article of Webster et al. (Webster III and Jones, 2010).

$$\mathbf{H}_i^{i-1} = \begin{bmatrix} \cos(\phi)\cos(\theta) & -\sin(\phi) & \cos(\phi)\sin(\theta) & r\cos(\phi)(1-\cos(\theta)) \\ \sin(\phi)\cos(\theta) & \cos(\phi) & \sin(\phi)\sin(\theta) & r\sin(\phi)(1-\cos(\theta)) \\ -\sin(\theta) & 0 & \cos(\theta) & r\sin(\theta) \\ 0 & 0 & 0 & 1 \end{bmatrix} \tag{5.2}$$

Taking into account that r can be rewritten as the curvature $\kappa = 1/r$ and that $\kappa = \theta/s$, with s being the point along the length of the backbone of the module (cm), the following matrix can be derived

$$\mathbf{H}_i^{i-1} = \begin{bmatrix} \cos(\phi)\cos(\kappa s) & -\sin(\phi) & \cos(\phi)\sin(\kappa s) & \frac{\cos(\phi)(1-\cos(\kappa s))}{\kappa} \\ \sin(\phi)\cos(\kappa s) & \cos(\phi) & \sin(\phi)\sin(\kappa s) & \frac{\sin(\phi)(1-\cos(\kappa s))}{\kappa} \\ -\sin(\kappa s) & 0 & \cos(\kappa s) & \frac{\sin(\kappa s)}{\kappa} \\ 0 & 0 & 0 & 1 \end{bmatrix} \tag{5.3}$$

Due to the fact that only a 2D scenario is considered at the moment, the rotation behaviour around the z-axis is left out of the scenario, which is equal to filling in $\phi = 0$ into Equation 5.3. This simplification results in the following relation

$$\mathbf{H}_i^{i-1} = \begin{bmatrix} \cos(\kappa s) & 0 & \sin(\kappa s) & \frac{(1-\cos(\kappa s))}{\kappa} \\ 0 & 1 & 0 & 0 \\ -\sin(\kappa s) & 0 & \cos(\kappa s) & \frac{\sin(\kappa s)}{\kappa} \\ 0 & 0 & 0 & 1 \end{bmatrix} \tag{5.4}$$

These homogeneous matrices form the basis of the endoscopic module simulation in the environment.

5.2 Integrating Modified Model

In order to validate the path planning model, the difference found between the constant curvature approximation with respect to the bending performance of the endoscopic module has been approximated by means of adjusting the model. A representation of the alternative model can be seen in Figure 5.2.

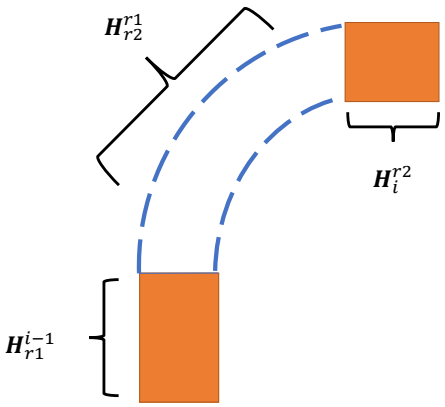

Figure 5.2: Decomposition of Modified Model, which consists of two rigid blocks and has a constant curvature section in the middle. The section contributing to the bending of the module is reduced in size compared to the Constant Curvature Model.

The new model consists of three parts, of which first and the last are rigid. The first section, $\mathbf{H}_{r1}^{i-1}$, has a length of 1.5 cm, which is the length of the connector piece together with the initial part of the module. The constant curvature approximation, represented by $\mathbf{H}_{r2}^{r1}$, is now reduced in length to 3 cm. This is in line with the chamber length in the physical module. The top layer has a size of 1 cm, represented by $\mathbf{H}_{i}^{r2}$.

The Modified Model has been implemented into the Endoscope Kinematic Planner algorithm, in order to see its performance. This has been done as follows.

The approach to define the homogeneous matrices with respect to the world frame, following equation has been used

$$\mathbf{H}_{i}^{0} = \mathbf{H}_{i-1}^{0}\mathbf{H}_{i}^{i-1} \tag{5.5}$$

in which $\mathbf{H}_{i-1}^{0}$ serves as the homogeneous matrix of the previous module with respect to the world frame. To include the rigid bodies on the bottom and the top of the module, the Equation 5.5 has been altered towards

$$\mathbf{H}_{i}^{0} = \mathbf{H}_{i-1}^{0}\mathbf{H}_{r1}^{i-1}\mathbf{H}_{r2}^{r1}\mathbf{H}_{i}^{r2} \tag{5.6}$$

where $\mathbf{H}_{r1}^{i-1}$ and $\mathbf{H}_{i}^{r2}$ are the lower and upper rigid parts of the module, respectively. An example of the homogeneous matrix $\mathbf{H}_{r1}^{i-1}$ in Equation 5.7 is given below

$$\mathbf{H}_{r1}^{i-1} = \begin{bmatrix} 1 & 0 & 0 & 0 \\ 0 & 1 & 0 & 0 \\ 0 & 0 & 1 & 1.5 \\ 0 & 0 & 0 & 1 \end{bmatrix} \tag{5.7}$$

where 1.5 is the length in cm for the initial module section. The implementation of a these rigid connections was accompanied with a shorter backbone length, on which the constant curvature was executed.

5.3 Comparison Models and Physical Module

The bending performance of the models have been highlighted in Figure 5.3. Here, the Constant Curvature Model is plotted next to the Modified Model, for an angle of 90 degrees. These models are compared to the physical representation of the bending module, represented in the left image of the figure. This approximation is based on the centerline selection of the bent module. In the right image, the Modified Model is adjusted to approach the physical response, which is done by scaling the constant curvature section of the Modified Model. The length of the Constant Curvature Model in the right image is scaled as well.

The results of implementing both models in the simulation algorithm have been compared in the next chapter, in for example Figure 6.13 and Figure 6.19.

5.4 Discussion

As the currently addressed models are mere approximations of the endoscope module behaviour, some remarks must be taken into account when considering its implementation.

5.4.1 Physical Module vs. Modified Model

When regarding the left image of Figure 5.3, the shape of the physical response seems to be more similar with respect to the Modified Model compared to the Constant Curvature Model. The approximation of the physical module response also contains rather straight sections at the base and the tip, similar to the Modified Model.

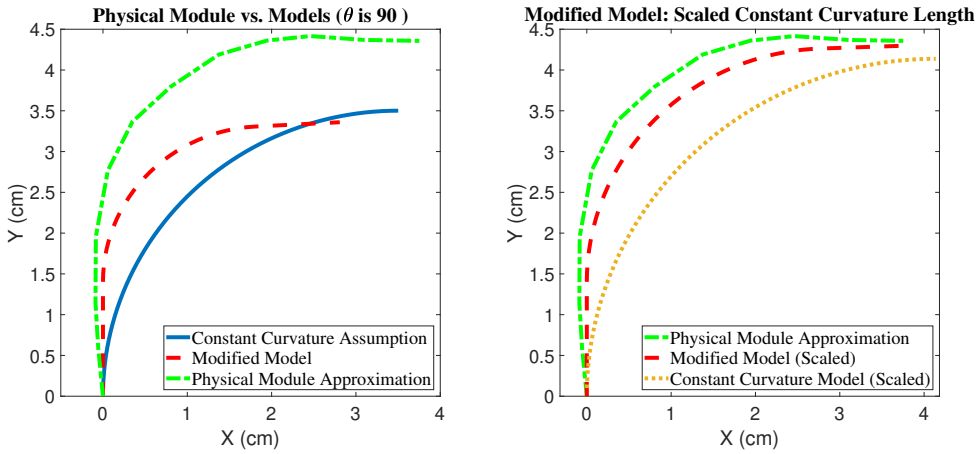

Figure 5.3: Comparison between model(s) and physical module response. The left illustration shows the responses of the physical module, the Constant Curvature Model, and the Modified Model. On the right, the physical approximation is compared to the Modified Model response with an increased size of the constant curvature section (from 3 cm to 4.5 cm), as well as to a scaled version of the Constant Curvature Model (from 5.5 cm to 6.5 cm).

It must be mentioned that the approximation of the physical response is constructed from manual selection of the centerline of the module during bending, which is subject to errors in representation. Due to a failed attempt using image processing, in which the module skeleton was deformed, and the lack of time available, this method for choosing the corresponding centerline is chosen. Therefore, the comparison serves merely as an indication of physical module growth and an increased similarity with respect to the Modified Model, as little can be said about the actual differences.

Furthermore, it must be taken into account that this comparison is solely based on one scenario, which is the 90 degrees bending. More scenarios should be examined to be able to confidently state the claim of approximating the behaviour rather closely, together with defining the lengthening behaviour throughout the bending.

5.4.2 Lengthening Principle

As could be seen in Figure 5.3, there seems to be a misfit between the models and the actual module response, mainly regarding the size. Arguing from a physical point of view, module bending occurs due to chamber expansion, which is not accounted for in the models itself. The right image of Figure 5.3 is showing the Modified Model response when the length of the constant curvature section would be increased from 3 cm to 4.5 cm, an increase of 50 %. The scaled version of the Constant Curvature Model has a different length compared to the Modified Model, as a bigger length would result in a worse approximation of the physical response. The Modified Model seems to approximate the physical response better compared to the Constant Curvature Model.

The phenomenon of lengthening of the module during bending is thus far excluded from the bending approximation, although it is affecting the response quite a lot. Due to lack of time, this was not researched in detail. Using the data from the EM tracker, the module (tip) position could be mapped and compared the (tip) position of Modified Model, to examine the difference. By means of adjusting the length of the constant curvature section, which is the principal section for expansion, an estimate can be defined for lengthening per bending angle. This would hold under the condition that the remaining part of the model represents the behaviour rather well. These results could be integrated in the current model as well. During

experimentation, it was found that the module increased in size more when bending with two chambers compared to one. This also has to be taken into account.

The lengthening has not been incorporated in the implemented model for the rest of the study, and remains a recommendation for future research.

5.5 Conclusion

Regarding the model of the bending endoscope module, two approaches have been considered; the Constant Curvature Model and the Modified Model. The Modified Model contains a constant curvature section with the length of a module chamber, surrounded by two rigid blocks that do not attribute to the further bending. The Modified Model seems to have a more similar shape with respect to the physical bending scenario than the Constant Curvature Model. Regarding physical inspection, the Modified Model is also deemed a better approximation. Lengthening of the modules seems to affect the bending response, which should be focus for future research. The Modified Model is eventually taken into account in the Endoscope Kinematic Planner, as well as integrated into the final experiments regarding path planned insertion.

6 Path Planning Algorithms

The knowledge obtained from the fabricating and characterizing the modules (Stage A1 and A2), in combination with the defined model of the endoscopic module bending behaviour (Stage B), serve as a basis for the development of algorithms that define the path for the endoscope to follow, as well as determine and store the necessary bending angles to so. The angles, together with the discovered pressure-bending relationships, will define the necessary pressures for the physical endoscope response.

The following sections describe the algorithms developed to create a path throughout the environment and to simulate the endoscope movement throughout the scenario when following this path. These two separate tasks, defining a path and simulating the endoscope movement when following it, are represented by the Path Planning algorithm and the Endoscope Kinematic Planning algorithm (also referred to as Path Tracker algorithm), which are stages C1 and C2, respectively. This chapter covers the answer to sub-question 4.

6.1 Path Planner

To determine the path the soft robotic endoscope has to follow, path planning is used. This section will treat the working principle of the currently used Path Planner algorithm, which starts with the working principle and is ending with simulations of the utilized scenarios. As has been addressed before, the RRT-algorithm is chosen for planning the path throughout the pre-defined scenarios.

6.1.1 Elaboration of the Principle

To eventually let an endoscope follow a path in simulation, first a path needs to be acquired. Knowing the environment and the dimensions of the endoscopic modules, a path can be determined. The goal is to let an algorithm define this path automatically, while also considering several criteria that come with the control of the soft robotic endoscope inside an environment.

Some general requirements need to be fulfilled for the algorithm:

- A path should be defined between the starting point and the target point.
- This path should be collision-free.

In general, path planning algorithms also take care of the mapping of the obstacles inside the given environment, as well as include obstacle margins, such that the dimensions of the moving object are taken into consideration. Several criteria concerning the current study application should be met as well:

- The dimensions of the endoscope should be taken into account in the obstacle margins.
- The endoscope dimensions should fit in the environment.
- The path should not contain corners which the endoscope should not be able to make.

To realize this, the RRT principle is utilized, which has been described in Section 2.2.1. The 2D path planning algorithm that has been used throughout this study is inspired by the work of Sai Vemprala (Vemprala, 2017), who based his work on the work of LaValle (LaValle, 1998) and Karaman et al. (Karaman and Frazzoli, 2011). The code consists of an RRT* algorithm, which is a variation of RRT and has been discussed earlier. The work of Sai Vemprala (Vemprala, 2017) has been adjusted to fit the conditions of the current study.

More details regarding the separate sections of the algorithm can be found in Chapter H of the Appendix.

Modifications to the Algorithm

Several scenarios have been predefined, representing parts of the endoscopic environment. These scenarios are shaped using obstacle coordinates, which limit the growth of the tree in certain directions. The starting point and the target point also have been defined beforehand. To increase speed of computation, the points that spawned inside the obstacles were disregarded, just like the approach in the study of Noreen et al. (Noreen et al., 2016b). Furthermore, a target region was selected around the target point, which also is mentioned in the study of Alterovitz et al. (Alterovitz et al., 2011). In this way, the goal is reached earlier. To limit the angles found inside the created tree, and thus the eventual angles inside the path, an algorithm is used to define the angle and quit when the potential angle surpasses the threshold.

To determine the angle, the following formula was utilized:

$$\theta_{\text{tree}} = \cos^{-1}\left(\frac{(\mathbf{A}\cdot\mathbf{B})}{||\mathbf{A}||||\mathbf{B}||}\right) \tag{6.1}$$

Where **A** and **B** are respectively the vectors from the q_{near} to the new point and the q_{near} to the previous point. The lengths of these connections are determined by taking the norm. A multiplication of these vector lengths serves as the denominator, whereas the numerator is the dot product of the two vectors. A representation of the angle determination can be found in Figure 6.1.

6.1.2 Simulations

To test the applicability of the path planner, two scenarios have been developed. These scenarios are basic representations of the segments inside the human colon and can be seen as the two main alternative bending scenarios. The shape of the endoscope environments is kept rather basic; in reality, the colon consists of flexible curved corners and does not really contain

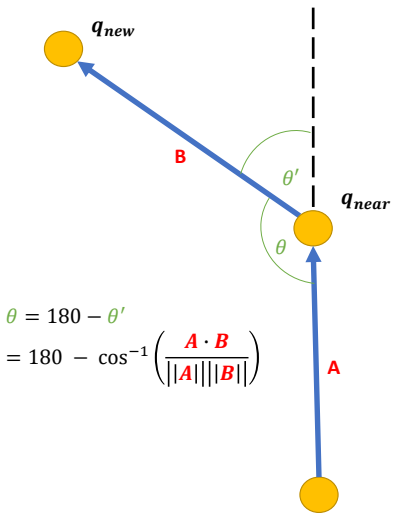

Figure 6.1: Representation of how the angle between the potential tree connections is determined.

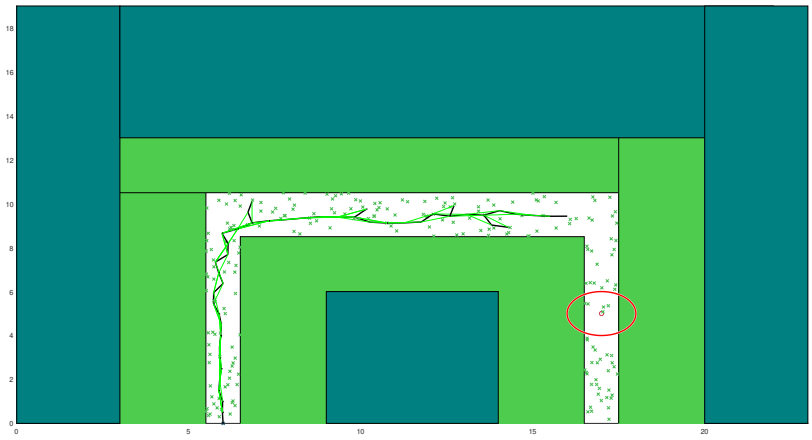

Figure 6.2: The RRT* algorithm performing the search for a path in Scenario 1. Obstacles are indicated in green, the target region in red. The coordinates of the path are transferred to the Endoscope Kinematic Planner.

any straight segments. Furthermore, the environment of the colon is rather dynamic, meaning that the consistency also shifts over time. It was attempted to find the dimensions of the colon in literature and use them as a reference for the sizes of these scenarios. Several sources were found, investigating the dimensions of the colon (Witmer, 2007) (Sadahiro et al., 1992)(Hounnou et al., 2002). Based on Witmer (Witmer, 2007), one could define the average colon diameter to be between 4 cm and 8 cm, which is why an average diameter of 6 cm is chosen.

Scenario 1 consists of a double-cornered bend, which requires bending in only one direction. The second scenario, Scenario 2, includes bending towards both sides. Simulations of both scenarios will be addressed below.

Scenario 1

A representation of Scenario 1 can be seen in Figure 6.2. The Path Planner algorithm is given the dimensions of the obstacles, together with information regarding the module width and length, as well as the potential bending capacity. Furthermore, the position of the starting point as well as the target has been given. Based on this information, the algorithm finds a suitable path. In the figure, the dark green indicates the obstacles, whereas the lighter green is representing the module dimensions. At this moment in the image, the target is still searched for. When the target is reached, the path is traced back towards the base. The black lines indicate the tree growth, whereas the green lines show the RRT* property, attempting to reduce the distance cost.

The resulting path with respect to the centerline, which is created by the Path Planning algorithm, is shown in Figure 6.3. What stands out from Figure 6.3 is the deviations of the planned path with respect to the corners of the centerline. Due to the angle limitations set in the Path Planner, these corners are avoided. This benefits the eventual behaviour of the endoscope during simulation, as this promotes more gradual transitions.

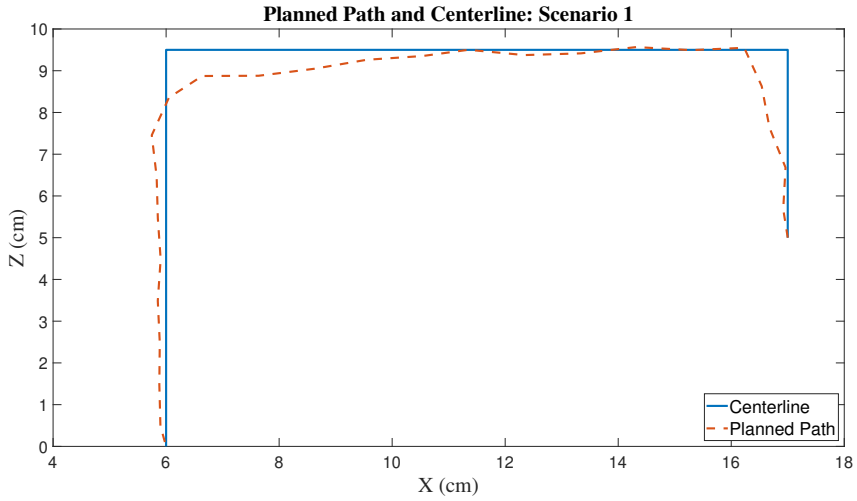

Figure 6.3: The planned path with respect to the centerline of Scenario 1. As can be seen, the planned path avoids the sharp corners of the centerline.

Scenario 2

Scenario 2 is rather similar to Scenario 1, but it has the second corner in the opposite direction. Figure 6.4 shows the building of the path inside Scenario 2. Similar settings were used.

The results of this scenario can also be converted in a comparison between centerline and planned path, as is depicted in Figure 6.3.

Duration

The simulations are performed using MATLAB on a Dell Latitude E6540 with 8 GB RAM and 2.7 GHz CPU. Regarding Scenario 1, it takes the algorithm on average around 5.9 ± 1.2 seconds to compute a path for this scenario (N=10). For Scenario 2, the average duration is about 10.2 ± 1.6 seconds to realize a path (N=10). Simple ways to improve speed of computation are by building the algorithm using faster platforms such as Python and C++, by using a faster computer or by removing visual computation during simulation.

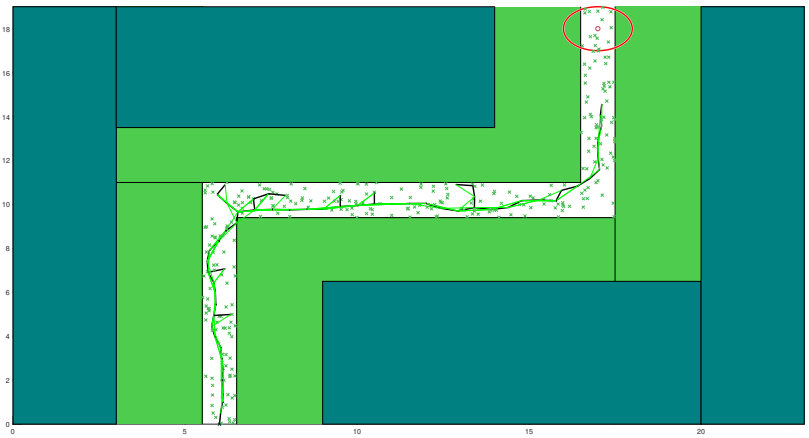

Figure 6.4: The RRT* algorithm performing the search for a path in Scenario 2.

6.2 Endoscope Kinematic Planner

The Endoscope Kinematic Planner makes use of the resulting path that has been created by the Path Planner, in combination with the module bending kinematics described in Chapter 5, to simulate the endoscope moving through the scenario. This section describes the processes connected to Stage C2 (see Figure 3.1).

6.2.1 Elaboration on Procedure

The stages in the Endoscope Kinematic Planner can be described as Insertion, Target Selection, Bending Optimization, and Data Storage. They will be treated in the subsections below.

Insertion

After initialization of the environment and the developed path from the path planner, the characteristics of the endoscope modules are used to determine how the endoscope behaves when performing insertion. Based on the length of the modules and the number of modules included in the endoscope, the initial base distance is chosen from the environment:

$$\mathbf{p}_1^0 = [x_c, 0, -(NL+2)]^T \tag{6.2}$$

where $\mathbf{p}_1^0$ describes the base location with respect to the global frame, x_c is the x-coordinate for the middle of the environment at the starting position, N is the number of modules used and L is the module length (cm). The endoscope starts to build up from the base, with its modules positioned in the middle of the environment. Every cycle, the base is moved up in z-direction, by addition of 0.5 cm per step. The base could be described as the $\mathbf{H}_1^0$. Pre-multiplying the base with the next modules, the actual positions of the module tips can be determined

$$\mathbf{H}_n^0 = \underbrace{\mathbf{H}_1^0}_{\text{Base}} \mathbf{H}_2^1 .. \mathbf{H}_n^{n-1} \tag{6.3}$$

with

$$\mathbf{H}_1^0 = \begin{bmatrix} 1 & 0 & 0 & (\mathbf{p}_1^0)_x \\ 0 & 1 & 0 & (\mathbf{p}_1^0)_y \\ 0 & 0 & 1 & (\mathbf{p}_1^0)_z + 0.5k \\ 0 & 0 & 0 & 1 \end{bmatrix} \tag{6.4}$$

where $(\mathbf{p}_1^0)_x$ describes the x-component of the base with respect to the world frame, as well as $(\mathbf{p}_1^0)_y$ and $(\mathbf{p}_1^0)_z$ do so for the y-component and the z-component, respectively. Here, k is the current step number.

Target Selection

After an insertion step, the algorithm checks for every module inside the simulated endoscope which point in the path is closest to the module tips. These are selected as the tip target points for those specific modules. The target point refers to the eventual goal, whereas the tip target point is a local target on the path at that point in time, regarding the treated module. This has been realized by taking the norm of the points in a local coordinate frame. Equation 6.5 shows the principle of retrieving the local difference:

$$\mathbf{p}_2^3 = (\mathbf{H}_3^0)^{-1} \mathbf{p}_2^0 = \mathbf{H}_0^3 \mathbf{p}_2^0 \tag{6.5}$$

where $\mathbf{p}_2^3$ describes the local difference between the third module and the second point, both represented initially with respect to the global frame.

After finding a relation between the path points and the module bases, described in the local frame, some boundary conditions are applied to filter out some bad combinations.

- The point has to be a distance of at least 90% of a the module length away from the module base. A shorter distance would make it more difficult to reach the point.
- Points that are behind the module base are also receiving a penalty, as only forward motion is stimulated.

After penalties are applied to these options, the norm is taken of all local points, resulting in a list of distances. This minimum of these distances is selected as tip target point for the module.

Bending Optimization

After selecting the tip target points for the modules to bend towards, the optimal bending has to be found for the module to perform. This is realized by means of a MATLAB function called fminsearch, which makes use of the Nelder Mead principle (Wright et al., 2010) (MathWorks, -a). This function looks for the value of a defined variable that creates the optimal solution for a pre-defined cost function.

Before the ideal solution is sought for, the algorithm first requires a starting point for the optimal search to occur. This starting point is provided by means of calculating the curvature between the module and the tip target point. This is done by taking the arctangent of the local x-value and local z-value, which results in the generated curvature of the respective module after dividing by the length. The step can be seen in Equation 6.6, taking the local difference between module three and the second point again as example.

$$\kappa = \frac{1}{L}\tan^{-1}\left(\frac{\left(\mathbf{p}_2^3\right)_x}{\left(\mathbf{p}_2^3\right)_z}\right) \tag{6.6}$$

Here, κ is the curvature (rad cm^{-1}), $\left(\mathbf{p}_2^3\right)_x$ describes the distance in x-direction of the difference vector between module three and point two (cm), $\left(\mathbf{p}_2^3\right)_z$ describes the distance in z-direction between the two (cm), and L is basically the module length (cm). An exception is made for $\theta = 0$, as this would eventually result in a difficult situation when calculating the homogeneous difference matrix. Therefore, when it is detected that θ has the value of zero, this is converted to a very small number.

After a starting point was found, the optimization procedure could commence. The cost function to be optimized is as follows:

$$J_{\text{cost}} = \alpha J_{\text{d}} + \beta J_{\text{o}} + \gamma J_{\text{c}} \tag{6.7}$$

where J_{d} is a cost with respect to the distance of the tip target point in the path, J_{o} is the cost describing the difference between orientation of the tip with respect to the points near the tip target point in the path, and J_{c} is a cost laid upon the number of collisions of sub-sections of the module. The variables α, β and γ describe the magnitude of the penalty towards these certain aspects of the cost function. The corresponding values are chosen to be: $\alpha = 2$, $\beta = 1$, and $\gamma = 1000$.

The following equation describes the cost with respect to the distance in more detail:

$$J_{\text{d}} = \frac{1}{L}\left\|\mathbf{p}_i^0 - \mathbf{p}_t^0\right\|_2 \tag{6.8}$$

Here the inverse of the module length (cm^{-1}) is used to normalize the function, based on a chosen standard of one module length, whereas $\mathbf{p}_t^0$ is the target point of the respective module

and $\mathbf{p}_i^0$ is the current module tip position with respect to the world frame. The function seems similar to the before mentioned equation regarding distance, although in that situation the distance of the tip target point with respect to the base of module was taken into account, whereas here the distance of the point with respect to the module tip is described.

It was found from experience that, when the orientation of the tip of the modules would not be considered, the module would often tend to bend such that it would get very close to the tip target point, with whatever orientation possible. Problematic orientations would occur, making it more difficult for the upper modules to build upon. This would often cause some undesired behaviour. Equation 6.9 describes the cost function regarding the orientation of the module. Here, it is desired to have the tip of the module in the same orientation as the path around the tip target point. The difference in orientation was computed as follows:

$$J_{\mathrm{o}} = \frac{1}{2} \left\| \mathbf{R}_0^i \mathbf{R}_y - \mathbf{I}_3 \right\|_2 \tag{6.9}$$

where $\mathbf{R}_0^i$ represents the inverse of the rotation segment from the homogeneous matrix $\mathbf{H}_i^0$ and where

$$\mathbf{R_y} = \begin{bmatrix} \cos(\theta_{\mathrm{p}}) & 0 & -\sin(\theta_{\mathrm{p}}) \\ 0 & 1 & 0 \\ \sin(\theta_{\mathrm{p}}) & 0 & \cos(\theta_{\mathrm{p}}) \end{bmatrix} \tag{6.10}$$

As can be seen from Equation 6.9, the rotation part of the homogeneous matrix is selected, or better said; the inverse of the rotation matrix. The inverse is taken, which is equal to the transpose for rotation matrices (Evans, 2001), to get the difference in rotation between the path angle and the module tip angle. From this resulting matrix, the identity matrix $\mathbf{I}_3$ is subtracted. The norm is taken to retrieve a value from this difference, which can range between zero and two. This is why this function is normalized by the factor 2. The angle θ_{p} is based upon the arctangent between the positions of the point before and after the tip target point:

$$\theta_{\mathrm{p}} = \tan^{-1}\left(\frac{\left(\mathbf{p}_{t+1}^{t-1}\right)_z}{\left(\mathbf{p}_{t+1}^{t-1}\right)_x} \right) \tag{6.11}$$

where $\left(\mathbf{p}_{t+1}^{t-1}\right)_z$ represents the distance (cm) in z-direction between the point next to the tip target point, with respect to the point previous to the tip target point. The same holds for the x-direction, regarding $\left(\mathbf{p}_{t+1}^{t-1}\right)_x$.

The last cost formula, J_c, determines the number of segments from the module that are intersecting with the obstacle (margins). In this case, the modules are separated in five segments, which are all individually checked on occurrence inside the predefined boundaries. Equation 6.12 gives a notion of what is meant:

$$J_{\mathrm{c}} = \frac{1}{5} \sum_{n=1}^{5} O_{\mathrm{c},n} \tag{6.12}$$

where O_{c} is representing the occasion of collision of one of the points in the module with respect to the environment. This value is either one or zero. Based on the comparison between obstacle coordinates and module point coordinates, potential interactions can be found. Currently, the algorithm compares only a discrete number of five points, representing the module shape with the obstacle coordinates. This is why the cost function is normalized by 5.

Using these cost function components in one whole function, the optimal curvature is determined for each module, which is implemented further using the model kinematics.

Data Storage

After the process of choosing the optimal curvature for the module, the curvature value is inserted in the homogeneous matrix for that respective module, which, together with a potential multiplication chain of module matrices, results in a position and orientation with respect to the global reference frame. For every module and during every cycle, these matrices are stored. Based on the orientation and position of the module, which can be retrieved from these values, the module tips and several segments in between are plotted inside the environment. When the tip module approaches the target of the path, which is defined by means of a Pythagorean distance threshold, the simulation is put to a stop. Optional functionality is built in that counts and projects the number of collisions of the module tips with respect to the obstacles, after simulation has completed. Furthermore, the defined angles found during the simulation are plotted together, representing the movement throughout the environment.

3D Endoscope Kinematic Planner

Potential options to expand towards a 3D environment have been considered and implemented into the algorithm. Pre-defined obstacles and paths are prepared, to show the performance of the endoscope in 3-dimensional space. This process seemed to work rather well, although the current focus of this study was not on developing 3D solutions. As recently it was found that there also is a 3D RRT* algorithm ready, this might be a fruitful future approach.

6.2.2 Simulations

The Endoscope Kinematic Planner algorithm would simulate endoscope movement along the path, based on the created paths of the Path Planning algorithm (Chapter 6.1). Simulation results are depicted in the sections below, with respect to Scenario 1 and Scenario 2. In this section, the Constant Curvature Model is used.

Scenario 1

In Figure 6.5, the separate modules can be seen, together with the path (indicated with black dots) and the environment. The green part of the environment resembles the real obstacle, whereas the red sections are the mapping of the endoscope module dimensions upon the obstacles. This is similar to the representation of the Path Planner. The tips of every module are indicated with frames, showing the position and orientation of the respective modules. This makes it easier to understand the behaviour of the separate modules. The black dots encircled with a red circle are indicators for the tip target points in the path, to which the modules tend to bend. The simulation keeps track of the number of modules inside of the environment, as well as their maximum bending, their dimensions and the potential collisions with the environment. The simulation also outputs the required angles necessary for the modules to move towards the target.

After the path has been run by the endoscope, the errors with respect to the planned path and the centreline can be determined. These are again based upon the tip positions over time, and are calculated from the instant they are found inside the environment. Figure 6.6 shows the error results for all modules inside this simulation.

Here, it is possible to see that the fourth module contains the errors the other modules also posses. This is because the optimal solution for every module at the specified points is the same, meaning that the fourth module angles will be found in the other modules during a later stage as well. This principle is similar to the follow-the-leader approach, where the tip defines the path of the rest of the segments. Zooming in on the error result of module 4 in Figure 6.7, the phases can be clearly depicted. The differences between ending stage of module responses seems to correspond with 11 steps. Taking into account that every insertion step is 0.5 cm

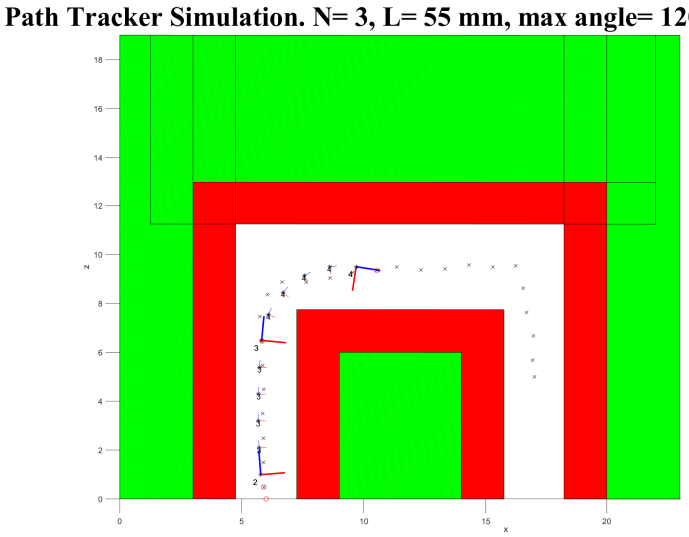

Figure 6.5: Illustration of the Endoscope Kinematic Planner at work in Scenario 1. The frames of the module tips are plotted as well, giving an indication of the orientation from the tip of the modules. Small frames in between are indicated in black, such that the resemblance of a bending module is more clear.

in size, this is equal to a length of 5.5 cm. This is one module length, which means that the behaviour is as expected.

Scenario 2

After the path has been created for Scenario 2, the endoscope was moved through the environment (Figure 6.8).

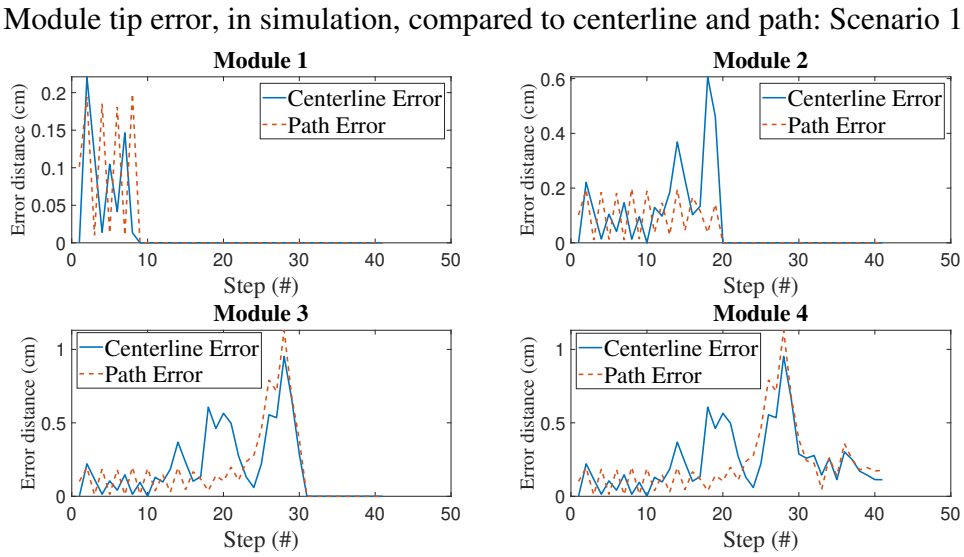

Figure 6.6: The errors found, during simulation of the endoscope inside the environment, with respect to the planned path and the centerline. This is performed for Scenario 1.

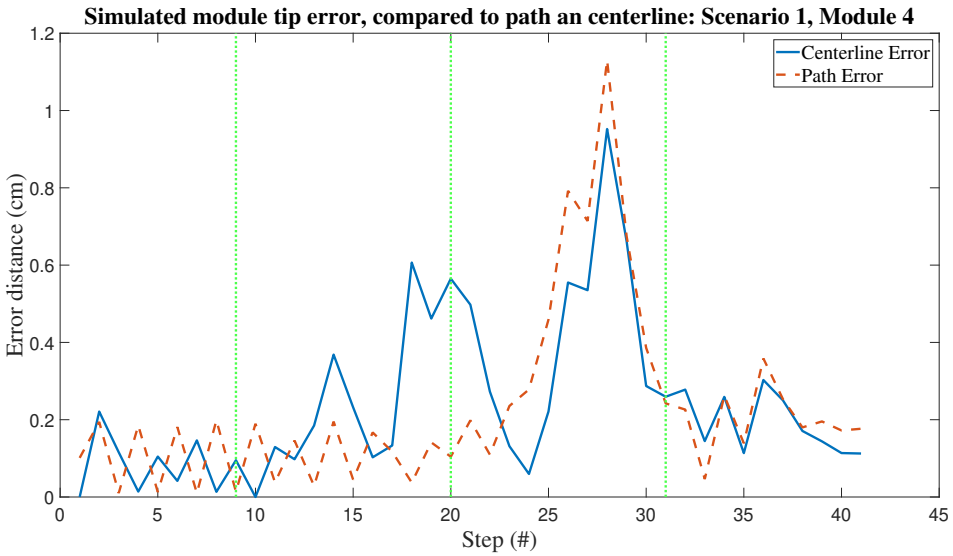

Figure 6.7: Simulated error of Module 4 inside Scenario 1. The green lines indicate the stages for which the other module behaviour stops.

The performance of the simulated endoscope throughout the path is again compared to the planned path and the centerline of the environment. Relatively small errors were found inside the simulation results. Figure 6.9 depicts the errors of the modules inside the environment.

6.2.3 Endoscope Simulated Response

The eventual goal is to define the pressures that have to be inserted into the physical endoscope to make it move through the specified environments. This is realized by combining the modelled behaviour of the algorithms with the actual response of the endoscope modules. To do so, the output of the simulation in terms of bending angles should be converted into eventual pressure steps. This Section describes the results of Step 6 in Figure 3.1.

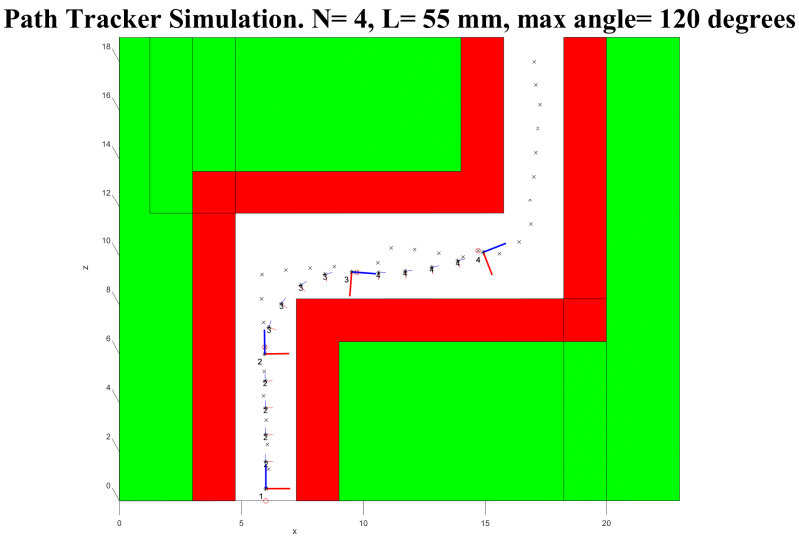

Figure 6.8: The Endoscope Kinematic Planner algorithm performing the endoscope simulation.

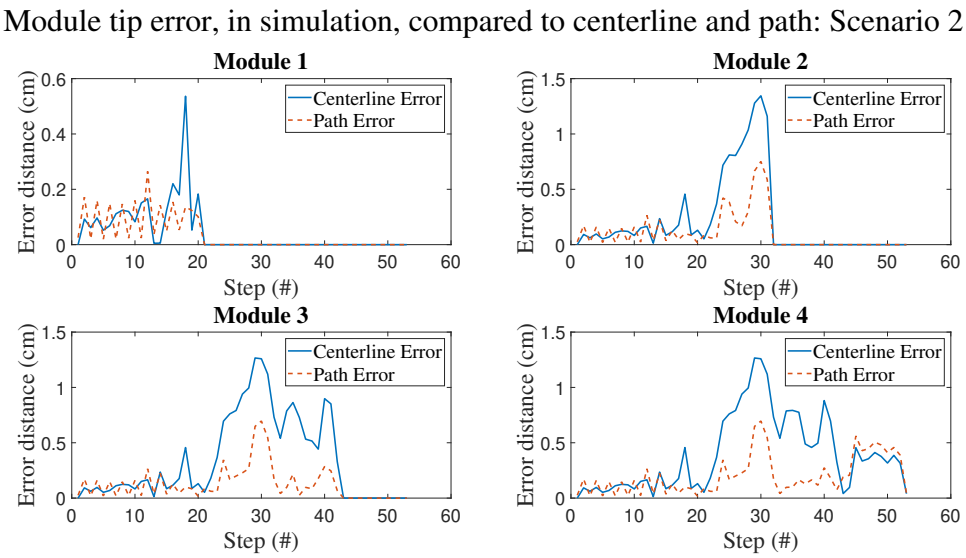

Figure 6.9: Errors with respect to the planned path, which was followed inside the Endoscope Kinematic Planner. More steps were required to complete this environment. The rest is later similar in behaviour, although the overall response seems to be more uniform.

After the Endoscope Kinematic Planner is complete, the angles used during the simulation are defined and stored for every separate module. The actual response from the simulation of Scenario 1 can be seen in Figure 6.10. As can be seen in the left image of the Figure, the response is not really smooth, resulting in a lot of switching between values during the actual response. A Savitzky-Golay filter is used to smooth out the angle response, making it more organic (MathWorks, -b). The result of this filtering can be seen in the right image of Figure 6.10. Figure 6.11 depicts the angles resulting from Scenario 2.

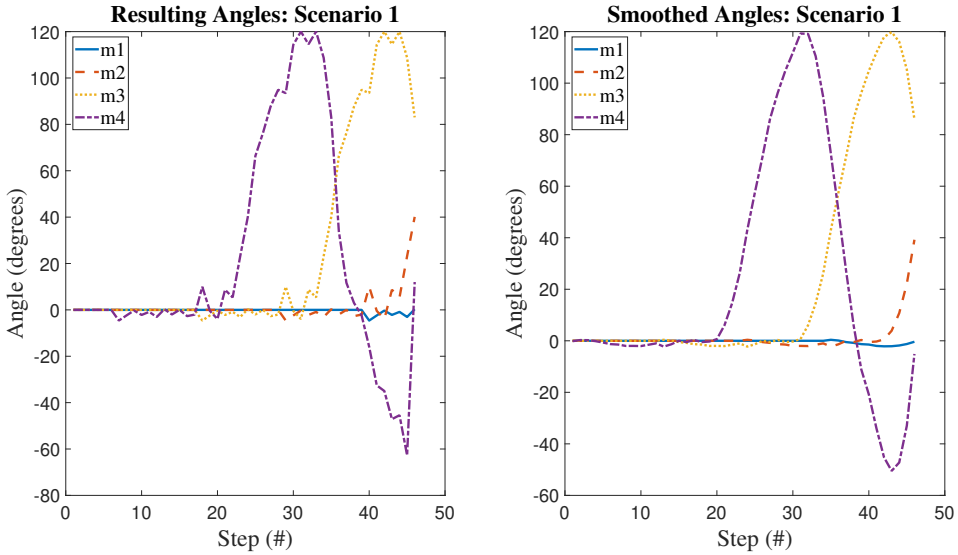

Figure 6.10: Resulting endoscope module angles for Scenario 1. The left image represents the raw resulting angles, whereas the right plot shows the smoothed version.

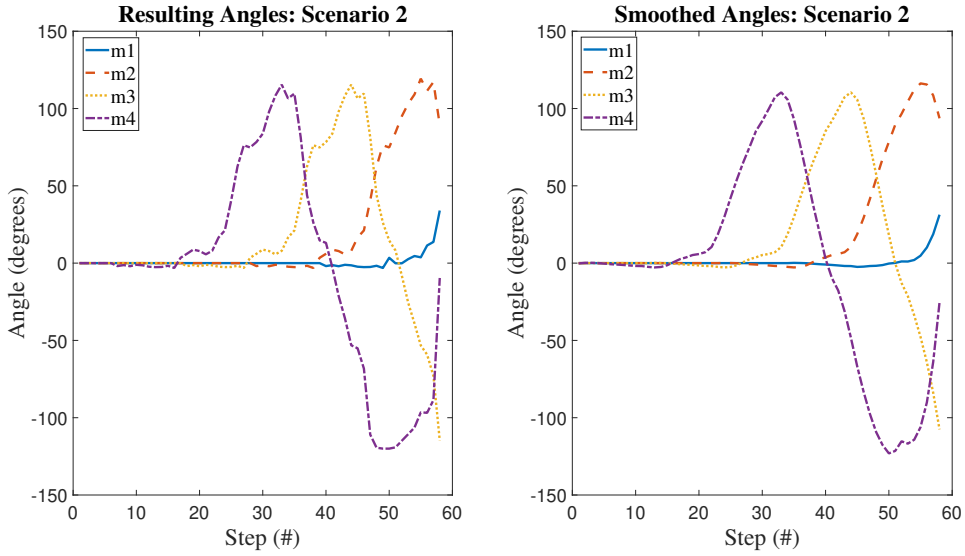

Figure 6.11: Representation of resulting angles within Scenario 2, depicting both the raw data on the left and the smoothed response on the right.

From the results of Figure 6.10 and Figure 6.11, it can also be seen that the pattern of the upper modules is being followed by the lower modules, being separated at the number of steps equal to the length of the module.

The angles from Scenario 2 are not very different from Scenario 1. The fact that it is going towards negative bending in Scenario 1 is due to the fact that, during simulation, the fourth module ends up straight and even has to compensate for excessive bending of the third module, which makes it have to bend towards the left. This is also partly due to the path that has been created, which sometimes makes a greater turn in the second corner compared to the centerline, which is why the top module sometimes have to bend up again.

6.2.4 Early Simulation Results - Design Impact

Throughout this study, several simulations were run to analyse the performance of the endoscope throughout the environment. One of the early results based on Scenario 1 pointed out that an maximum bending angle of 40 degrees was not enough to move through the selected environment. Furthermore, the number of modules inside the environment based on early work was found to be four. These two points have been considered as design criteria in the physical development of the endoscope. After development of Scenario 2, it was found that five endoscope modules were needed for that specific environment.

6.2.5 Application of Modified Model in Simulation

These modifications to the model, which are found in Section 5.2, have been integrated into the Endoscope Kinematic Planner as well. Based on Equation 5.6, the Modified Model is integrated into the homogeneous matrices of the endoscopic modules. Furthermore, the modification had to be taken into account in the initial guess of the optimal curvature κ, as well as in the plotted representation, the angle limitation and the realized curvature. The angle limit still depends on the bending of the whole module, which is converted to the curvature section to enable comparison. This also occurs for the initial curvature determination, as the angle between target point and module base has been defined for the whole module. The change has also been implemented in the adjustment for the cost function that determines the optimal angle.

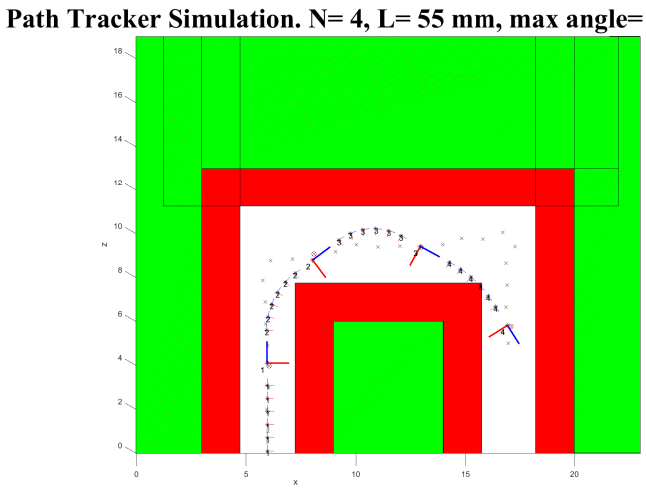

Figure 6.12: Endoscope with Modified Model performing the pre-defined path through Scenario 1.

Based on the final hysteresis curves and the corresponding angles that could be reached for x-axis rotation, a requirement could be set for the Endoscope Kinematic Planner to follow. This limit was put on 80 degrees maximum bending for Scenario 1 and since this complicated Scenario 2, a maximum angle of 100 degrees was used there.

The resulting behaviour can be viewed in Figure 6.12, in which the endoscope module bending is limited to 80 degrees bending. In Figure 6.13 the resulting path for the fourth module is displayed. The result of the Modified Model (right) is compared to the Constant Curvature model (left). Furthermore, the performance of a variant in which the bending is limited to 120 degrees has been plotted as well, to show the effect of increased bending.

In Figures 6.14, the results of the Endoscope Kinematic Planner can be seen for the Modified Model in Scenario 1, in terms of error with respect to the planned path and the centerline.

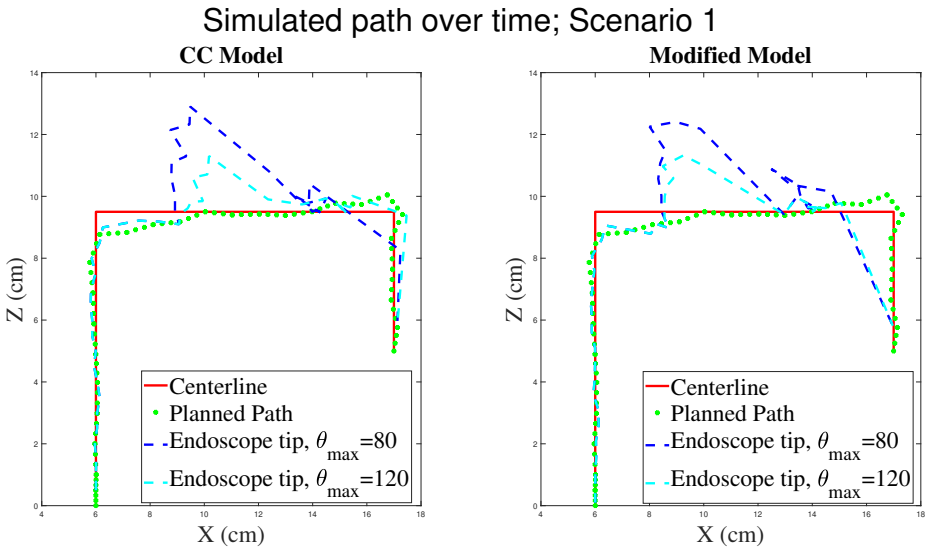

Figure 6.13: Errors regarding the distance between the modules of the endoscope and the planned path, as well as compared to the centerline. On the left, the performance of the Constant Curvature Model can be seen, whereas the right indicates the behaviour of the Modified Model. Both are executed with the same scenario and path, Scenario 1.

Figure 6.14 shows the error with respect to the planned path and centerline, regarding the simulation of the Modified Model endoscope.

The resulting angles for Scenario 1 and Scenario 2 are depicted in Figure 6.15 and Figure 6.16, respectively. The results show similarities with respect to the previously found angles, especially when regarding Scenario 2. In Scenario 1, it shows that the bending angle of the modules in a later stage have less tendency to bend back, which is more in accordance with the expected behaviour for the bending throughout the Scenario, as it was not expected the reach bending towards the opposite direction.

Due to the nature of defining local optima, the bending performance for each module following each other is still repeatable. In the Figures, the limitation of the possible bending angle can be seen clearly. However, due to smoothing the responses, the values sometimes tend to reach higher than the set limit.

After the responses of the endoscope simulation throughout the environments for Scenario 1 and Scenario 2, the resulting angle profiles could be transformed into required pressure profiles, based on the previously described characterization.

6.2.6 Duration Endoscope Kinematic Planner

Using the same laptop as with the Path Planner, the resulting average simulation duration has been found to be 128.9 ± 4.8 seconds (N=5), whereas for Scenario the average duration is 240.2 ± 18.6 seconds (N=5).

6.3 Path Planned Endoscopic Pressures

After simulations for both scenarios, when implementing the Modified Model, the resulting angles from simulation can be transferred into pressure profiles using the previously addressed characterization fit (see Chapter 4). The middle line fit is used, in which the middle fit is neglected due to complications. The pressure is limited to 0.4 bar maximum, whereas very small values are put to 0 bar.

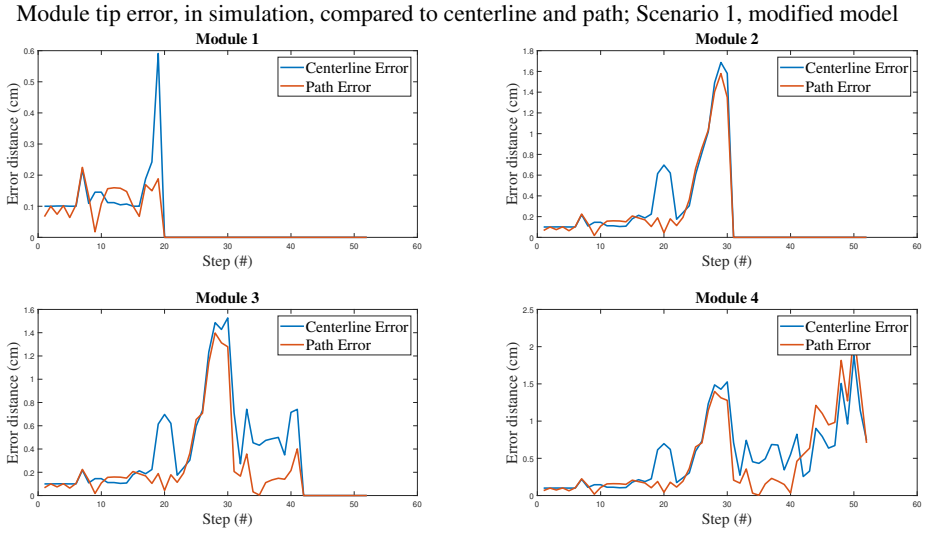

Figure 6.14: Errors regarding the distance between the modules of the endoscope and the planned path, as well as compared to the centerline. The simulation is performed using the Modified Model in Scenario 1.

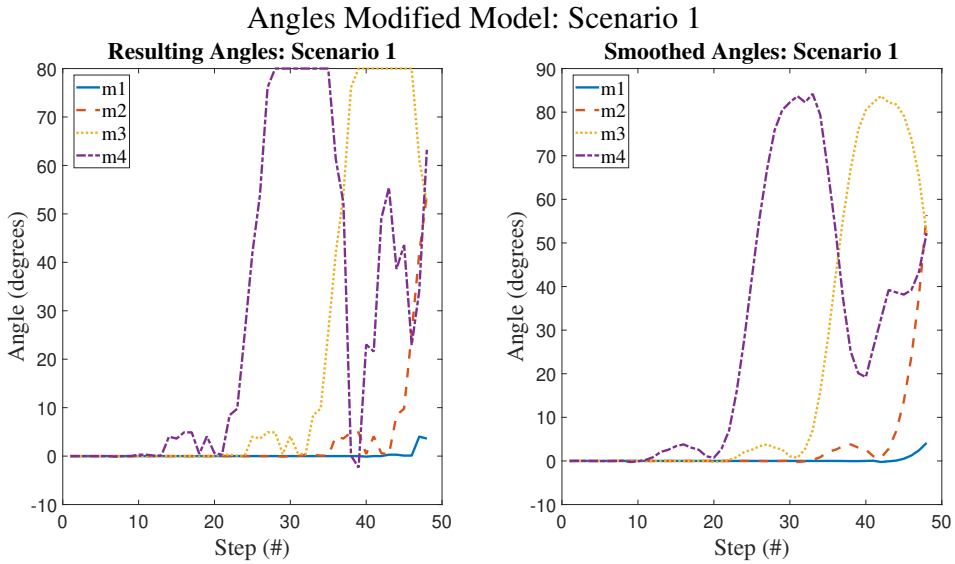

Figure 6.15: Resulting filtered and unfiltered angles from the Endoscope Kinematic Planner simulation, regarding Scenario 1 using the Modified Model.

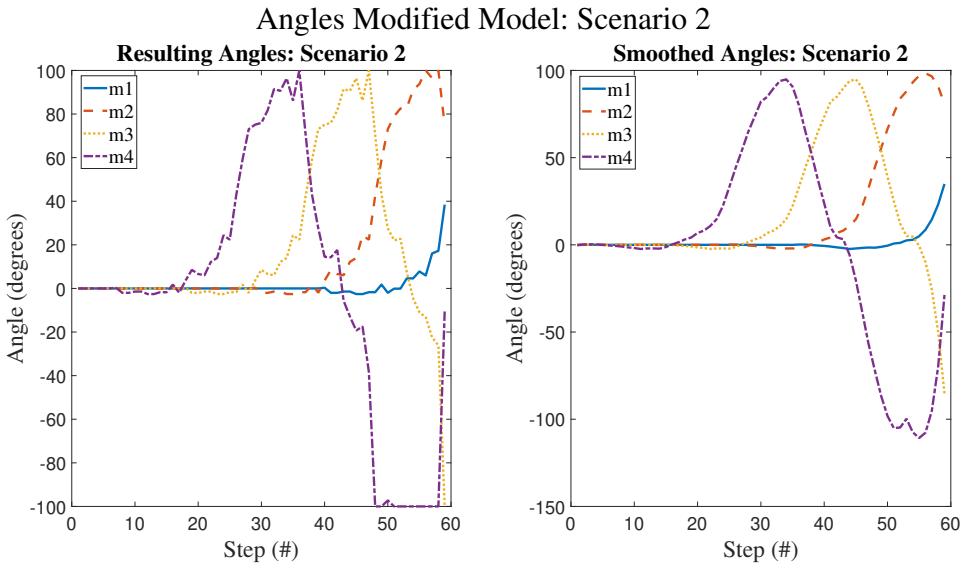

Figure 6.16: Resulting filtered and unfiltered angles from the Endoscope Kinematic Planner simulation, regarding Scenario 2 using the Modified Model.

The resulting pressure profiles for Scenario 1 and Scenario 2 are represented in Figure 6.17 and Figure 6.18, respectively.

6.4 Comparison Weighted Centerline Error

To be able to compare the results of the simulation with respect to physical data obtained using image processing upon camera footage, the data from simulation has been processed in similar fashion. Every intermediate point represented in the simulation of the Endoscope Kinematic Planner has been stored, such that not only the position of the tip is known, but also the aspects of the rest of the endoscope. Here the Modified Model is taken into account, as well as the limitations of the previously stated bending per scenario. Per step, the coordinates present in

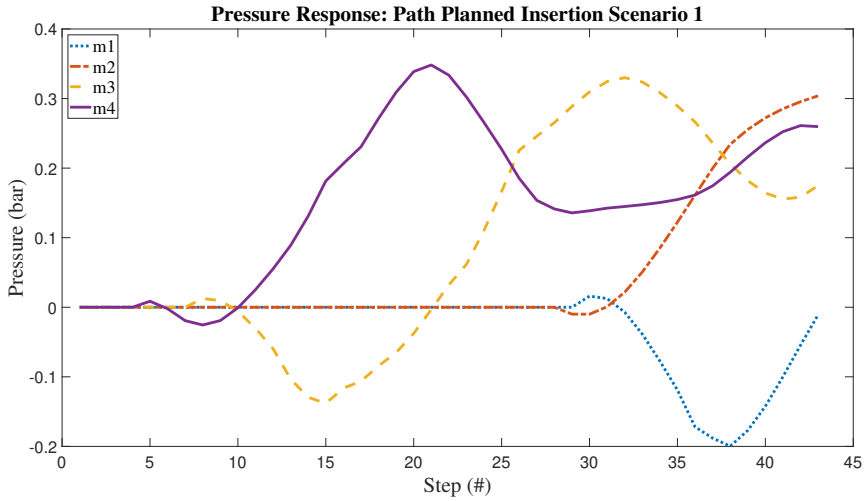

Figure 6.17: Resulting pressure profiles regarding Scenario 1, when transforming the resulting angles from the Endoscope Kinematic Planner, using the Modified Model.

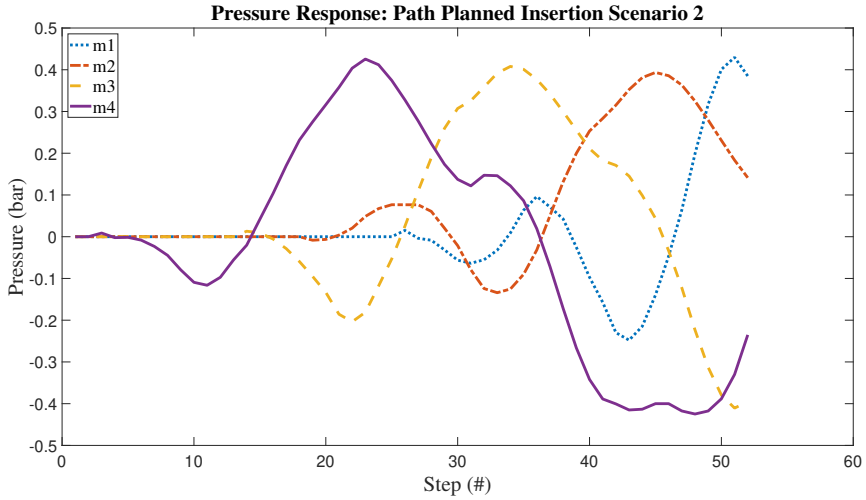

Figure 6.18: Resulting pressure profiles regarding Scenario 2, when transforming the resulting angles from the Endoscope Kinematic Planner, using the Modified Model.

the environment at that moment are compared with the defined coordinates of the centerline, to get the total distance for the endoscope with respect to the centerline. This is divided by the total number of data points of the endoscope inside the environment to get the weighted error. This is done per step, combining data of all the modules.

6.4.1 Results Weighted Error

The results of this computation are visible in Figure 6.19, in which both Scenario 1 and Scenario 2 are depicted, as well as describing both the Constant Curvature Model and the Modified Model. The total weighted error is computed per simulation step.

As can be seen from the figure, several peaks appear throughout the simulation. These can be mainly related to the difficulties passing the first corner in Scenario 1. Here, the first peak is from the last step before the third module actually bends the tip module back towards the center. The same occurs for the second module, causing the other peak. Regarding to Scenario

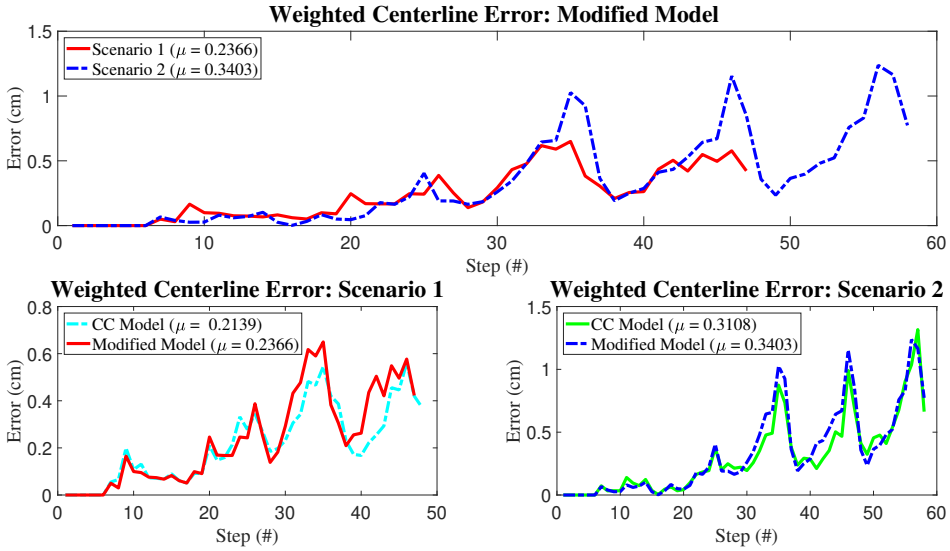

Figure 6.19: Representation of resulting weighted errors with respect to the centerline. Upper image describes error of the Modified Model for both Scenario 1 and Scenario 2. The lower graphs compare the results between the Constant Curvature Model (CC Model) and the Modified Model.

2, similar peaks occur at similar moments in time. Both the first and second peak originate mostly from the error due to going through the first corner. The endoscope takes a very wide turn through the second corner, together with a wide turn through the first, which result in the last error peak.

From the results of the Modified Model compared to the Constant Curvature Model, it can be deduced that the Modified Model has a bigger error with respect to the centerline. Furthermore, as has been detected earlier, less steps are necessary for Scenario 1 compared to Scenario 2.

6.5 Discussion

In general, the used environment throughout simulations was rather abstract. Therefore, proper comparison with the human body is currently difficult. More organic and dynamic environments should be accounted for. Furthermore, basic environment limited the full potential of the RRT-algorithm. More complex scenarios with multiple branching options would be more ideal to show the full potential of the searching algorithm, as now the finding of the path is quite straightforward. A future redefinition of the plotting environment is recommended.

6.5.1 Path Planner

Although a limitation of the tree angles was attempted, it did not always seem to succeed. More attention has to be paid to the angle constraint algorithm. Furthermore, the curvature of the modules could be implemented as tree splines, instead of straight lines. As of now, the RRT algorithm is used in a rather basic way, whereas it could implement more of the endoscope kinematics potentially.

6.5.2 Endoscope Kinematic Planner

The inaccuracies in the model also translated into discrepancies in the simulated behaviour. Due to the fact that the model did not take into account the lengthening phenomenon that occurred in the physical behaviour, it took the algorithm also more steps to complete both scenarios. This made it more difficult to implement the results in the physical scenario.

Another factor that could have been improved regarding the algorithm is the way it treats bending optimization. At the moment, the algorithm determines the optimal angle for the respective module, by means of minimizing a cost function for each module. This process is starting from the bottom module and going up to the tip module. A negative effect of this approach is that the next modules have to deal with the starting point that has been given by the best bending action of the previous module, which might not always be optimal. It would be far more desirable to optimize the position and orientation of all modules simultaneously per step, such that the most optimal position is developed. This might result in improved overall performance.

Due to the local optimization it could be noted from the resulting angles that the behaviour of the tip is followed by the other modules over time.

This behaviour can also be found in the follow-the-leader principle, where movement of the tip section determines the bending behaviour of the rest Chen et al. (2014). However, in terms of efficiency, the currently used approach is less efficient than that, as it constantly re-calculates the optimal solution, whereas the alternative algorithm stores the motion profile to distribute it to the lower modules in a later stage. Therefore, when it is desired to approach this algorithm, this would be suggested as a first step.

The smoothing of the resulting angles might affect the angle magnitude and thus the computed pressures.

6.5.3 Comparison Weighted Centerline Error

Several aspects should be pointed out regarding the process of creating a weighted centerline error that could serve as a comparison for the upcoming experimental results.

First of all, the amount of endoscope points used for the computation of the error with respect to the centerline is rather limited. Only five points per module are considered, which results in a rather coarse approximation of the distance error.

Next to that, it should be considered that the development of the simulation results is expressed in cycle steps, whereas the development of experimental results will rely upon duration expressed in time. This increases the difficulty in terms of comparison.

Furthermore, the weighted centerline error has only been computed for one simulation round thus far. Therefore, the representation of these errors might not provide a strong foundation for comparison. Multiple simulation rounds for path creation are necessary to improve the reliability.

Furthermore, the endoscope simulation starts computing before the endoscope is entering the environment. This situation might differ with respect to the physical experiments, so this should be accounted for in the eventual comparison.

6.6 Conclusion

The RRT* algorithm successfully creates paths inside both Scenario 1 and Scenario 2, after which the Endoscope Kinematic Planner simulates the endoscope following the path.

Furthermore, the bending angle- and error results both indicate repetitive behaviour for the bending of the separate modules, where lower modules follow the pressure profile of the tip module. This is due to local optimization for every module bending angle.

The average weighted error found for Scenario 1 is about 0.24 cm, whereas the average error found for Scenario 2 is 0.34 cm. As can be seen, Scenario 1 contains a lower (average) error with respect to Scenario 2. Furthermore, Scenario 1 contains less steps, which was also found in previous simulations. Next to that, the Constant Curvature Model contains less error with respect to the centerline compared to the Modified Model.

The found angles for the simulated endoscope response, taking into account the Modified Model, are converted into pressures using the relations found in Chapter 4. Due to differences in module bending capacity, the conversion into pressure profiles also affects symmetry of the response.

7 Evaluation of Path Planner Performance

This chapter addresses theo procedures that are connected to the experimental verification of the endoscope behaviour based on the path planner performance, which is Stage E in Figure 3.1 of Chapter 3. This chapter deals with the search for the solution of research sub-question 6. To investigate the potential of using path planning to control the soft robotic endoscope, the manual endoscope steering performance of several participants is compared to the performance of the autonomous path planned soft robotic endoscope, for both the scenarios described earlier. Both experiments are described below.

7.1 Manual Insertion Experiment

To verify the use of the path planning algorithm for determining a better path with respect to the manual insertion method, a comparison has to be made based on several criteria. As the main focus point is to improve the safety of the performance, there a the key metrics to be tested. The aspect of safety can be approached using several metrics; limitation on the amount of force exerted on the environment, maximum distance from the obstacles and a minimum number of collisions with the environment. Due to time constraints and lack of resources at hand, the main focus will be on the determination of the latter two metrics. The maximum distance with respect to the environment walls will be computed by means of determining the distance of the endoscope skeleton with respect to the centerline of the environment. The centerline basically is the line furthest away from all the obstacles, simulating the best possible interaction-free scenario. The centerline is often computed in virtual endoscopy to simulate the potential path the surgeon has to take (Wan et al., 2002)(Wang et al., 2011).

Another aspect that will be considered is the amount of air pressure used to control the endoscope, as less pressure would imply safer conditions. Furthermore, the times required to complete the procedure are tracked, as this duration has an effect upon safety and operation cost. Ideas for future work regarding interaction force are presented in the Chapter 10.

7.1.1 Experimental Setup

In combination with the characterization setup described in Section 4.3, this subsection describes the answer to research sub-question 5. An experiment is defined, in which operators have to control the endoscope through a defined static environment, with as objective to reach the target while trying to avoid collisions with the wall as much as possible. In total, two environments are defined which contain different bending corners, such that the performance in different situations can be tested. The two scenarios are depicted in Figure 6.4 and Figure 6.2, in Section 6.1.2. Using a graphical representation of the environment, a transparent platform on which the endoscope is moved and a camera, the positions of the endoscopic modules are tracked and potential interactions with the environment are noted. This approach has been inspired by the work in the article of Chen et al. (Chen et al., 2014). Due to time constraints and long experiment duration, the number of different scenarios is limited to two. After the two scenarios were completed, a short questionnaire followed, containing questions regarding the experience of controlling the endoscope. To enable insertion of the endoscope inside the environment, a pneumatic stepper motor is attached. This is elaborated upon in a section below. The endoscope insertion is guided by means of a rails. By using the same endoscope for both scenarios, the influence of endoscope-specific characteristics upon the performance is limited. In Figure 7.1, a participant performing the experiment can be seen.

Figure 7.1: The experimental setup together with one of the participants, who is currently performing the experiment. On the right the screen is placed, from which the participant can see the position inside the environment.

7.1.2 Subject Group

A group of 15 participants was assembled to perform the experiments, of which three had medical training background with operational use of flexible endoscopes. The group consists of four females and eleven males, ranging from the age of 19 up to 29 years old. A more detailed description is given in Table 7.1.

7.1.3 Pre-Experimental Procedure

Before the experiment commenced, there were several steps taken during the process. These will be explained below. An information letter was provided, containing a description of the project, the current experiment, potential risks and the notion of data use from this experiment. Furthermore, a consent form had to be signed. All participants gave their consent and were aware of their options and risks. After the experiment was introduced, the participants were allowed to practice with the tip module inside the environment, to get a feeling for the bending behaviour and response. The application was used to control the tip module towards both sides and for various amounts of pressure. The training time ended when participants felt ready to perform the experiment. Before the actual start, all systems were reset to avoid unusable data. For every new participant, the order of the two environments was swapped, such that the effect of learning is spread over both environments.

Table 7.1: Subject Group Specifications

	Untrained	**Trained**
Amount (#)	12	3
Age Range (years)	19-27	26-29
Average age (years)	23.8 ± 2.4	27.7 ± 1.5
Male/Female (%)	(75%)/(25%)	(66.7%)/(33.3%)
Number of Operations (#)		
- Rigid Endoscopes	0	0
- Flexible Endoscopes	0	<20 (100%)

7.1.4 Insertion

The insertion was done by the researcher, using a pneumatic actuator that was designed by Vincent Groenhuis (Groenhuis and Stramigioli, 2018). Using push buttons that are connected to the Arduino, the actuator was designed to make steps of 0.5 cm for each time the button was pressed. This is to be consistent with the steps taken in simulation. Each time the participant completes its desired orientation of the endoscope, the researcher would insert the endoscope one step further in the environment. To make room for the connection with the pneumatic actuator with the endoscope base, the starting point is shifted 9 steps. The effect of this is assumed to be small, as during the initial steps correction by means of pressure is often not needed.

7.1.5 Interface

The MATLAB application interface can be seen in Figure 7.2. It combines information regarding input pressure with possibilities to alter the pressure. An image is presented in the app to clarify the connection between the pressure insertion fields and which modules they will actuate, as well as which pressure corresponds to which direction (positive is right bending, negative is left bending). The button 'Insertion Step Completed' has to be used when the researcher is done with the insertion step of the endoscope inside the environment. Pressing the button will start a timer, which will be stopped when the button 'Lock Pressures' is being pressed. This button has to be pressed when the operator is satisfied with the current orientation of the endoscope. Upon pressing this button, the pressure values also will be stored. In this way, the time taken to find the correct pressure values for the desired orientation is being documented, as well as the final pressures. After this button is being pressed, the researcher starts inserting again.

7.1.6 Data Collection

As has been mentioned above, the MATLAB application facilitates the storage of duration, inserted pressure, and realized pressure for every step. Furthermore, a camera is placed above the environment, to be able to capture the movement of the endoscope throughout the experiment. With the footage of the camera and the implementation of image processing techniques, the distance of the endoscope with respect to the centerline can be defined. By means of an image processing algorithm, the endoscope was tracked and the points of the endoscope skeleton were compared to the derived centerline coordinates of the environment. The skeleton of the endoscope found in one of the video frames is depicted in Figure 7.3. A more detailed elaboration can be found in Chapter I in the Appendix. To evaluate performance, distances of all points of the endoscope were normalized per frame, which was averaged to get to a score metric. This is termed the average weighted error, or $E_{\mathrm{w,av}}$.

The number of collisions during the experiment were monitored manually. The camera view is also displayed on a screen in front of the operator, such that the operator has the possibility to view the state of the endoscope inside the environment. It has been mentioned to the participant that both looking at the screen and viewing the actual environment is considered to be fine. Furthermore, a questionnaire is used to define more specific experiences of the participant during experimentation.

7.2 Path Planned experiment

To compare the performance of the path planned trajectory with the manual insertion experiment, the resulting pressures from the path planner had to be used to redo the experiment for both scenarios. To facilitate this, an Arduino script has been written that incorporates to control of the pneumatic actuator as well as the pressure regulators and solenoid valves. Using one Arduino board with the attached shield, the bending and insertion mechanisms could be

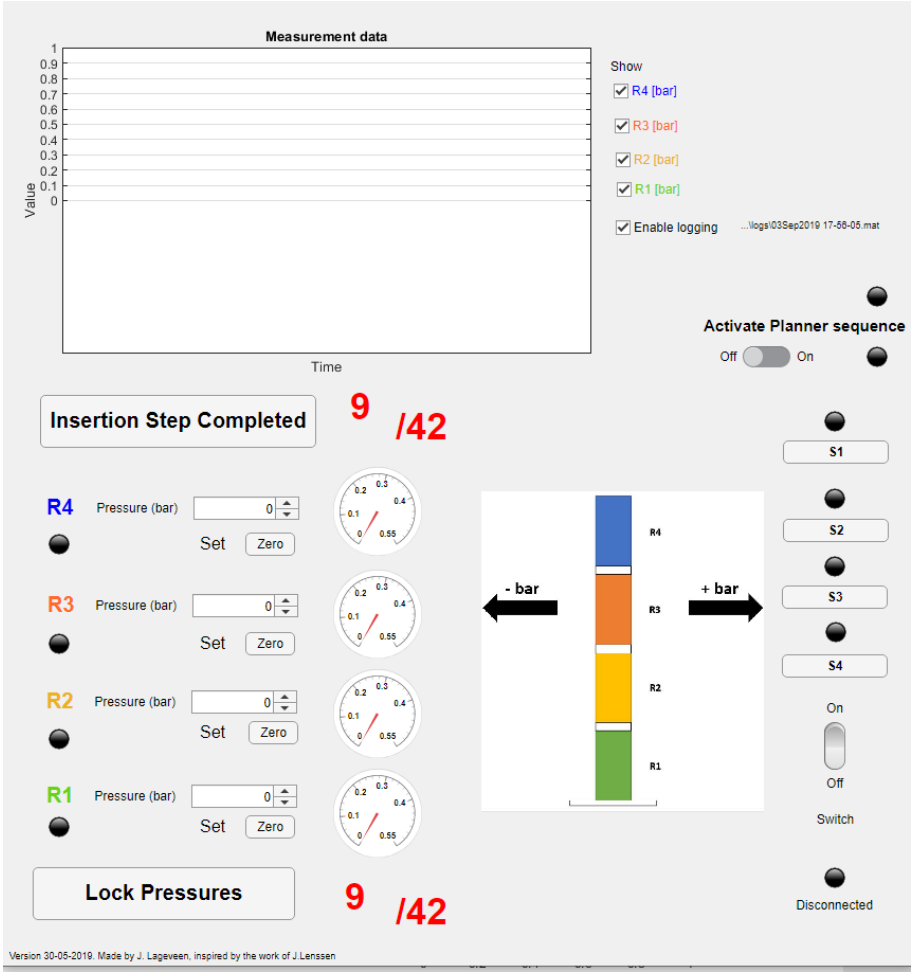

Figure 7.2: The interface which the participants had to use to control the endoscope with. Pressures could be inserted on the left.

combined. A pressure button was added to enable the start of the sequence. The planned path was performed autonomously, without using any kind of feedback.

7.2.1 Data Collection

As has been done with the manual performance, the times, pressures and video material of the performance are stored. Similar approaches have been utilized for the path planned endoscope compared to the manual insertion experiment, although no use has been made of the MATLAB application described before. Duration of pressure insertions have been monitored using a timer inside the Arduino code. The pressure profiles are known beforehand, as they serve as a basis on which the Arduino executes the pressures. Motion is captured using the same camera and using the same approaches as before. Manual collision detection is performed as well.

7.3 Results Evaluation of Path Planner Performance

7.3.1 Manual Experiment

The results of the manual insertion experiments can be categorized into several sub-sections; the time spent, amount of pressure used, amount of collisions detected and the overall positioning of the endoscope with respect to the centerline. Furthermore, the results of the questionnaire give some useful insights in the experience of the participants. The following section will deal with each of these categories.

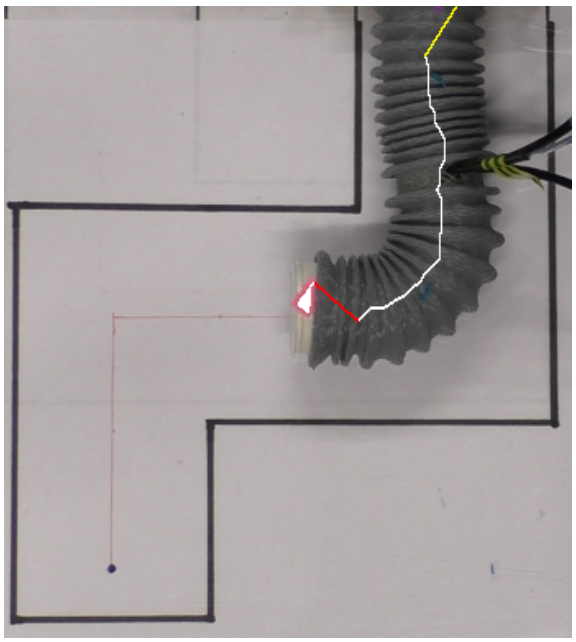

Figure 7.3: A display of one frame during image processing. The white line depicts the endoscope skeleton, the red line connects the tip with the skeleton, and the yellow line defines the part between base and skeleton. Due to complications, the yellow line is excluded from the total distance cost.

Exerted Pressures

The average response of the participants when moving through Scenario 1 can be found in Figure 7.4.

The initial part of the experiment contains a low amount of pressure in total, as not a lot of bending occurred in the first section. After about ten steps, the participants tend to start bending the tip module, Module 4. This is soon followed by the bending of the third module, as well as the second module a bit later. The dotted line indicates the limit to which all participants

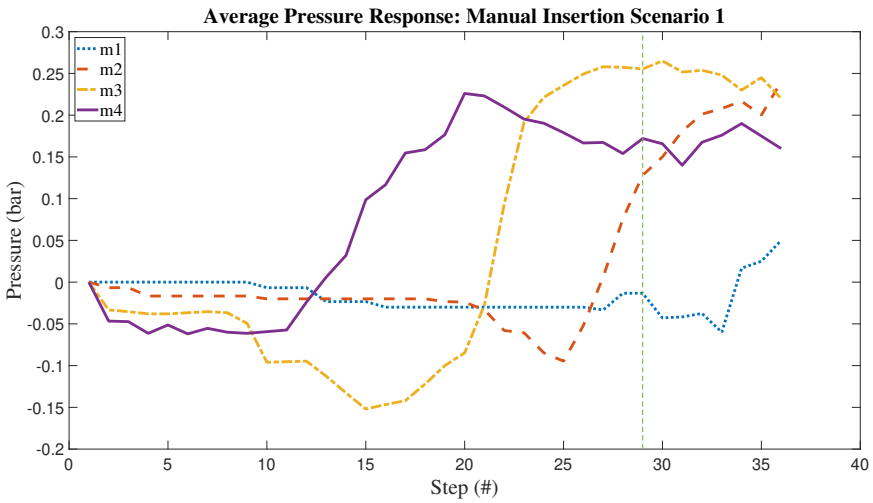

Figure 7.4: Averaged pressure response of the participants during the manual insertion, per cycle step. The vertical dotted line is used to indicate the limit in size of the number of steps, since not all participants had the same number of steps to complete the scenario.

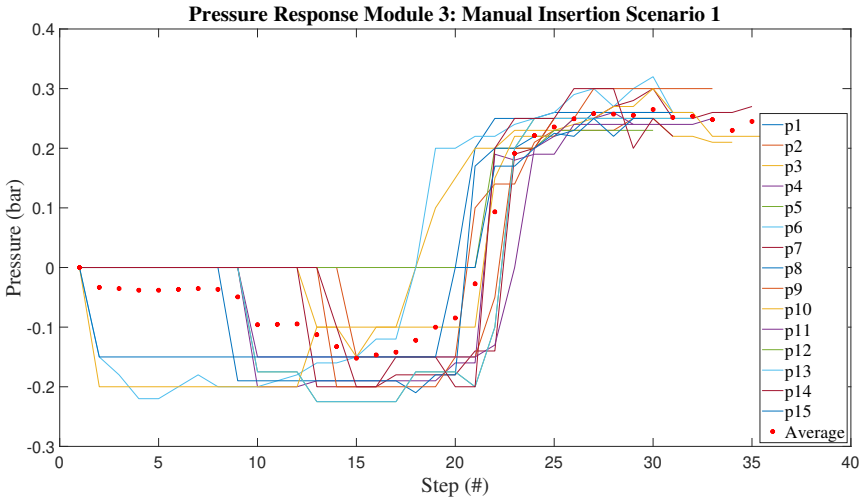

Figure 7.5: Pressure response of Module 3, during manual control throughout Scenario 1. The average of the lines is represented with a dotted line.

have the same number of steps performed. This is since there is a difference in the number of steps taken to complete the environment.

In Figure 7.5, the pressure response for Module 3 of all participants has been given. This representation indicates that the chosen pressures for Module 3 have been rather similar throughout the environment, which can be found in the behaviour of controlling the other modules as well.

Figure 7.6 shows the average pressure response of the participants inside Scenario 2. Here it can be seen that the response of all modules except the tip module are rather similar to the response found in Scenario 1, as can be seen in Figure 7.4. This is in accordance with the consistency of the environment, as it is similar except for the second corner. The fourth module in Scenario 2 is switched from bending to the right towards bending to the left. A similar dotted line is used in this graph, indicating a difference in number of steps until completion.

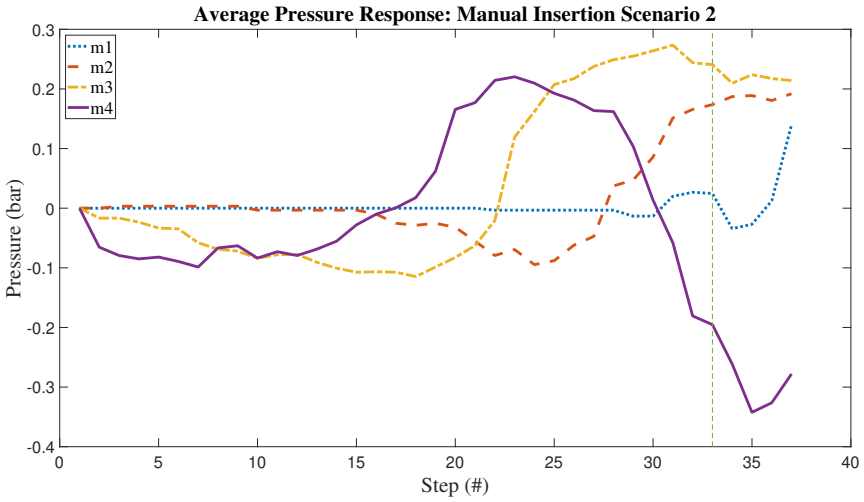

Figure 7.6: Average pressure response of the particpants during manual insertion of the endoscope in Scenario 2. The green vertical dotted line indicates the step for which the first participant has finished the insertion.

Furthermore, the average endoscope pressure per step has been determined for every participant, as well as for the path planned pressure profiles from Figure 6.17 and Figure 6.18. The average endoscope pressure per step of the manual insertion experiment was found to be 0.34 ± 0.12 bar for Scenario 1 and 0.36 ± 0.08 bar for Scenario 2. The path planned endoscope used an average endoscope pressure per step of 0.37 bar for Scenario 1 and 0.53 bar for Scenario 2.

Time

Next to storing the amount of pressure used during performance of the experiments, the amount of time per cycle has also been saved, excluding the time necessary to execute the insertion step.

The total completion time excluding insertion steps has been depicted in Table 7.2, together with the total completion time information of the path planned scenario.

Results Questionnaire

The results of the questionnaire can be found in Chapter J in the Appendix. Throughout the experiment, the general opinion expressed by the participants was that the control of the endoscope throughout the scenarios was rather difficult and they had to focus a lot to get the endoscope to stay away from the boundaries. The majority of the participants with medical training in flexible endoscopes stated that the control was rather not intuitive, it was hard to control the four modules to get to the desired configuration and that they did not really feel confident to control the endoscope.

Number of Obstacle Collisions

See Table 7.3 for the collision data that was obtained from the experiments (first three columns). The number of unique collisions have been noted. This implies that, after a collision, the endoscope should first be free of collision or hit another boundary, before another collision is indicated.

Centerline Deviation

To see how safe participants could guide the endoscope through the environment, the distance with respect to the centerline (which is the safest path) is determined. Based on the results obtained by using image processing for the data from the video footage, a metric of performance could be defined per participant. The weighted average error (average error per frame determined, after which the average is taken over all frames) is determined for both scenarios. The result can be seen in Table 7.3, in the two later columns.

7.3.2 Path Planned Experiment

In Table 7.4, the average weighted error of the path planner performance is depicted. The number of different collisions during operation is also indicated. It has to be taken into account that the number of different collisions might be low, but the continuation of the collisions was found to be rather long. This is due to the fact that the control is open loop, in which the endoscope does not have any means to correct itself. In Scenario 1, the path planned endoscope reaches the target, whereas in Scenario 2 it only came very close.

Table 7.2: Total Experiment Completion Time Characteristics

Experiment	**mean (s)**	**std (s)**	**max (s)**	**min (s)**
Manual: Scenario 1	646	376	1756	378
Path Planner: Scenario 1	53.3	0.1	53.4	53.1
Manual: Scenario 2	1252	563	2405	652
Path Planner: Scenario 2	67.5	0.003	67.5	67.5

Table 7.3: Collisions and Centerline Error during Experiment

Participant	**Collision # Scenario 1**	**Collisions # Scenario 2**	**Average weighted error; Scenario 1**	**Average weighted error; Scenario 2**
1	4	9	0.83	1.04
2	0	9	1.5	0.96
3	5	3	1.32	0.56
4	8	14	1.40	1.94
5	11	16	1.49	0.87
6	1	6	0.75	0.68
7	7	8	1.01	0.65
8	1	11	0.76	0.71
9	9	22	2.29	1.89
10	3	7	0.81	0.89
11	3	19	1.15	1.06
12	*	11	*	2.03
13	6	19	1.13	0.69
14	8	17	0.64	0.90
15	5	15	0.89	1.46
Average	**5.1**	**12.4**	**1.12**	**1.09**

*Data regarding participant 12 is partly missing, therefore left out

Two rounds are mentioned in Table 7.4. Round 1 corresponds to the automated endoscope performance using the resulting values from the path planner. The path planned trajectory includes more pressure steps compared to what has been realized in manual performance, and is also larger than the possible available steps the pneumatic stepper can provide. Round 1, therefore, is limited to the number of steps that could be realized before the limit has been reached. Round 2 is a variation of Round 1, as the pressures used in Round 1 have been interpolated to fit the limit of the pneumatic stepper motor. The number of steps to complete for Scenario 1 is set to 33, whereas Scenario 2 is set to 35 steps. Round 2 performed worse compared to round 1 in terms of resemblance; it seemed to be a cut off version of Round 1.

In Figure 7.7, the weighted average of the path planned endoscope is depicted, considering Round 1. As can be seen, a high error was found in the end stage of the endoscope performance, before eventually reaching the finish. The error peak corresponds to the orientation depicted in the same Figure. The lower plot corresponds to the performance of one of the participants in Scenario 1.

Table 7.4: Centerline Error Data: Path Planned Endoscope

Round	$E_{\mathbf{w,av}}$ **Scenario 1 (cm)**	$E_{\mathbf{w,av}}$ **Scenario 2 (cm)**	**Collisions Scenario 1 (#)**	**Collisions Scenario 2 (#)**
1	1.53	1.72	4	5
2	1.25	0.94	3	5

7.4 Discussion

7.4.1 Manual Insertion Experiment

During the execution of the manual insertion experiment, several aspects were noted to either be of influence on the eventual result or to be deviating from the desired experimental condi-

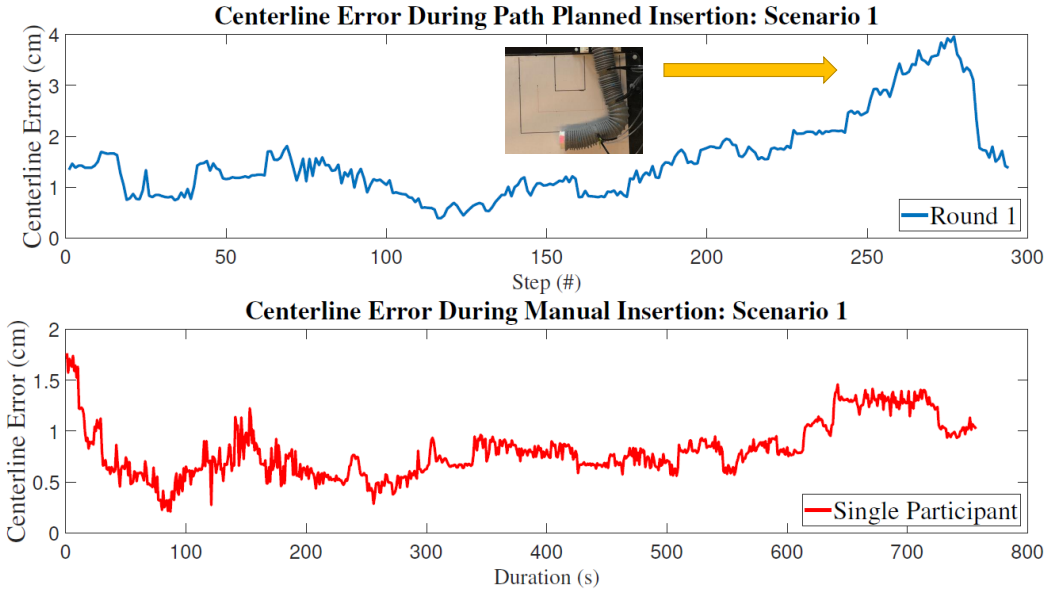

Figure 7.7: Display of the weighted error per time step, considering the endoscope skeleton with respect to the centerline of the environment.

tions. These points are mainly found while executing the experiment and due to the feedback received during performance of the participants.

One of the points that was addressed during the experiment was the influence of the interface upon the eventual experience while controlling the soft robotic endoscope. As can be seen from Figure 7.2, the participant could either control the modules by using arrow steps of 0.05 bar or by manually inserting values. This approach was chosen such that the participant could make bigger steps to speed up the process, as well as smaller steps to get more accurate movements. However, this might not have been as intuitive as, for example, pressing a button to go a step more left or more right. As this approach would be rather basic, the effect of understanding such an interface would have less impact upon the eventual outcome. Furthermore, the difference in approach might cause bigger differences in duration and performance error between different participants. Next to that, it would be a more realistic scenario when the operator had to choose the desired bending angle instead of trying to find the corresponding pressure. However, as mentioned before, the inaccuracies in modelling the pressure-bending relation would then also be included.

The interface of the application contained buttons that had to be pressed during operation, which was sometimes forgotten. This meant that there are some artefacts in the recorded times. Later on, indexes were added to the interface to ensure clear indication of pressing a button or not. In future work, it is recommended to make use of a sequence that disables continuation of the experiment until the buttons are pressed.

Another aspect that could be pointed out is the potential effect of the camera view upon the performance of the participants. Since the camera was placed upside down due to lack of space, the participants had more difficulty with orienting.
Furthermore, the vision throughout the experiment differs from the actual scenario, in which an endoscopic camera is used. The effect of this is yet unknown, but it is hypothesized that using an endoscopic camera view would worsen the performance of manual insertion compared to the current study. In general, it is recommended to consider the implementation of

vision within the soft robotic endoscope itself and how this affects MRI compatibility, module stiffness and control performance.

It was attempted during the experimental procedure to reduce the friction of the endoscope with the bottom plate, by means of using mould release spray, which tends to have a lubricating effect. The effects of the implementation are rather unknown, but it is expected that this effect is rather small. It is recommended for future work to consider reducing the friction and hysteresis, since it makes it very complicated for the participants to execute the experiment, as the expected movement often will vary with the actual response. One idea that was thought of but eventually not realized is the idea of having a platform filled with holes, through which air would be blown to reduce the contact pressure.

In general, control of the soft robotic endoscope is really complicated, having to deal with hysteresis effects as well as stick-slip phenomena. Many participants expressed their frustration resulting from the uncontrollability of the endoscope throughout the experiment. These complications have to be tackled in order to make manual control more feasible.

7.4.2 Path Planned Experiment

The resulting behaviour of the endoscope has not entirely met the expected response during the path planned insertion inside both scenarios. This can be due to several factors, such as a mismatch in mapping of bending to pressure, an inaccurate modelling of the endoscope module in simulation, and environmental disturbances such as friction and reaction forces of the pressure tubes that affect the bending performance. These points will be addressed shortly below.

Regarding the mismatch between the mapping of pressure to the corresponding necessary bending, it was also found during the experimental procedure that the endoscope tip module bent much more than was anticipated for, in both scenarios. Data from an additional characterization round of the tip module showed an increased bending capacity for the defined pressure limit, which could possibly be due to a different orientation of the endoscope modules with respect to the Aurora EM Tracker, as expressed before. Furthermore, aspects as plastic deformation causing enhanced bending capacity of bending module over time and a mismatch in placing the sensor could be of influence to the result. The first and third point of attention can be compensated for by maintaining similar posture throughout the experiment as well as the characterization phase. The second aspect is harder to map and therefore should be countered by means of frequent inspection of the bending capacity. It is recommended for future research to investigate which reason or reasons apply here.

Results from the simulation contain more steps to reach the target compared to the steps necessary for the manual insertion experiment to be completed. This showcases a mismatch in behaviour between simulation and the physical response. Due to a limitation on the number of steps the stepper motor can make, the response of the path planned endoscope is also cut of compared to its full motion profile. This affects the total performance of the path planned endoscope. It has been attempted to interpolate between values, such that a response appears that is in line with this stepper motor limitation. However, the resulting response of this action regarding visual inspection is rather poor. The overall modelling of the endoscope therefore needs improvement, mainly in the area of size increase during bending.

The effect of the environment upon the eventual performance is difficult to map and has been discussed in this chapter before. Due to the nature of the current control being open loop, it is rather important to retrieve the desired response behaviour. The current path planned endoscope has no ability to correct itself, whereas from manual experiments it was found that even with compensation of behaviour the target was already hard to reach without making

any collisions. It is highly recommended to consider feedback for future use of path planned control.

7.4.3 Data Analysis Experiments

Regarding the data processing of the video footage acquired during several experiments, some remarks remain. These are mainly formulated in the discussion section of Chapter I in the Appendix. Due to the video footage not being pre-processed, this sometimes makes for errors in measured data, as well as difficulties for image processing. Furthermore, the centerline of the endoscope often contained holes or branches, resulting in errors in data. Next to that, the current setup resulted in difficulties regarding image processing. The pressure tubes for example influenced the detection of the endoscope during image processing. Furthermore, the detection of the centerline of the environment was not always correct, mainly due to the black surrounding of the environment influencing the environment edge detection. The algorithm should be made more robust, together with a better consideration of setup display for image recognition. More attention should be paid to fixed position of the camera, visibility of markers throughout the scene, more clear distinction between tracked object and environment and fixed dimensions of the footage.

7.4.4 Results Experiments

Concerning the comparison between the resulting pressures from simulation with respect to the average pressures found in the manual insertion performance, several remarks can be made. Since the participants required a varying amount of steps to complete the scenario, taking the average response would not totally grasp a proper representation of manual behaviour. It would have been better to set a fixed amount of steps which the participants had to use.
The overall pressure profiles of the path planned endoscope and the average manual insertion response are also difficult to compare, due to having a different amount of steps required to complete the scenario. It can be seen that similar events occur during the pressure profiles, although no clear conclusion could be drawn from this. It can be observed from the plots that the path planned pressures seem to be higher compared to the manual experiment. This is also in line with the average endoscope pressure per step found.

With regard to the comparison between manual completion time and path planner completion time, it comes to no surprise that the path planner would be much faster. However, as their main objective was reaching the target while avoiding the obstacles, this also stimulated participants to take their time. An interesting phenomenon is the rather big deviation between completion time of the participants, ranging from about 6 minutes to about 29 minutes for Scenario 1 and ranging about 11 minutes up to even around 40 minutes for Scenario 2. Important to note here is that only the time between the moment the stepper motor is finished and the time the pressures are inserted is counted, excluding the stepper motor process.

The error with respect to the centerline is higher regarding the path planned endoscope, mainly due to its lack of feedback. The number of separate collisions counted for the path planned endoscope is actually lower, which is mainly due to the fact that the open loop behaviour refrains the endoscope from getting out of the initial collisions. Computing the percentage of insertion duration being in collision with the environment might improve the comparison.

Interestingly enough, the results regarding the average weighted errors considering the distance of the endoscope with respect to the centerline seem to be lower for Scenario 2 with respect to Scenario 1, when looking at the manual experiments. This is not in line with the hypothesized behaviour. However, it was found that Scenario 1 often contained rather big errors in the start of the experiment. Since the start often mainly concerns insertion, it was deemed unlikely to be in line with the actual error. After further investigation, it was found to be due to

an error, connecting the endoscope tip with the upper left corner and determining the error by means of that.

In general, other performance metrics are required to more accurately assess the performance of the path planned endoscope, as from these metrics it is hard to derive the behaviour. With for example the computation of the vicinity of the endoscope tip with respect to the target, in combination with the current (modified) centerline error, one can already assess the performance better.
Due to the limited performance of the path planned endoscope, the current comparison with manual insertion might not be that suitable at this stage. Improvements in physical response are necessary before it can properly complete the insertion. Therefore, the performance of the separate blocks should be investigated and improved. Furthermore, the use of feedback might be required to further improve the response.

7.5 Conclusion

The total duration of inserting pressures was on average much shorter for the path planned endoscope compared to the manual endoscope control. Scenario 2 took longer for both path planned endoscope and manual procedures.

The path planned endoscope seems to use more pressure per step compared to manual insertion. Similarities can be found in the pressure profiles of the manually inserted endoscope experiments with respect to the output of converted angles from simulation, although no concrete conclusion could be drawn.

A majority of participants stated that they had to concentrate a lot to stay away from the obstacles. The majority of the participants with medical training in flexible endoscopes stated that the control was rather not intuitive, it was hard to control the four modules to get to the desired configuration and that they did not really feel confident to control the endoscope.

In general, more collisions were found for the manual performance, compared to the path planned performance. This is considered due to the lack of correcting behaviour. More collisions occurred in Scenario 2 with respect to Scenario 1, for both manual experiments and path planned experiments. Current average weighted errors for Scenario 1 are higher compared to Scenario 2. At this point in time, the path planned endoscope performs less compared to manual insertion in terms of error with respect to the centerline. When regarding the simulation error, represented in Figure 6.19 of Chapter 6, a lower weighted error with respect to the centerline was found, for both scenarios.

From observation, it was clear that the open-loop path planned control had difficulty to reach the target. However, the shape in some cases was not too far off. Better defined conditions for control are necessary, and the potential use of feedback could be of use to get closer to the manual performance.

8 Discussion

As has been mentioned in previous chapters, several aspects of the process could be improved. These chapters could serve as separate studies, improving the overall knowledge and quality of the soft endoscopic control process.

The module design that has been used throughout the study suffered from lengthening properties and hysteresis behaviour, making response estimation more difficult. The current model serves as merely an approximation of the real behaviour. It would be more desirable to combine model and design with an underlying explanation based on the physics behind the bending response based on pressure input. Furthermore, it should be attempted to limit the effect of lengthening and hysteresis upon module behaviour in future iterations, as opposed to attempting to compensate for them.

The modified model that is currently used to describe the bending behaviour of the module is chosen based on similarities in shape and physical comparison, but has not been extensively compared using different bending scenarios, regarding different bending angles. Validation of accurate model representation is lacking, which affects both simulation and physical performance.

Currently, the physical phenomena such as lengthening of the modules, hysteresis behaviour, stick-slip effects, and characterization errors due to orientation difference as well as simplified fitting severely impact the in open-loop performance of the endoscope. It has been found almost impossible for the path planned endoscope to reach the target throughout the scenarios. Attempts have been made using proportional gains for the pressure profiles of the separate modules, as well as trying to reduce the amount of necessary steps to fit the response inside the environment. Both are results from the inaccuracies between planned and realized response, and merely compensate for the problem rather than solving it. For a more structural solution that would contribute to current knowledge, improvements in the stages before the resultant pressure profiles are necessary.

During this study, several intermediate experiments have been performed to get more insight regarding the origin of the hysteresis behaviour. From the results of these experiments, it was found that the hysteresis might not only be due to friction or the use of external sheathing, but could also be a result of the material characteristics of the module. However, the magnitudes of these aspects upon the hysteresis behaviour is yet unknown, and should be elaborated upon in future research.

Mapping the pressure-bending relation during characterization by means of an average response of the hysteresis curve is currently used for the definition of pressures throughout the path planned trajectory, which might be an oversimplified approach that causes certain inaccuracy. Alternative approaches were deemed unfit due to misalignment with similar hysteresis profiles or presumed cause of oscillatory pressure profile response. However, a proper comparison between the defined fitting methods and their corresponding output is currently lacking. Furthermore, a more detailed validation is necessary to define the best response. More knowledge should be obtained regarding the best fitting approach, while also taking into account different characterization pressure profiles.

Although the path planning algorithm currently bridges the model with the desired output response throughout the scenario, it could also serve as a basis for the design process once the desired application environment is known. Based on these tools, one could define accurately modelled designs which would suit the application purpose. However, the algorithm currently does not take into account dynamic environments as well as scenarios in which interaction with the environment occurs. Furthermore, RRT has a limited performance concerning nar-

row passages (Rilk et al., 2009), which might be problematic when concerning some of the realistic application scenarios. The simulation currently lacks physical resemblance, which should be taken into account for future work. Furthermore, the accuracy of predicting the physical response from simulated motion has not been taken into account in the computation, which might be a valuable addition to the performance evaluation during simulation.

At this point in time, this study has not yet treated the implementation of imaging to develop the scenarios for the path planning algorithm. However, this factor might play a big role in the implementability of the eventual infrastructure, as without proper definition of the environment, the whole trajectory will be complicated. Furthermore, vision of the endoscope inside the environment might play an important role for the future potential application of on-line path planning, which can use the imaging feedback to readjust the trajectory throughout the environment.

Throughout the study, there have been some inconveniences with respect to the use of angles from the Aurora EM Tracker. It has to be taken into account that the bending angle in terms of Euler angles will probably be less high compared to the results when using the angle from rotation matrices, based on quaternions. This is because of the difference in plane selection.

Although it was found that the duration of the pressure insertion of the path planned endoscope was much faster, it must be mentioned that the processes before getting to the final pressure profiles also take time. Current simulation procedures are rather slow, which has to be improved concerning potential future on-line path planning purposes.

Finally, the used metrics to determine the performance of the manual insertion with respect to path planned insertion might not totally cover the complete performance differences of both experiments. Without visual inspection of the path planned performance, the actual resemblance of insertion performance is rather difficult to grasp. Discrepancies between the scenarios for manual insertion and path planned insertion, together with difficulties participants had with the interface of the experiment, further complicate the comparison and resemblance of performance.

9 Conclusion

This study has laid the first stones in the path that is yet to be discovered regarding the control of multi-module soft robotic endoscopes. Throughout the study, several stages were considered, from design and characterization to modelling and simulation to the physical response. All of these stages have been necessary to define the endoscope behaviour and develop the required response with respect to the physical scenario. The current infrastructure built from this research could not only serve as a means to evaluate current soft robotic endoscope designs, but can also be utilized as a tool to develop these designs. All in all, this study gives useful insights for future soft robotic applications.

A big hurdle was found in the form of hysteresis behaviour, which can be due to friction, sheathing or material properties of the modules. This highly affected performance and mapping of the physical response. It became clear that more knowledge regarding the overall behaviour of the modules as well as the endoscope as a whole is required to improve the eventual performance, both for simulation and in the physical environment. Currently, the open-loop response has difficulties realizing the desired path, due to potential limitations in characterization and modelling as well as the influence of external factors. These challenges have to be faced in the future, together with the implementation of imaging and potential use of feedback.

The following sections contain answers to the previously stated sub-questions, which were also stated in the beginning.

Which path planning algorithm would suit the steering of a soft robotic endoscope? The path planning algorithm that was deemed suitable for the current application was based on the RRT* principle. RRT was mentioned in literature to have several benefits, such as being able to deal with (non-) holonomic constraints, being fast in terms of computation and being able to deal with high dimensional complex problems. This path planning principle was combined with the Endoscope Kinematic Planner algorithm, simulating the endoscope response based on a bending module model.

What bending characteristics can be found regarding the endoscope module performance? The average bending response for the endoscopic modules from the EcoFlex 0030 design with outer sheath was found to be around 107 degrees, when actuating the module in upright position while only using a single chamber for actuation. From the pressure profiles combining left and right bending, hysteresis behaviour was found. The hysteresis behaviour was not solely the cause of friction, but was also due to the module design. Signs point towards the EcoFlex material having hysteresis properties as well. During bending, it was found that bending with two chambers resulted in a lower effective bending angle compared to the bending of one chamber.

In what way can the algorithm(s) be coupled to the actual behaviour of the endoscope modules? This can be done by means of using information regarding the pressure-bending behaviour of the endoscopic modules. Every separate module is characterized and the resulting pressure-bending relation is extracted by means of fitting the respective data. Several variations of fitting the behaviour were considered, whereas currently segments of the middle line from the hysteresis plot are fitted into several pressure functions. Due to the hysteresis behaviour of the modules, together with other factors such as the stick-slip effect, the actual bending performance of the whole endoscope as well as the separate modules are difficult to predict. It is recommended to investigate better ways to either predict or correct the behaviour during control.

Another connection between actual behaviour and the algorithms is the development of the model, which approximates module bending behaviour. Two models have been compared;

the Constant Curvature Model and the Modified Model. Both models have been used in simulation. The Modified Model showed similarities in terms of shape with respect to the physical response, as well as being more in line with the physical structure of the module.

Which approaches can be used in combination with the path planning algorithm to make a safe path that can be followed by the soft robotic endoscope? Based on information regarding the shape and size of the endoscopic modules, safety measures could be taken during computation to ensure an obstacle-free path is be computed. One of those safety measures is the implementation of obstacle margins based on the dimensions of the soft robotic endoscope modules, which is a principle often used in path planning approaches. Furthermore, a cost function was used to steer the endoscopic modules, which implemented a high penalty on obstacle collisions. Therefore, the simulated endoscope would refrain from touching the boundaries. Furthermore, the information regarding the bending capacity of the endoscopic modules was used in both the Path Planner and Path Tracker, to constrain the maximum bending of the path and the endoscope.

What setup can used to be able to experimentally test the developed path planning algorithm? A platform was developed, which allowed for testing of several scenarios. A pneumatic stepper motor was used to insert the endoscope into the environment, guided by a rails. The endoscope was assembled using four EcoFlex 0030 modules, surrounded by an outer sheath. This module design was chosen because of the highest module bending results compared to the alternative designs. The modules were further analysed by means of using the Aurora EM tracker, which enabled the recording of position and orientation of the sensor connected to the module. To control bending of the endoscope, four pressure regulators (VEAB-L-26-D2-Q4-V1-1R1) and four solenoid valves (MHE2-M1H-3/2G-QS-4-K) were used. During the manual experiments and the path planned experiment, a camera setup was used in combination with a written image processing algorithm, in order to define positions and orientations of the endoscope throughout the environment. A pneumatic stepper motor was used to insert the endoscope in the environment. Regarding the path planned insertion, the setup was controlled using an Arduino. Manual insertion experiments were performed using a MATLAB application as interface for the participants.

How would the path planning algorithm perform compared to manual operation in terms of safety and speed? In terms of speed, it is fair to say that the automated insertion of pressures is much faster compared to the human manual insertion of the pressures. However, since the path planned endoscope had severe difficulty to accomplish reaching the target inside the environment, the approach cannot yet be considered safer with respect to manual insertion. Due to several factors that affect the performance of the endoscope inside the environment, together with the aspect of the current control law being open loop, the eventual response was not yet deemed desirable. More attention has to be paid on the pressure-bending relationship for soft robotic modules in various circumstances. Nevertheless, results from the participant experiments show that manually steering the endoscope through the scenarios was not found easy. Numerous collisions with the environment occurred in both scenarios. The participants stated that the control was not intuitive and they had to concentrate a lot to stay away from the boundaries. This indicates that an alternative method to manual control might be desired. Regarding the centerline error, the manual insertion currently outperforms path planned insertion. However, from simulation of the path planned endoscope, a lower error has been found regarding both scenarios, indicating that the path planning cannot be performed ideally due to practical effects. Improvements in relating simulation to physical response or the implementation of feedback could help to improve path planned performance compared to manual insertion performance.

10 Future Recommendations

In the time span in which this research was conducted it has become increasingly evident that more research has to be done in this field. There are still some steps to make, both in technology as well as the knowledge gained from the clinical perspective. Subjects such as scalability of the modules, integration of sensors and knowledge regarding interaction with the environment will play a major role in this. Several ideas for future improvement are depicted below.

10.1 Current Behaviour Mismatch

At this moment, several processes could influence the performance of the actual physical response with respect to the simulations. Examples are the inaccurate representation of the module behaviour in the simulation, as well as the deviation between characterized module response and actual response. The last one could be divided into three categories; the mismatch in fitting the hysteresis response, the mismatch in orientation between characterization and the external influences that affect performance. These effects should be investigated in separate experiments, such that the magnitude of their influence could be determined. Furthermore, it is recommended to simplify the current experimental setup, as this would stimulate more accurate insights. The same holds for the hysteresis behaviour. Since currently several potential causes are found, it is key to define the effects of these causes upon the overall hysteresis behaviour, such that these effects could be accounted for and preferably limited.

10.2 Algorithm

A real contribution to the currently existing algorithm would be the inclusion of a global optimization function. At the moment, the current algorithm determines an optimal bending for each module, starting from the bottom module. These local optima do not necessarily provide a global optimal solution. Instead, it would be better to determine the optimal position for the complete endoscope at once, using a cost function that directly incorporates all modules.

Next to this point, a recommendation for future work would be to include the lengthening of the module during bending in the kinematic description as well, to get a better approximation with respect to the physical bending behaviour.

Furthermore, modification of the algorithms towards 3D environments is close. A modification made by Sai Vemprala (Vemprala, 2017) is found for RRT* in 3D space. Combining this with current knowledge and the currently made algorithms will make 3D path planning for the endoscope possible. It is recommended to integrate the kinematic model in the use of developing tree splines in the RRT*-algorithm as well. Furthermore, the knowledge regarding bending performance for all modules should be incorporated in the simulation algorithms, to improve the accuracy of response.

10.3 Imaging Connection

To make the current algorithm and soft robotic endoscope more application oriented, the environment scenario should be based on medical images. In this way, realistic scenarios can be examined, which might improve design aspects and at the same time access the quality of the current algorithm. Different imaging methods should be analysed to define the potential difficulties and target applications.

10.4 Module Design

It has been mentioned earlier that the current endoscope design has its limitations in size and composition. At the moment, work is already being done in the area of downscaling the design.

An important and problematic aspect of the pressure controlled endoscope is the fact that the size increases due to the additional tubes that have to facilitate the pressure. This is one of the greatest bottlenecks in design, as this severely limits downscaling possibilities. Solved this would increase the potential for future application.

Next to that aspect, the current design made it difficult to fix broken modules. A start has been made into the design of modular connectors, which enables the modules to be taken out of the endoscope easily. At the moment, the modules have to be cut from both sides, damaging the modules and the connection with the connector pieces. These new connector pieces enable easy switching when a module is damaged or another endoscope module composition is desired, and facilitate experimenting with different combinations of module designs.

10.5 Actuation

As has been experienced before, exact mapping of the endoscopic movement is rather difficult. The effect of the friction combined with the weight and bending of other modules make mapping without errors impossible. This is why it would be interesting to consider on-line path planning instead. In this case, the planned path serves as a base and by means of sensors the path can be adjusted when necessary. An interesting way of sensing the deformation of the endoscope would be the principle of fiber Bragg grating (HBM, -)(Park et al., 2008). By means of analysing the wavelengths of the reflected light, the strain of the fiber can be determined. (Park et al., 2008) The work of Park et al. (Park et al., 2008) showed the use of fiber Bragg grating in analysing the deflection of a needle, while operating in an MRI environment. Another article used the principle of fiber Bragg grating for detecting respiration motion inside an MRI environment (Dziuda et al., 2013). Both articles state that the use of this method did not affect MRI image quality, as well as considering the method to be usable inside an MRI (Dziuda et al., 2013)(Park et al., 2008). Other methods might also be interesting to look at, such as the use of multiple Aurora EM tracker sensors, or the connection of camera footage and image processing to correct the bending performance.

During the experiments, the participants had to make a connection between pressure inputs and the resulting bending. For future manual control, it would be more convenient to already do this mapping beforehand, such that participants can more easily control the endoscope themselves. However, the side mark here is that this mapping must be rather accurate, otherwise errors could still occur. Next to that, the control interface has to be made more convenient and easier to understand for the user.

Furthermore, there has been an interesting alternative for controlling the endoscope, which slightly resembles the currently used method of path planning, but can also be used in other ways. This control approach is based on follow-the-leader motion, in which the tip module motion is the reference for other modules to follow, as can also be seen in the article of Chen et al. (Chen et al., 2014). Other work based on similar principles can be found as well (OCRobotics, 2014) (Choset et al., 2017). This approach would simplify manual control drastically, as the operator only has to control the tip manually, after which other modules would follow the bending profile of the tip, when considering having knowledge regarding the insertion status.

Regarding actuation of the pneumatic stepper motor, it would be desired to develop a motor with more smooth transition steps, to prevent shocking behaviour. Implementation of potentiometers for the modules and stepper motor in a demo setup would help to improve insights in behaviour of the endoscope in an early stage.

10.6 Interaction

One of the most important aspects that should be considered in future research is the effect of interaction with the environment. In practice, the aspect of interaction with the surroundings

is almost unavoidable. As this interaction affects the behaviour of the endoscope itself as well as potentially influencing the consistency of the environment, it is of key importance to examine these effects. This interaction goes both ways, as both the effect of the environment upon behaviour of the endoscope as well as the effect the endoscope has upon the environment in terms of force and torque are interesting for future applications. Regarding surgical manipulation, it might be interesting to look at the target orientation and position of the endoscope before the manipulation procedure, as well as the change in structure during the procedure. Instead of selecting a target in the middle of the environment, what should be done to make the endoscope move through the environment and eventually place itself in an optimal position corresponding to the next operation?

Several ideas were thought of to investigate the potential effect of the endoscope upon collision with the environment during navigation. One involves the use of deformable sheets at the edges of the environment, which would not be attached to the environment, but would be fixed to the fixed world. The deformation of the deformable sheet can be related to the force exerted by the endoscope upon the walls.

Another idea includes the use of a movable platform, which is connected to the world by means of springs. The endoscope would be inserted from the fixed world into the moveable platform. The interaction with the environment could be related by means of the deformation of the springs. However, it would be rather hard to design the springs to suit this experiment, as well as distinguish the individual interactions with the environment from a resulting platform displacement.

The aspect of dynamic environments has also been treated very little in this research. It was considered to develop an algorithm that would alter the positions of the obstacles through time, such that the path planner had to deviate its path through time. However, this unfortunately has not been implemented. It might be a very interesting concept, together with the use of sensory feedback, to develop an on-line path planning algorithm that can take those deviations into account. Eventually, a study was found dealing with deformable environments in combination with endoscopes (Rilk et al., 2009), in which they used a path planner to define the path for Robot Assisted Functional Endoscopic Sinus Surgery.

10.7 Medical Knowledge

During this study it also became clear that very little is known regarding the interaction forces during in vivo operation, as well as the conditions of the human body during operation. Several attempts were done in search for information regarding maximum allowable air pressure inside the lumen, dimensions of the colon, interaction forces during operation etcetera. Even research upon endoscope tool performance has only been covered up to a very small extent. It must be said that several answers were found, but this often was based on one study or a couple of scenarios which differed from actual human operations. It would benefit the research on medical devices greatly if more knowledge would be gained regarding the impact the operations currently have and the conditions that are currently present, such that this can serve as guidelines for the future.

Bibliography

(2015), STIFFness controllable Flexible and Learn-able Manipulator for surgical OPerations. http://sssa.bioroboticsinstitute.it/projects/STIFF-FLOP

Abayazid, M., G. J. Vrooijink, S. Patil, R. Alterovitz and S. Misra (2014), Experimental evaluation of ultrasound-guided 3D needle steering in biological tissue, **vol. 9**, no.6, pp. 931–939.

Ahmad, D., S. K. Sahu and K. Patra (2019), Fracture toughness, hysteresis and stretchability of dielectric elastomers under equibiaxial and biaxial loading, *Polymer Testing*, **vol. 79**, p. 106038.

Alterovitz, R., S. Patil and A. Derbakova (2011), Rapidly-exploring roadmaps: Weighing exploration vs. refinement in optimal motion planning, in *Robotics and Automation (ICRA), 2011 IEEE International Conference on*, IEEE, pp. 3706–3712.

Ambu (2019), Endoscopy, Website. https://www.ambu.com/products/flexible-endoscopes/all-products

Blanco, J. L., M. Bellone and A. Gimenez-Fernandez (2015), Tp-space rrt–kinematic path planning of non-holonomic any-shape vehicles, **vol. 12**, no.5, p. 55.

Borenstein, J. and Y. Koren (1991), The vector field histogram-fast obstacle avoidance for mobile robots, **vol. 7**, no.3, pp. 278–288.

Chakravarthy, A. and D. Ghose (1998), Obstacle avoidance in a dynamic environment: A collision cone approach, **vol. 28**, no.5, pp. 562–574.

Chen, Y., J. Liang and I. W. Hunter (2014), Modular continuum robotic endoscope design and path planning, in *Robotics and Automation (ICRA), 2014 IEEE International Conference on*, IEEE, pp. 5393–5400.

Choset, H. M., A. Wolf and M. A. Zenati (2017), Steerable, follow the leader device, uS Patent 9,591,964.

Cianchetti, M. (2013), The octopus as paradigm for soft robotics, in *2013 10th International Conference on Ubiquitous Robots and Ambient Intelligence (URAI)*, pp. 515–516, doi:10.1109/URAI.2013.6677325.

Coloplast (2019), Integrated, single use system for independant stent removal by flexible cystoscopy, Website. https://www.isiris-scope.com/isiris-performance/

van Dorp, J. J. (2019), Development of a Soft Robotics Diaphragm to Simulate Respiratory Motion. https://essay.utwente.nl/78278/1/Master%20thesis%20Jeroen%20van%20Dorp%2024-06-2019.pdf

Dziuda, Ł., M. Krej and F. W. Skibniewski (2013), Fiber Bragg grating strain sensor incorporated to monitor patient vital signs during MRI, **vol. 13**, no.12, pp. 4986–4991.

Elbanhawi, M. and M. Simic (2014), Sampling-based robot motion planning: A review, *Ieee access*, **vol. 2**, pp. 56–77.

Evans, P. R. (2001), Rotations and rotation matrices, **vol. 57**, no.10, pp. 1355–1359.

Falatehan, K. (2012), Advanced Path Planning for a Neurosurgical Flexible Catheter: Improving the performance of sampling-based motion planning.

Festo (2013), Website specs sheat. https://www.landefeld.com/shop/media/festo/Datenblaeter_DE_2016_06/196136_de.pdf

Festo (2018), Proportional pressure regulators VEAB, Website regarding specs sheat.
http://www.erwi.nl/uploads/veab.pdf

Fox, D., W. Burgard and S. Thrun (1997), The dynamic window approach to collision avoidance, **vol. 4**, no.1, pp. 23–33.

Fraś, J., J. Czarnowski, M. Maciaś, J. Główka, M. Cianchetti and A. Menciassi (2015), New STIFF-FLOP module construction idea for improved actuation and sensing, in *Robotics and Automation (ICRA), 2015 IEEE International Conference on*, IEEE, pp. 2901–2906.

Fujifilm (2019), ADVANCING DEEPER INSIGHTS IN ENDOSCOPY.
https://www.fujifilm.eu/fileadmin/countries/EU/endoscopy/Brochures/Mastercatalogue_2019_72dpi.pdf

Galceran, E. and M. Carreras (2013), A survey on coverage path planning for robotics, **vol. 61**, no.12, pp. 1258–1276.

Gao, Y., K. Takagi, T. Kato, N. Shono and N. Hata (2019), Continuum Robot with Follow the Leader Motion for Endoscopic Third Ventriculostomy and Tumor Biopsy, *IEEE Transactions on Biomedical Engineering*.

Garry, R. (2006), Laparoscopic surgery, **vol. 20**, no.1, pp. 89 – 104, ISSN 1521-6934, doi:https://doi.org/10.1016/j.bpobgyn.2005.10.003, gynaecological Surgery: Techniques, Training, Skills and Assessment.
http://www.sciencedirect.com/science/article/pii/S1521693405001252

Gasparetto, A., P. Boscariol, A. Lanzutti and R. Vidoni (2015), Path planning and trajectory planning algorithms: A general overview, in *Motion and operation planning of robotic systems*, Springer, pp. 3–27.

Gayle, R., P. Segars, M. C. Lin and D. Manocha (2005), Path planning for deformable robots in complex environments, in *Robotics: science and systems*, volume 2005, pp. 225–232.

Giacoboni, N. (2018), *Custom Arduino Library for HX711*.

Gifari, M. M. (2018), *Study on the Design of Soft Surgical Robots for Endoscopic NOTES Applications*, Master thesis, University of Twente.

Gomes, P. (2011), Surgical robotics: Reviewing the past, analysing the present, imagining the future, **vol. 27**, no.2, pp. 261–266.

Groenhuis, V. and S. Stramigioli (2018), Rapid prototyping high-performance MR safe pneumatic stepper motors, **vol. 23**, no.4, pp. 1843–1853.

Hachour, O. (2008), The proposed genetic FPGA implementation for path planning of autonomous mobile robot, **vol. 2**, no.2, pp. 151–167.

Han, L., Q. H. Do and S. Mita (2011), Unified path planner for parking an autonomous vehicle based on RRT, in *2011 IEEE International Conference on Robotics and Automation*, IEEE, pp. 5622–5627.

HBM (-), What is a Fiber Bragg Grating?
https://www.hbm.com/en/4596/what-is-a-fiber-bragg-grating/

Hounnou, G., C. Destrieux, J. Desme, P. Bertrand and S. Velut (2002), Anatomical study of the length of the human intestine, **vol. 24**, no.5, pp. 290–294.

Hu, C., X. Wu, Q. Liang and Y. Wang (2007), Autonomous robot path planning based on swarm intelligence and stream functions, in *International Conference on Evolvable Systems*, Springer, pp. 277–284.

ImageJ (-), Image Processing and Analysis in Java, website.
https://imagej.nih.gov/ij/

Jansen, J. (2018), Endoscopic end effector control using soft actuator, Bachelor Thesis.

Karaman, S. and E. Frazzoli (2011), Sampling-based algorithms for optimal motion planning, **vol. 30**, no.7, pp. 846–894.

Katrakazas, C., M. Quddus, W.-H. Chen and L. Deka (2015), Real-time motion planning methods for autonomous on-road driving: State-of-the-art and future research directions, *Transportation Research Part C: Emerging Technologies*, **vol. 60**, pp. 416–442.

Khan, G. N. and D. F. Gillies (1996), Vision based navigation system for an endoscope, **vol. 14**, no.10, pp. 763–772.

Khatib, O. (1986), Real-time obstacle avoidance for manipulators and mobile robots, in *Autonomous robot vehicles*, Springer, pp. 396–404.

Kim, S., C. Laschi and B. Trimmer (2013), Soft robotics: a bioinspired evolution in robotics, **vol. 31**, no.5, pp. 287–294.

Kuwata, Y., G. A. Fiore, J. Teo, E. Frazzoli and J. P. How (2008), Motion planning for urban driving using RRT, in *2008 IEEE/RSJ International Conference on Intelligent Robots and Systems*, IEEE, pp. 1681–1686.

LaValle, S. M. (1998), Rapidly-exploring random trees: A new tool for path planning.

LaValle, S. M. (2006), *Planning algorithms*, Cambridge university press.

LaValle, S. M. and J. J. Kuffner Jr (2001), Randomized kinodynamic planning, **vol. 20**, no.5, pp. 378–400.

Lee, J., G. Kim, H. Lee, B.-S. Shin and Y. G. Shin (2008), Fast path planning in virtual colonoscopy, **vol. 38**, no.9, pp. 1012–1023.

Lenssen, J. (2019), *Towards a steerable multi-module soft robotic endoscope for NOTES applications*, Master's thesis, University of Twente.

Liu, Y.-C. (2017), Constrained path planning of unmanned vehicles.

Loeve, A., P. Breedveld and J. Dankelman (2010), Scopes too flexible... and too stiff, **vol. 1**, no.3, pp. 26–41.

Lozano-Pérez, T. and M. A. Wesley (1979), An algorithm for planning collision-free paths among polyhedral obstacles, **vol. 22**, no.10, pp. 560–570.

MathWorks (-a), fminsearch, Website.
https://nl.mathworks.com/help/matlab/ref/fminsearch.html

MathWorks (-b), sgolayfilt, Website.
https://nl.mathworks.com/help/signal/ref/sgolayfilt.html

Medtronic (2016), ENT Product Catalog, Catalog.
http://endomedproekt.ru/upload/products_f/f_6_111.pdf

Merritt, S. A., L. Rai, J. D. Gibbs, K.-C. Yu and W. E. Higgins (2007), Method for continuous guidance of endoscopy, in *Medical imaging 2007: physiology, function, and structure from medical images*, volume 6511, International Society for Optics and Photonics, p. 65110O.

Naghibi, H., M. W. Gifari, W. Hoitzing, J. W. Lageveen, D. M. van As, S. Stramigioli and M. Abayazid (2019), Development of a Multi-level Stiffness Soft Robotic Module with Force Haptic Feedback for Endoscopic Applications, in *2019 International Conference on Robotics and Automation (ICRA)*, IEEE, pp. 1527–1533.

Noreen, I., A. Khan and Z. Habib (2016a), A comparison of RRT, RRT* and RRT*-smart path planning algorithms, **vol. 16**, no.10, p. 20.

Noreen, I., A. Khan and Z. Habib (2016b), Optimal path planning using RRT* based approaches: a survey and future directions, **vol. 7**, no.11, pp. 97–107.

OCRobotics (2014), OC Robotics - Introducing the Series 2 - X125 system, Youtube.
https://www.youtube.com/watch?time_continue=82&v=_gU6TWGynkU

Olympus (2018/2019), Endoscope Overview, Website brochure.
https://www.olympus-europa.com/medical/rmt/media/en/Content/Content-MSD/Documents/Brochures/ENDOSCOPE-OVERVIEW-2017-2018.pdf

Paik, D. S., C. F. Beaulieu, R. B. Jeffrey, G. D. Rubin and S. Napel (1998), Automated flight path planning for virtual endoscopy, **vol. 25**, no.5, pp. 629–637.

Park, J.-H., W. J. Park, C. Lee, M. Kim, S. Kim and H. J. Kim (2015), Endoscopic Camera Manipulation planning of a surgical robot using Rapidly-Exploring Random Tree algorithm, in *2015 15th International Conference on Control, Automation and Systems (ICCAS)*, IEEE, pp. 1516–1519.

Park, Y., S. Elayaperumal, B. Daniel, E. Kaye, K. Pauly, R. Black and M. Cutkosky (2008), MRI-compatible Haptics: Feasibility of using optical fiber Bragg grating strain-sensors to detect deflection of needles in an MRI environment, *International Society for Magnetic Resonance in Medicine (ISMRM) 2008*.

Patil, S. and R. Alterovitz (2010), Interactive motion planning for steerable needles in 3D environments with obstacles, in *Biomedical Robotics and Biomechatronics (BioRob), 2010 3rd IEEE RAS and EMBS International Conference on*, IEEE, pp. 893–899.

Raja, P. and S. Pugazhenthi (2012), Optimal path planning of mobile robots: A review, **vol. 7**, no.9, pp. 1314–1320.

Rilk, M., F. M. Wahl, K. W. Eichhorn, I. Wagner and F. Bootz (2009), Path planning for robot-guided endoscopes in deformable environments, in *Advances in Robotics Research*, Springer, pp. 263–274.

Robb, R. (2000), Virtual endoscopy: development and evaluation using the Visible Human datasets, **vol. 24**, no.3, pp. 133–151.

Sadahiro, S., T. Ohmura, Y. Yamada, T. Saito and Y. Taki (1992), Analysis of length and surface area of each segment of the large intestine according to age, sex and physique, **vol. 14**, no.3, pp. 251–257.

Shiller, Z. (2015), Off-line and on-line trajectory planning, in *Motion and Operation Planning of Robotic Systems*, Springer, pp. 29–62.

Smooth-On, I. (-), Ecoflex™ 00-50, Website.
https://www.smooth-on.com/products/ecoflex-00-50/

van der Stap, N., F. van der Heijden and I. A. Broeders (2013), Towards automated visual flexible endoscope navigation, **vol. 27**, no.10, pp. 3539–3547.

Trivedi, D., C. D. Rahn, W. M. Kier and I. D. Walker (2008), Soft robotics: Biological inspiration, state of the art, and future research, **vol. 5**, no.3, pp. 99–117.

Vadakkepat, P., K. C. Tan and W. Ming-Liang (2000), Evolutionary artificial potential fields and their application in real time robot path planning, in *Evolutionary Computation, 2000. Proceedings of the 2000 Congress on*, volume 1, IEEE, pp. 256–263.

Vemprala, S. (2017), 2D/3D RRT* algorithm, Website / Git.
https://nl.mathworks.com/matlabcentral/profile/authors/4026649-sai-vemprala

Vitiello, V., S.-L. Lee, T. P. Cundy and G.-Z. Yang (2013), Emerging robotic platforms for minimally invasive surgery, *IEEE reviews in biomedical engineering*, **vol. 6**, pp. 111–126.

Voermans, R., M. V. B. Henegouwen and P. Fockens (2007), Natural orifice transluminal endoscopic surgery, **vol. 39**, no.11, pp. 1013–1017.

Vyas, L., D. Aquino, C.-H. Kuo, J. S. Dai and P. Dasgupta (2011), Flexible robotics, **vol. 107**, no.2, pp. 187–189.

Wan, M., Z. Liang, Q. Ke, L. Hong, I. Bitter and A. Kaufman (2002), Automatic centerline extraction for virtual colonoscopy, **vol. 21**, no.12, pp. 1450–1460.

Wang, J., T. Ohya, H. Liao, I. Sakuma, T. Wang, I. Tohnai and T. Iwai (2011), Intravascular catheter navigation using path planning and virtual visual feedback for oral cancer treatment, **vol. 7**, no.2, pp. 214–224.

Wang, Q., W. Wang and Y. Li (2012), A multi-RRT based hierarchical path planning method, in *2012 IEEE 14th International Conference on Communication Technology*, IEEE, pp. 971–975.

Webster III, R. J. and B. A. Jones (2010), Design and kinematic modeling of constant curvature continuum robots: A review, **vol. 29**, no.13, pp. 1661–1683.

Witmer, L. M. (2007), Clinical anatomy of the large intestine, *Centers for Osteopathic Research & Education*.

Wright, M. H. et al. (2010), Nelder, Mead, and the other simplex method, *Documenta Mathematica*, **vol. 7**, pp. 271–276.

Xu, J., V. Duindam, R. Alterovitz and K. Goldberg (2008), Motion planning for steerable needles in 3D environments with obstacles using rapidly-exploring random trees and backchaining, in *2008 IEEE international conference on automation science and engineering*, IEEE, pp. 41–46.

Yang, K., S. Moon, S. Yoo, J. Kang, N. L. Doh, H. B. Kim and S. Joo (2014), Spline-based RRT path planner for non-holonomic robots, **vol. 73**, no.1-4, pp. 763–782.

Appendix A: Literature review

A.1 Abstract

An important aspect of robotics is path planning. Path planning can be described as the process of building a path from starting point to finish, while avoiding potential collisions with obstacles and considering relevant performance criteria. These criteria can range from the amount of energy used, to time spent, but can also consider robot-specific boundaries regarding motion or other characteristics. This research addressed several path planning algorithms and made a distinction between on-line and off-line approaches, of which on-line is based on dynamic environments and having to react to moving obstacles, whereas off-line approaches mainly address the paths that are pre-defined in a stationary non-changing environment. Furthermore, the concept of trajectory planning is introduced. Most attention was spend on types of algorithms suitable for endoscopic purposes. Next to these approaches, some alternative approaches to path planning were mentioned. One of the outstanding methods was the use of lumen centralization and visual odometry to steer the endoscope in the correct direction. Although a broad selection of path planning algorithms is presented in this review, further investigation of certain approaches is needed to draw proper conclusions regarding the future path planning direction for endoscopic applications.

A.2 Introduction

The aspect of path planning can be described as creating a path from starting point to target point that can be followed without colliding with any object in the environment, often combined with one or more performance criteria (Raja and Pugazhenthi, 2012). Path planning is a very important step in the process of controlling trajectories of autonomous robots (Raja and Pugazhenthi, 2012).

The article of Lozano-Perez et al. is one of the initial articles mentioning path planning algorithms (Lozano-Pérez and Wesley, 1979). It was stated that the 'generate and test' method, which boiled down to a structured trial and error, lacked global insight in path making, which made this approach to potentially be very costly (Lozano-Pérez and Wesley, 1979). In the years to come, many algorithms were created, dealing with all kinds of scenarios and specializing in several aspects.

This review will showcase several path planning algorithms and will attempt to clarify distinctions that can be made between those different approaches. The goal of this literature review is to get a grand overview of path planning possibilities, which may help in the development of a path planning approach for soft robotic endoscopes. Path planning methods could help improving several aspects of endoscopic operation. Examples are, among others, limited interference of the endoscope with the surroundings and minimum energy used during operation.

The structure of the article is as follows. In Section A.3 some conventional path planning algorithms will be discussed. The topic of trajectory planning will be introduced in Section A.4. In Section A.5, a selection of novel approaches in path planning are introduced. In Section A.6, some alternative methods to path planning are described, which differ from the traditional notion of path planning, but turned out to be useful when considering autonomous steering. Section A.8 will describe possible solutions for soft robotic endoscopes.

A.3 Conventional Path Planning Algorithms

The article of Raja et al. (Raja and Pugazhenthi, 2012) mentions the development of the configuration space (C-space), which was a relevant development for the conversion of the robot

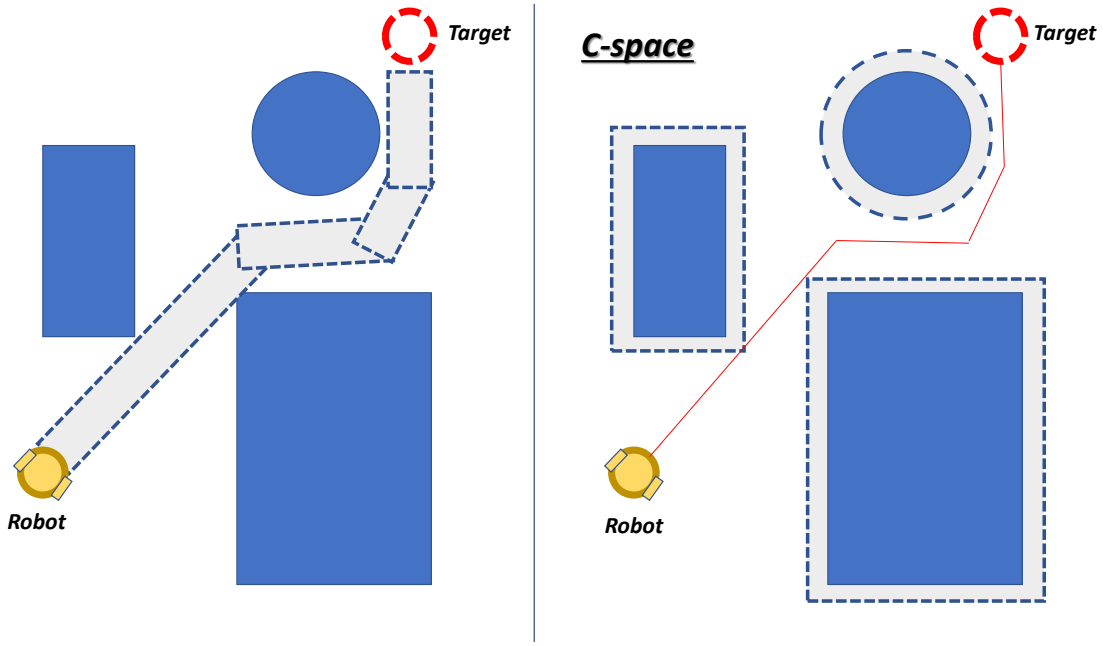

Figure 1: Example of the C-space implementation, inspired by footage found in the article of Lozano-Perez et al. (Lozano-Pérez and Wesley, 1979). The figures show the addition of the robot dimension to the obstacle environment, eventually adjusting the size of the environmental obstacles and reducing the robot to a spot in the image.

in an environment into a 2D map of the surrounding. One of the early articles in which the C-space made an appearance was in the article of Lozano-Perez et al. (Lozano-Pérez and Wesley, 1979). In the article, some useful simplifications are stated, of which one of them is the transformation of the obstacles with respect to the robot. In essence, the simplification means that the object size is increased by means of the dimensions of the robot. This is stated in the article as "growing O by A"(Lozano-Pérez and Wesley, 1979), implying the creation of a new obstacle by adding the object size (or robot size) to the obstacle. (Lozano-Pérez and Wesley, 1979) In Figure 1, an illustration is given of how the obstacle space is adjusted with the size of the object or robot (Lozano-Pérez and Wesley, 1979). This approach is utilized in many cases of path planning approaches (Raja and Pugazhenthi, 2012).

A distinction can be made between two types of path planning: off-line path planning and on-line path planning (Raja and Pugazhenthi, 2012). As Raja et al. describes, off-line path planning is based upon knowing the path in advance. On-line path planning basically includes knowledge of the path beforehand, but adjusting the path to changes that occur in the environment during the movement. Other words for on-line path planning and off-line path planning are local path planning and global path planning. (Raja and Pugazhenthi, 2012)

A.3.1 Off-line path planning algorithms

Off-line path planning is also called model-based path planning (Hachour, 2008), as it functions based on a model of the environment constructed beforehand. Its approaches can be subdivided into roadmap techniques and cell decomposition approaches (Raja and Pugazhenthi, 2012). Of the roadmap techniques, the visibility graph and the Voronoi diagram are well-known (Gasparetto et al., 2015) (Raja and Pugazhenthi, 2012). The visibility graph consists of nodes, which are connected by edges and show the C-space. The resulting path from this is the shortest Euclidean path in the C-space (Gasparetto et al., 2015). This method was presented by Lozano-Perez et al. (Lozano-Pérez and Wesley, 1979), who introduced the before

mentioned C-space in the same article. The algorithm for finding the shortest path in this visibility graph was named by Lozano-Perez et al. as being the VGRAPH algorithm (Lozano-Pérez and Wesley, 1979). The Voronoi diagrams (Gasparetto et al., 2015) (Raja and Pugazhenthi, 2012) comprise of an algorithm which checks that every distance the path and the obstacles is maximum, meaning that the path chosen has maximum distance between all objects. This often results in a longer path, but can be considered a safer option (Gasparetto et al., 2015).

Next to road mapping techniques, the cell decomposition approach was mentioned (Raja and Pugazhenthi, 2012). This method is based on dividing the C-space into separate cells and creating a path between cells that are empty. An important factor with cell decomposition is the grid size, as it determines the precision with which the algorithm can greate the optimal path, but this also has effect upon computation speed. (Raja and Pugazhenthi, 2012) A so-called connectivity graph is created, creating a link between cells through which a path connection is made (Gasparetto et al., 2015). The method can be categorized into exact cell decomposition- and approximate cell decomposition methods, where exact cell decomposition does have an exact computation of the free space and the approximate cell decomposition does not exactly know the boundaries of the free space. In other words, with exact cell decomposition the cells that are used to connect span a certain amount of space which is all free space, but when no clear distinction can be made between free space and obstacles, approximate cell decomposition can be used to split cells and eventually find cells that only contain free space. (Gasparetto et al., 2015)

As off-line techniques are static and do not take into account any deviation in the environment, it might be more interesting to consider dynamic and on-line path planning as approach. This is because the human body will also show forms of dynamic behaviour during operation, such as the deflation of organs and so on. The next section will discuss on-line path planning approaches.

A.3.2 On-line path planning algorithms

On-line path planning approaches have gained more popularity, as it becomes more important that autonomous mobile robots are capable of dealing with dynamic environments (Raja and Pugazhenthi, 2012). The on-line path planning approaches can also be termed sensor-based approaches (Galceran and Carreras, 2013)(Hachour, 2008). The main conventional approaches in terms of on-line path planning are Artificial Potential Field (APF), the dynamic windows approach, the vector field histogram approach and the collision-cone approach. (Raja and Pugazhenthi, 2012)

The APF approach is developed by Khatib (Khatib, 1986) and makes use of a potential field to steer the robot towards targeted goals. This potential field is created by assigning objects to a repelling force and creating a function based on the distance to the object that increases this repelling force. The target goal is assigned an attraction force. The article mentions that the application of APF can help reduce the high level control effort, as this approach moves part of the path planning towards low level control. Here, high level control implies algorithms to compute the optimal path, whereas low level control more relies upon sensors for example. The addition of APF improves the real-time performance speed of the robot control system, although it has been mentioned that there are drawbacks to this technique. The main drawback mentioned in the article is the occurrence of local minima, which could lead to the robot already settling before reaching target position. However, solutions to these problems exist and have been proposed, which were called navigation functions. (Gasparetto et al., 2015) It was mentioned that this method is known for simplicity and elegance, as little computation is needed (Raja and Pugazhenthi, 2012).

The dynamic window approach takes into account the linear and angular velocities and optimizes these for obstacle avoidance. This is dependent on vehicle dynamics. (Raja and

Pugazhenthi, 2012) According to Fox et al. (Fox et al., 1997), the dynamic window approach takes into account velocity limits based on dynamic constraints. Furthermore, it contains a limitation of velocities which are safe in combination with the obstacles. An optimization function is used to take these aspects into account (Fox et al., 1997). The function considers heading towards the target, distance with respect to the objects and the suitable velocities. (Fox et al., 1997)

The Vector Field Histogram (VFH) approach (Raja and Pugazhenthi, 2012) (Borenstein and Koren, 1991) makes use of polar histograms that are generated every instant. The approach is based upon improvements of the Virtual Force Field (VFF) algorithm, which creates a histogram grid of one cell each range reading and uses a probability distribution to estimate the obstacle appearance. The potential field method is used afterwards to eventually control and steer past obstacles. The VFH approach improves upon the shortcomings of the VFF approach, of which loss of local obstacle distribution information due to computational heavy load is one of them. The VFH introduces some intermediate steps to reduce the data set needed. In the histogram grid, the chance that an obstacle is present is represented by means of size and certainty values. As mentioned in the article, the VFH method is a local path planner, so it is not looking for the optimal path and can also get stuck for various reasons. (Borenstein and Koren, 1991)

The collision cone concept was created by Chakravarthy et al. (Chakravarthy and Ghose, 1998) and takes into account velocity paths that avoid collision with obstacles. The approach is derived from the field of aerospace, where they analyze the possible collision courses of airplanes. The method is suitable for a dynamic environment containing moving objects. (Chakravarthy and Ghose, 1998)

A.4 Trajectory planning algorithms

Trajectory planning, as is mentioned in the paper of Gasparetto et al. (Gasparetto et al., 2015), combines the path planning output and kinematic and dynamic characteristics of the robot to create trajectory information for the joints, assigning velocity, acceleration and jerk. This is done in the joint configuration space. Due to inverse kinematics and interpolation functions, the joint trajectory can be determined. Furthermore, this trajectory keeps in mind the boundaries of dynamics and kinematics of the system, which is good for avoiding singularities. However, it is mentioned that it might be difficult to transform motion from joint space to operation space, as non-linearities make this mapping less accurate. Important for trajectory planning is to receive a smooth path planning output together with clear boundaries of the system. (Gasparetto et al., 2015)

The article of Shiller (Shiller, 2015) refers to trajectory planning as being a path with a velocity profile to it. It is being stressed that for robots that are required to be able to move quickly in dynamic environments, only path planning is not enough.

Trajectory planning can be divided into three target criteria for which they are created (Gasparetto et al., 2015). These criteria are minimum execution time, minimum energy in the form of effort and minimum jerk. Minimum jerk corresponds to minimum vibrations in the robot, which reduces the wear of the robot. (Gasparetto et al., 2015)

A.5 Novel Path Planning Approaches

Raja et al. (Raja and Pugazhenthi, 2012) describes a selection of evolutionary approaches in on-line path planning and off-line path planning.

Almost all of the approaches mentioned in the article were some form of combination between the use of potential fields in combination with the Particle Swarm Operation (PSO) algorithm,

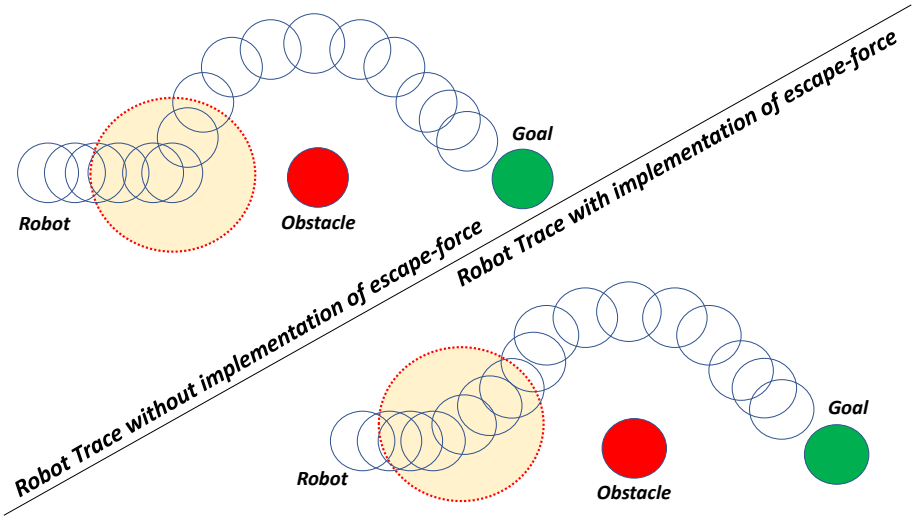

Figure 2: Representation from the illustration of the resulting escape-force algorithm mentioned in the article of Vadakkepat et al. (Vadakkepat et al., 2000). As can be seen from the image, the robot makes a smoother motion around the obstacle when compared to a situation in which the algorithm is not used. In this way, the motion may stay more continuous, reducing the risk of getting stuck.

which is an approach based on the flocking behavior of birds and fish (Raja and Pugazhenthi, 2012). One of the main reasons for the combination of algorithms is because of the possible occurrence of local minimums when using the APF algorithm. (Raja and Pugazhenthi, 2012)

The article of Vadakkepat et al. (Vadakkepat et al., 2000) proposes a new approach to APF; Evolutionary Artificial Potential Fields (EAPF). In the article, an evasion of local minimums is introduced, called the escape-force function. This method is claimed to be fast and suitable for real time path planning. One of the key remarks that has to be made with respect to this approach is that the same size of the objects is used. Figure 2 shows the resulting effect of the escape-force function included in the EAPF approach (Vadakkepat et al., 2000).

The article of Hu et al. (Hu et al., 2007) mentioned an approach to path planning introducing the stream functions, derived from another article, in combination with PSO. Stream Potential fields tend to be more smooth and seemed to be solving the local minimum problem of APF, but suffered from stagnation points where the velocity reaches zero. For this, swarm intelligence is used. (Hu et al., 2007)

A.6 Alternative methods for autonomous motion

A.6.1 Lumen centralization and visual odometry

Lumen centralization would not be considered a path planning technique, but is an other way of steering the endoscope in the right direction. This could be an alternative way of helping to improve the motion of the surgeon at hand.

The article of Khan et al. (Khan and Gillies, 1996) describes the use of dark regions and contours to guide the endoscope. The approach was tested in practice and remove a QL-tree structure was used for representation of the environment. The QL-tree approach is based on 2D cross-sections of the 3D environments, interconnecting the previous plane with the current plane and the next plane. From multiple 2D representations, a 2.5D representation of the colon is made. (Khan and Gillies, 1996)

The review paper of van der Stap et al. (van der Stap et al., 2013) concerns visual navigation approaches for the purpose of automating endoscopic mobility. During their literature review, their findings pointed towards two main proposed techniques for the navigation of en-

doscopes. These techniques are lumen centralization (mentioned earlier (Khan and Gillies, 1996)) and visual odometry. The motivation for defining systems to enable automation of the endoscopic movement is due to the fact that endoscopists think the steering of endoscopes is rather non-intuitive. Especially controlling flexible endoscopes was found challenging. The article states that the endoscopic environment is subject to dynamic behaviour, as the organs are often not completely stationary.(Khan and Gillies, 1996)

As the article mentions (van der Stap et al., 2013), lumen centralization is based on the physical features of the colon during illumination, resulting in lumen appearing to be darker with respect to the surrounding. This can be detected by means of camera imaging on the endoscope and is used to keep the endoscope central in the image. This helps to deal with tip orientation. Visual odometry implies the detection of displacements using camera images, leading to insights on tip orientation and tip direction. Both techniques are mentioned to be dependent on image quality and thus susceptible for various imaging-related problems, such as artifacts, image quality, unpredictable motion and so on. (van der Stap et al., 2013)

A.6.2 Path Covering Algorithm

In the article of Galceran et al. (Galceran and Carreras, 2013), different path planning algorithms are used, with as main target to cover all the space that is considered free space. Possible applications are for example an autonomous land mower or autonomous vacuum cleaning robots. Within this target, one can again assign different criteria to the path, such as minimum time and minimum path length. (Galceran and Carreras, 2013) As the goal of robotic endoscopy is not related to full coverage of the free space, this topic will not be further elaborated upon. In Table 1 of the article, a concrete overview of all the approaches mentioned is listed. (Galceran and Carreras, 2013)

A.7 Virtual Endoscopic Path Planning

The area of virtual endoscopy is a promising area for endoscopic operations in general. Virtual endoscopy can serve as a training platform for starting endoscopists (Robb, 2000), as well as a mental preparation of the operation to come. This could potentially decrease difficulties and risks for endoscopic operations, which could lead to improvements of the operation conditions for the patient. There is even a mentioning of performing inspection of regions that were not accessible before using conventional endoscopy. The article of Robb et al. (Robb, 2000) discusses the development of Virtual Endoscopy (VE) in combination with provided Visible Human Datasets. The aspect of having such a model of the human body might be of interest for our path planning application.

The techniques often found in literature are similar to techniques mentioned in the article of Lee et al. (Lee et al., 2008). Examples of applied path planning algorithms are topological thinning, Dijkstra's shortest path and Euclidean distance mapping. Most of these techniques resemble the working principle of the Voronoi diagram, implying that they create a path that is furthest form the edges of the colon, basically keeping the centerline. This article specifies a multi-resolution path tree propagation method using the farthest visible point in the model. Control points are created at maximum visible distance and are adjusted in amount depending on the orientation of the shape (see visible distance). The path tree basically connects all the voxels at maximum distance from the colon sides.

The article of Merritt et al. (Merritt et al., 2007) describes a very promising development, combining virtual planned image and real endoscopic image with included path visualization and marking regions of interest. The path planning in this study includes the use of centerlines, which are visualized on the camera view of both virtual and real endoscope. It is mentioned in the article that the virtual endoscope can be used to decouple and show images from the areas

up ahead or back, in this way scouting the area. However, the two endoscopes are also able to work in parallel, where it has been stated that this makes the virtual endoscopic view rather redundant. As registration or tracking methods can already cope with the speed, only the real interface can be used in combination with the continuously performing tracking. The article also states the possibility of including additional useful information, such as distance to target region and so on. (Merritt et al., 2007)

Some possible improvements upon this research could be the inclusion of for example optimal path planning. Currently, the most virtual endoscopic applications use centerlines or a method comparable to Voronoi approach to create a path through the environment. However, although this method is a safe way of providing motion through the channels, it will follow channel curvature as well. An approach could be thought of based on thee method of visualization of Merritt et al. (Merritt et al., 2007), but taking into account the curvature of the endoscope and keeping this to a minimum. Furthermore, the feedback that is given to the surgeon using the approach of Merritt et al. (Merritt et al., 2007) is rather passive. The surgeon is not encouraged to improve his path other than showing the correct path. One could think of a method that gives directional queues to the surgeon as well, providing an easier feedback system that less relies on the surgeons tracking capabilities.

A.8 Potential for Endoscopic Operations

As the Natural Orifice Transluminal Endoscopic Surgery (NOTES) operations using a robotic endoscope includes a change of path due to movement of organs and other body parts, it is assumed that the endoscopic robot will benefit from on-line path planning.

It has been mentioned that trajectory planning is needed when the robot has to move and react fast in its environment (Shiller, 2015). However, when regarding a robotic application such as the endoscope, the implementation of path planning will suffice, as the endoscope does not have to cope with high speeds or fast interacting environments.

One of the techniques that already is proposed in endoscopic continuum robots (Gayle et al., 2005) makes use of a motion planner that computes an estimated path that is furthest from all near obstacles and also resolves any collisions using a non-penetration constraint. (Gayle et al., 2005) In more detail, the article proposes an overlap algorithm to check whether collisions occur, together with an initial path based on a probabilistic roadmap planner and the approximate medial axis of the work space. The goal of the authors was to generate a collision-free path, while minimizing the energy used. To check for overlap, they used 2.5D overlap tests. Two experiments were performed in simulation, containing path planning of a spherical robot through walls and the simulation of catheters in liver chemoembolization. (Gayle et al., 2005)

The article of Chen et al. (Chen et al., 2014) provides some interesting path planning algorithms as well. In the article two techniques are mentioned; uncoiling path planning and follow-the-leader path planning. The first one provides a way to insert the endoscope without needing to use any extra actuator, whereas the latter approach helps in automatically steering the other segments of the continuum robot after the movements of the tip that have been performed. (Chen et al., 2014)

As mentioned earlier, the use of lumen centralization and visual odometry are visual-based planning techniques with lots of potential in terms of steering the endoscope (van der Stap et al., 2013) (Khan and Gillies, 1996). However, according to van der Stap et al. (van der Stap et al., 2013), no experiments in vivo have been executed.

A.9 Discussion

This review has covered several approaches developed throughout the history of path planning, as well as alternative movement methods. However, from this research it is still difficult to determine which approach would be most suitable for application in endoscopic feedback during operation. Essential information regarding performance, advantages and disadvantages is currently missing in this research. Future approach should consider a more elaborately drawn image of all techniques in a overview table. Furthermore, some recent developments in terms of algorithms should be included in the research.

Further ideas for future research include the further investigation of virtual endoscopy, a topic which has been more widely addressed in literature. Virtual endoscopy can be used to train and to pre-plan possible trajectories for operation, taking visual effort away from navigation during operation (Paik et al., 1998). Articles regarding virtual endoscopy also introduce new approaches that could be of interest for eventual application of path planning-based feedback during operation. This collection of information can be very insightful for determining the future target of this research.

A.10 Conclusion

An important aspect of robotics is path planning. Path planning consists of a starting point and an end goal, to which a path is drawn while evading potential obstacles along the way and taking possible performance criteria into consideration. These criteria can range from energy used, to time spent, but can also consider robot-specific boundaries regarding motion or other characteristics.

This research addressed several path planning algorithms and made a distinction between on-line and off-line approaches, of which on-line is based on dynamic environments and having to react to moving obstacles, whereas off-line approaches mainly address the paths that are pre-defined in a stationary non-changing environment. Furthermore, the concept of trajectory planning is introduced. Most attention was spend on types of algorithms suitable for endoscopic purposes, which was why new developments in on-line path planning approaches were highlighted.

Next to these approaches, some alternative approaches to path planning were mentioned. One of the outstanding methods was the use of lumen centralization and visual odometry to steer the endoscope in the correct direction.

Approaches in virtual endoscopy are also studied, of which some researches proposed interesting approaches to path planning. Path planning in virtual endoscopy mainly relies on the use of line centralization, which basically implies generating points that are furthest away from the walls, interconnected to create a path. This is quite similar to the approach of Voronoi diagrams. The article of Merritt et al. (Merritt et al., 2007) provides a novel approach in interfacing the planned path as visual feedback for the surgeon to use during operation.

Appendix B: Commercial Endoscopes

The current commercial endoscopes vary in terms of dimensions and other characteristics, such as bending capability and tooling options. Depending on the application, other aspects are of course of importance. Table 1 contains the data of several commercial endoscopes, which have been found in several brochures of commercial companies. It has been chosen to display only the biggest diameter in the endoscope, as sometimes the tip might be bigger than the overall diameter and vice versa. Furthermore, for the sake of overview, only the range per type of endoscope is shown.

Other sources were also investigated, but no clear information regarding flexible endoscopes for medical purposes were found in those sources. Other considered companies were looked at were Boston Scientific, Medtronic, Ethicon, Hologic, Comeg, B.Braun and Bayer.

Endoscope type	Source	d (mm)	Bending angle (degrees)	Remarks
Bronchoscopy	(Olympus, 2018/2019)	3.1-6.2	U:180-210/D:130/L:120/R:120	
	(Olympus, 2018/2019)	2.2-6	U:180/D:130/L:¬/R:¬	
	(Ambu, 2019)	4.2-6.2	U:130-180/D:110-180/L:¬/R:¬	
Colonoscopy	(Fujifilm, 2019)	11.1-12.8	U:180/D:180/L:160/R:160	
	(Fujifilm, 2019)	10.5	U:210/D:160/L:160/R:160	
	(Olympus, 2018/2019)	9.5-14.8	U:180/D:180/L:160/R:160	
	(Ambu, 2019)	18	U:180/D:180/L:180/R:180	
Duoendoscopy	(Fujifilm, 2019)	13.1	U:120/D:90/L:90/R:110	
	(Olympus, 2018/2019)	12.8	U:120/D:90/L:90/R:110	
Enteroscopy	(Fujifilm, 2019)	7.7-9.4	U:180/D:180/L:160/R:160	
	(Olympus, 2018/2019)	9.2	U:180/D:180/L:180/R:180	
Gastroscopy	(Fujifilm, 2019)	5.1-10.8	U:210/D:90/L:100/R:100	
	(Fujifilm, 2019)	9.8	U:210/D:120/L:100/R:100	
	(Olympus, 2018/2019)	5.8-12.9	U:210/D:90/L:100/R:100	
Cystoscopy &	(Olympus, 2018/2019)	2.7-5.5	U:210-220/D:120-130/L:¬/R:¬	
Uteroscopy	(Coloplast, 2019)		U:80/D:90/L:¬/R:¬	d unclear
	(Olympus, 2018/2019)	2.65-3.3	U:180-275/D:275/L:¬/R: ¬	
Laparascopy	(Olympus, 2018/2019)	5.4 -10	U:100/D:100/L:100/ R:100	
Rhinolaryngoscopy	(Olympus, 2018/2019)	2.2-5.0	U:130/D:130/L:¬/R:¬	
	(Ambu, 2019)	3.5-5.5	U:130/D:130/L:¬/R:¬	
	(Olympus, 2018/2019)	2.65-3.3	U:180-275/D:275/L:¬/R:¬	
Sigmoidoscopy	(Fujifilm, 2019)	12.8	U:180/D:180/L:160/R:160	
Choledochoscope	(Olympus, 2018/2019)	5.2	U:160/D:130/L:¬/R:¬	
Pleuroscope	(Olympus, 2018/2019)	7	U:160/D:130/L:¬/R:¬	
GI Fiberoscope	(Olympus, 2018/2019)	9.8-13.8	U: 160-210/D: 90-180/ L:100-160/R: 100-160	
Tracheal Intubation	(Olympus, 2018/2019)	2.2 -5.2	U:120-180/D:120-130/L:¬/R:¬	
Hysteroscope	(Olympus, 2018/2019)	3.1	U:100/D:100/L:¬/R:¬	
ENT Scope	(Medtronic, 2016)	3.2-3.8	120-160 U:125/D:125/L:¬/R:¬	$l_{\text{bend}} = 25$ mm

Table 1: Inventory of commercial endoscopes. As diameter- and bending angle columns suggest, this information is a summary of even more commercial endoscopes. For the sake of overview, these endoscopes are combined when they contain the same bending performance. Here, d is the biggest diameter.

Appendix C: Fabrication process

The modules used for the creation of the complete endoscope have been fabricated in house, using the various types of EcoFlex and Dragon Skin that have been present at the research group. This section will concern the fabrication process, explaining the steps taken during this procedure. It will mainly focus on the fabrication process of the EcoFlex 0030 modules, as these are mainly used throughout the experiments. First, a quick recap is given concerning the design of the most frequently used modules, after which their fabrication process is highlighted. Most of the fabrication process has been pioneered by Jan Lenssen (Lenssen, 2019), after which several adjustments have been made.

C.1 Design description

The EcoFlex 0030 modules consist mainly out of EcoFlex 0030 material, using EcoFlex 0050 for the chambers and Dragon Skin 10 for the lid of the module. The reason for having EcoFlex 0050 chambers is to increase the strength of the chambers, hopefully lasting longer during the process. The Dragon Skin 10 lid is used as an extra strong barrier to contain the expansion with, as the most pressure would be exerted in upwards direction.

C.2 Manufacturing the chambers

The chambers have been fabricated by means of pouring EcoFlex 0050 into a fabricated mould, which is created by Jan Lenssen (Lenssen, 2019) using the Stratasys Objet printer. The mould can hold six chamber pieces (also fabricated in the Stratasys Objet printer), used to build the chamber shell around. Initially, the chamber pieces and the mould itself have to be cleaned using Isopropanol, after which the mould can still be sprayed with mould release to reduce the sticking behaviour to the mould. After the parts are cleaned, the white chamber pieces are placed in the mould and the mould can be screwed tight. The mould then is placed upright (see Figure 3, on the left, to enable the mixture to run from top to bottom.

Figure 3: Image showing the poured mould (left) and the resulting chambers (right), together with a view on the inside of the mould and its fixation material (below and right). Process designed by Jan Lenssen (Lenssen, 2019).

After the mould is ready, the EcoFlex 0050 material can be prepared to be poured in. First, the EcoFlex has to be mixed together. For one of these moulds, it would suffice to use five grams of mixture A and five grams of mixture B of the EcoFlex 0050 package (names are indicated on the outside of the buckets). The weights have been defined using the small scale that is available in the lab. Be advised; this scale is fairly inaccurate every now and then and sometimes requires lifting the sample to see if any changes in weight occur. The mixture then is thoroughly mixed, going from counter-clockwise to clockwise and taking into account all the edges of the small cup in which the mixture is poured.

When the mixture is thoroughly mixed for about a minute, the mixture can be placed inside a vacuum chamber for a maximum of four minutes. This is to let the bubbles in the mixture escape, ending up with a uniform mixture. When keeping the sample in the vacuum chamber for longer, one risks the chance of having the mixture not fully running down the mould, as the solidification process prevents the mixture flow downwards any further.

After the mixture is taken out of the vacuum chamber, it can slowly be poured over the mould until the top part is covered. After around two minutes another layer can be added, since the level probably has been sinking by now. Adding this extra layer on top is assumed to stimulate flow downwards due to additional pressure from the top. When about 20 minutes have been passed, the level of the EcoFlex mixture can be inspected, as by now the level should be dropped all the way to the bottom. If this did not occur, there is a high chance of incomplete chambers after curing. Then the process must be restarted. If the level indeed dropped to the bottom, the chambers will highly likely become proper module chambers. The curing takes about three hours.

C.2.1 Removing the chambers

After the curing process is complete, the chambers can be carefully taken out of the moulds. This can be done by removing any material found on the outside, after which the screws can be removed. The top section in the grooves can be cut away to ensure the sides of the mould are not connected. After this has been done, the mould pieces can be slowly taken apart. During this process there is a high chance of having chambers being connected to each other. The connections can be carefully cut away, leaving behind the result that can be seen on the right in Figure 3.

The chambers have to be reshaped slightly to get rid of any unnecessary attachments, such as the ones seen on the right in the mould. After this, the chamber process is complete.

C.3 Pouring the first layer: EcoFlex 0030

When the chamber pieces are complete, the process of making the whole module can start. To do so, the chamber pieces are placed inside a bottom mould, which can be seen in Figure 4. After the chambers have been placed, the middle bar and the metal sidebars can also be inserted. The chamber pieces are placed in the holes with a lower ring that can be seen, whereas the metal bars fill the other holes. The middle hole is filled by a 3D-printed rod. After all is in place, the outside shell can be placed around the bottom part. The moulds are designed to facilitate moulding in two stages. For now, the outside shell will be levelled with the lower parts of the bottom part and fixed with two pins. The mould is now complete and ready for use.

C.3.1 Preparing EcoFlex 0030

The process of preparing the mixture of EcoFlex 0030 for the first layer of the module can be performed simultaneously with the preparation of the mould, as it can be put in the vacuum chamber for a rather long time. The principle is the same as for the EcoFlex 0050 chambers, but now an amount of about seven grams of mixture A and seven grams of mixture B are necessary to fill the module with. The mixture can stay up to 30 minutes in the vacuum chamber without

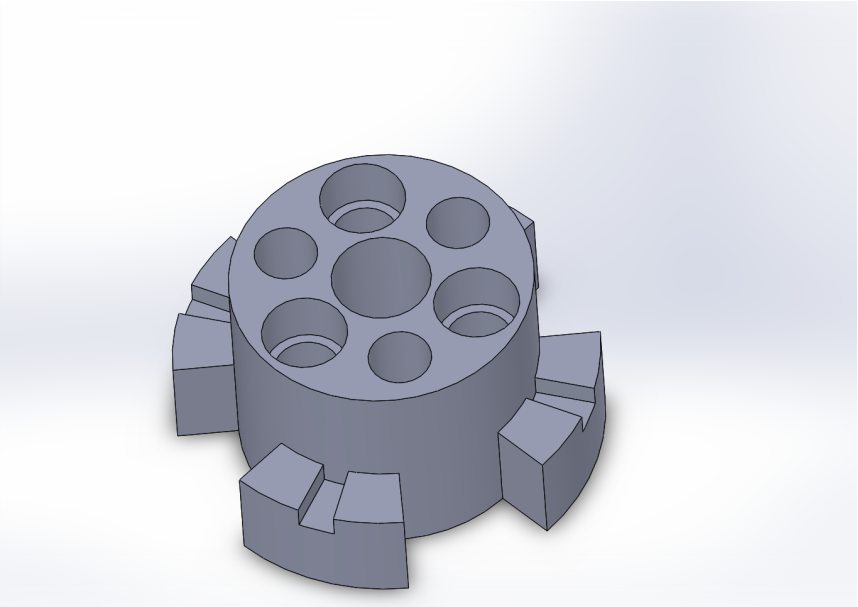

Figure 4: Bottom mould of the endoscope module fabrication process. Design based on the design of Jan Lenssen (Lenssen, 2019), but is adjusted to fit the use of extra holes in the module.

any problem, as the low viscosity property of the material enables it to still be poured rather easily in the mould. When the 30 minutes have passed, it is time to pour the mixture into the mould. To prevent spilling and the creation of bubbles, slow speed is advised. After the mould is topped off, a final check and correction can be done on the position of the chambers in the mould. Next to this, the top of the mixture is levelled with the top of the mould as much as possible. This is beneficial in a later stage of the process, when the module has to be glued to the connector piece. The curing takes about 2.5 hours. The result is shown in Figure 5, in which the metal bars are already taken out.

Figure 5: Result of the first layer of EcoFlex 0030 inside the module mould. The metal bars already have been taken out.

C.3.2 Module removal

The first part of the module can be removed as soon as the curing process has been completed. It is advised to push the rods out first, after which the bottom connection can be dismantled. Then, the outer shell can be taken off, after which only the module part with the inserted chamber pieces remains. Using small forceps, these chamber pieces can be taken out. This can be realized by first turning the chamber pieces, until the connection with the outside material feels rather loose. After that, the pieces can be pulled out slowly.

After complete removal of all the parts from the module, the module looks similar to the one depicted on the right in Figure 6. The module has to be smoothed by taking away the unnecessary residue, after which the module looks similar to the left module in Figure 6. Now, the first level of the module is complete.

C.4 Adding the top layer: DragonSkin 10

Now it is time to add the last layer of the endoscope module, using DragonSkin 10. This material is rather thick and strong, ensuring a proper coverage of the module. For this process, the same mould can be used. The already fabricated first part of the module is inserted back into the mould again, but the chamber parts that have been taken out have been replaced by other pieces, which look similar to 'baseball bats'. These pieces close off the top of the chambers, thus preventing DragonSkin 10 from leaking into the module chambers. These objects are placed just below the top of the chambers, such that a part of the chamber is filled and less interface problems might occur. An illustration of the structure is given in Figure 7. The outside cover will be placed higher this time, in the square holes on the top of the bottom connector, enabling closure at a higher level. This enables to pour the liquid in the new space above the previously made part.

C.4.1 Preparing and pouring DragonSkin 10

DragonSkin 10 is a mixture which cures very fast and has a high viscosity. The curing time is so short that caution has to be taken when pouring the mixtures together, as waiting too long

Figure 6: Bottom mould of the endoscope module fabrication process. Design based on the design of Jan Lenssen (Lenssen, 2019), adjusted to fit the use of extra holes in the module.

Figure 7: Re-assembled module part to prepare for the pouring of DragonSkin 10. The cover is placed on the top of the white base-connector, creating an extra space above to pour the material in.

might make the material unusable. For the cover of the module, two grams of mixture A and two grams of mixture B are used. The usual time taken inside the vacuum chamber is two minutes. After these two minutes, the sample can be taken out and can be poured over the mould. Same procedure holds as for the use of EcoFlex 0030 for this step. Curing is complete in about 1.5 hours. Removal follows the same procedure as before. After all these steps are taken, the module is ready for use!

C.5 Suggestions for future fabrication

Some remarks can be made regarding the current fabrication process. It is possible that having EcoFlex 0030 chambers would benefit the bending even more, together with cutting the time it takes to make the modules. However, due to time constraints this has not been verified. It is assumed that the effect of having EcoFlex 0030 chambers would not increase bending that much, but in terms of fabrication it might be interesting to look into. Furthermore, the necessity of using the vacuum chamber before pouring the EcoFlex 0050 and the DragonSkin 10 can be questioned, as the duration of the curing in the vacuum chamber seems not to be sufficient to get rid of all the bubbles and could even make matters worse in terms of bubble formation.

Appendix D: Data Analysis Characterization - Single Module

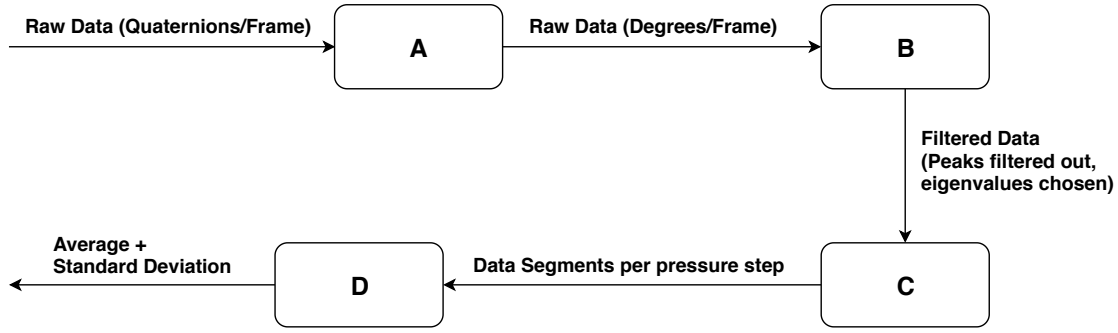

Figure 8: A block diagram showing the steps taken during the data analysis process. *A* transforms the dataset from quaternions to eigenvalues, *B* is the block filtering the artefacts out, *C* checks the transitions and divides transitions into parts per pressure step and *D* calculates the averages and standard deviations of these segments.

As mentioned before, the bending of the modules are investigated under various circumstances. The main principle behind this experiment is based on sensing using an EM tracker to detect position and bending angle of the endoscope module, when pressure steps ranging from 0 bar up to 0.55 bar are applied. In the initial characterization experiments performed with the EM tracker, the first pressure steps were 0.1 bar in size, going up to 0.2 bar. After that, steps of 0.05 bar were taken. The reasoning behind this was that the initial pressure steps did not contain big bending differences compared to the initial position. Later on, the choice was made to keep steps of 0.05 bar throughout the experiment, to keep the data spread more uniform.

The data stored by the Track app of the NDI software has the file extension '.csv' and can be read out using Matlab. Several steps are taken to eventually get to a pressure-bending characteristic. These steps are depicted in Figure 8.

The blocks A, B, C and D stand for several aspects of the algorithm that alter the consistency of the data. Starting with raw data expressed in degrees of bending angle per frame, this eventually is converted to bending angle (degrees) per pressure step (bar).

In block A, the data is being converted from quaternion information to bending angles in degrees. This has been done by means of a conversion form quaternions to rotation matrices, after selecting the correct data in the file. The rotation matrices of all time frames are divided by the initial rotation matrix, such that the relative differences in bending can be examined. From these corrected rotation matrices, the eigenvalues can be determined. The arctangent is taken of the imaginary part of these eigenvalues divided by the real part of these eigenvalues, which will give the angle in radians. Moreover in Chapter D.0.1 of the Appendix. After this, conversion to degrees follows. The result can be considered the raw bending data set, describing the amount of bending per frame. In Figure 9, an example of a raw bending data set is given. This is a result from an experiment with chamber A of module 2, loaded with a module on top.

In block B, the raw bending data in degrees is examined and the high peaks are taken out. The origin of these peaks is yet unknown, but these peaks occur mostly between 0.2 bar and 0.3 bar, as well as when the pressure goes back from 0.55 bar to 0 bar. One could reason that this phenomenon could be related to the rapid changes in bending angle, as the moments where they occur coincide with the two highest transitions in bending angle. Furthermore, during earlier experiments using Euler data instead of quaternions, these peaks did not occur that

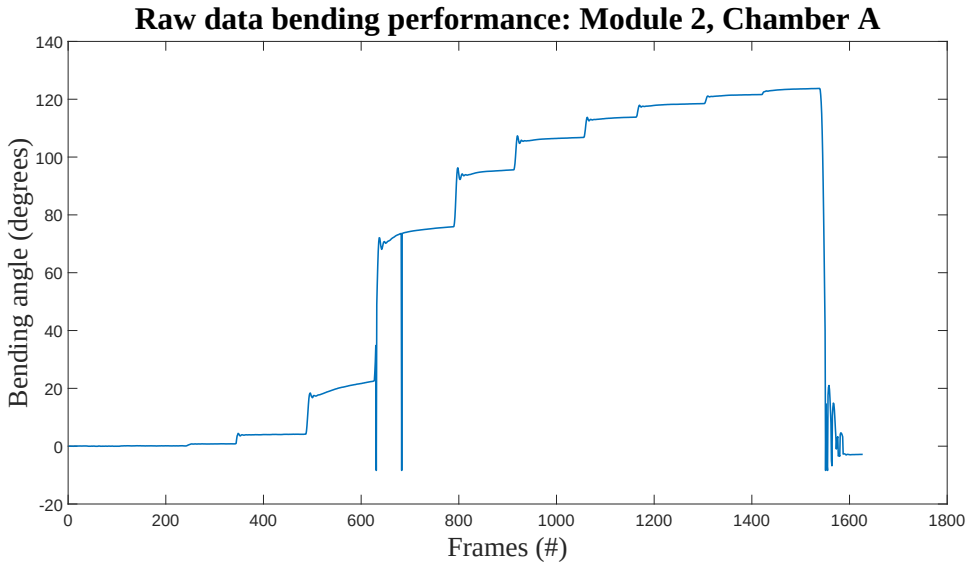

Figure 9: Raw data, converted from quaternions to rotation matrices, of which the angle between real and imaginary eigenvalues is computed. Some artefacts can be seen between frame 600 and frame 700.

much. The peaks can also be seen in Figure 9. The method for finding these sudden high peaks in the data is by means of looping through the data set and finding data points for which there is a big decrease when taking a step forward, but also a big decrease when taking a step back. When the decrease is bigger than a certain threshold, it can be considered an artefact. An example of the filtered and segmented data can be seen in Figure 10, which is a continuation of the raw data from a round of chamber A from module 2.

After the data has been filtered, block C divides the data into separate segments per pressure step. For every experiment, it is known which pressure steps are taken (namely the steps that are mentioned above). Furthermore, the pressure steps can be reviewed by examining the video material taken during every experimental round, as well as from the data stored by the Matlab app used to control the pressures via the Arduino. In the used algorithm, transitions are detected by checking the data for sudden increases in bending angle. Points are taken before and after the transition, giving a boundary for the number of samples per pressure setting. The drop from 0.55 bar to 0 bar is also detected by subtracting the previous value from the current value. When this crosses the threshold value, there mus be a pressure release. This serves as the last bound for 0.55 bar. Often it occurred that this way of detecting transitions did not include all pressure segments, as the initial set pressures did not have very much effect upon the bending of the module. Therefore, the value difference was too small to detect. This is why extra points were added between the beginning and the first clear transition, to ensure that these points were also taken into account. It must however be said that it would have been much more accurate to link the pressure data together with the bending data, had it not been that these contained different time stamps and could not be matched. As there was not much variation in bending values at all, it was assumed that taking these samples did not affect the characterization result to a great extent.

After these segments were determined, the separate data sets per pressure step were analysed and statistics were calculated (see block D). The average was computed, together with the standard deviation of the samples. Every pressure step contained roughly 100 data points, but due to the manual way of controlling the pressure level, the amount of points varied a lot. The pressures are stored, together with the calculated averages, standard deviations and transitions. Furthermore, the number of data points was stored per pressure step, together with the

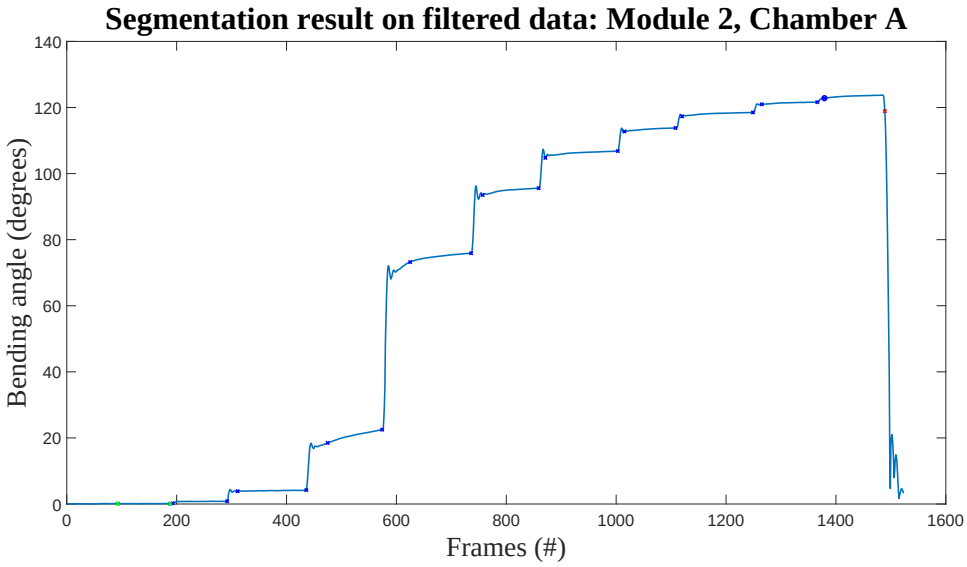

Figure 10: Filtered data, together with indications of segmentation. As can be seen, the artefacts have been removed. The transition from 0.55 bar to 0 bar again is indicated with the red dot, whereas extra transitions are added in green in the beginning.

complete data set. The result looks like the plot in Figure 11, where the averages are computed together with the standard deviation of the previously segmented data set from Figure 10.

D.0.1 Exceptions

During the data analysis procedure, several exceptions were found in the data structure. Every result was manually inspected to verify whether the estimated segments were taken correctly and whether no odd situations occurred. Sometimes a rare phenomenon was found, which

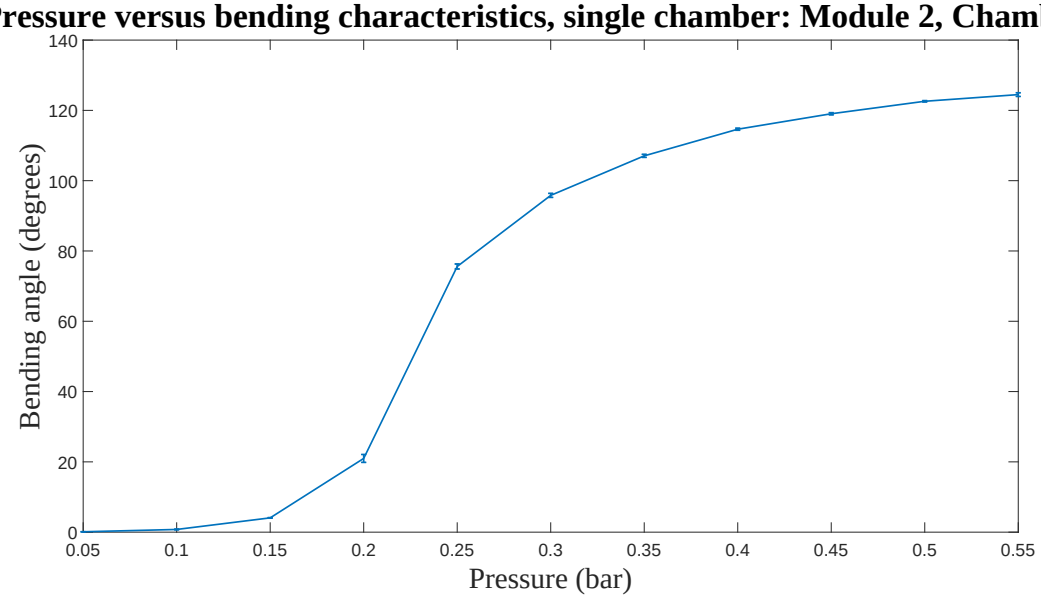

Figure 11: Result of taking the average of all the samples per pressure step, together with the standard deviation. The bending is plotted as a function of the taken pressure steps.

had to be handled separately using a collection of adjustments. This section will describe the majority of these odd cases.

Initially, it was found that not all data sets had the same position for their positive angle definitions in the computed matrix, meaning that special cases had to be made to ensure the correct selection per case was made.

It sometimes happened that not all of the data from the module returning to initial position was captured, leaving the data set with a 'missing end'. When this occurred, the initial way of computing the downwards transition could not be used. Thus, the last point of the data set, probably still at 0.55 bar, was selected to serve as last transition.

Furthermore, there were a certain number of cases in which the transitions between pressures continued after dropping to 0 bar. Due to some oscillations still, there would be a possibility for the algorithm to detect them as possible transitions. To counter this, for some situations the a loop was run to check whether there were any next transitions with a lower value in bending angle than the current transition, such that these transitions and the ones that would follow are taken out.

Another situation had to do with the length of the data set, which was sometimes found smaller than the detected transition to zero. To ensure this could not happen, a small function was written to detect and change the position of this downwards transition.

In general, there were some measures taken to ensure that the results were more precisely focussed upon the actual bending angle in rest. To ensure that the initial transition was not taken directly, a filter has been placed there. In other words, there could not be a transition in the first 5 frames of the experiment, as the initial pressure was kept at zero. It is assumed that not enough should happen at rest to directly have a transition. Furthermore, when transitions were rather small in size (small difference in bending angle), it was assumed that the steady position of the module under certain amount of pressure was not yet reached. Therefore, the transition was moved slightly to the right, hopefully creating a better representation of the angle difference. Lastly, during the application of several pressure values, the module tends to bend further than its steady state position for that pressure, due to it having momentum. This causes a small

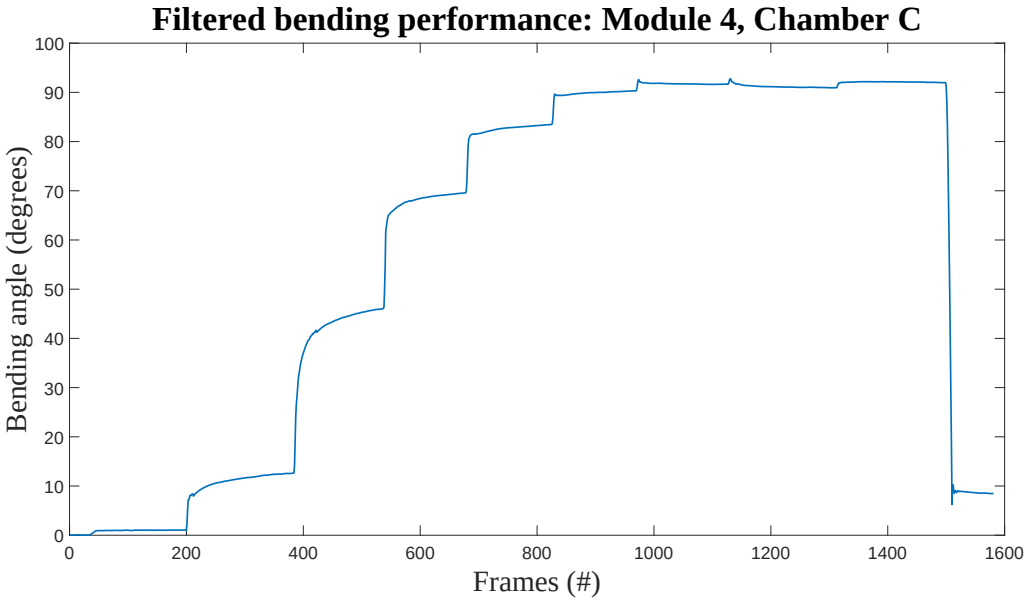

Figure 12: Result of the failed connection, displayed in Figure 4.10. For pressures of 0.45 bar and 0.5 bar, the bending seemed to decrease, rather than increase.

peak upwards after every transition. To ensure that mostly the steady position of the module under certain pressure is measured, the transition is also moved from that part.

During characterization of the modules without load, it occurred that the sensor connection got loose during the measurement, causing the sensor to actually bend away from the whole module. This could be retrieved from the data, as the increase in pressure did not deliver an increase in bending performance. Due to this effect, this measurement was not taken into account and was deemed an outlier. An image of this measurement can be seen in Figure 4.10, presented earlier in this report. In Figure 12, the result of this failed connection can be seen, mainly for higher pressures.

Aside from these occasions, there were several individual cases that required for example an extra transition, since the algorithm did not catch a point clearly enough. Therefore, also these special cases were dealt with.

Appendix E: Data Analysis Characterization in Quaternions - Endoscope Modules

Throughout the study, the Aurora EM Tracker has been used rather frequently. The output of the EM Tracker consists of position coordinates and rotation angles, which could either be described in Euler angles or in quaternions. For a rather long period of time, the bending of the endoscopic modules has been approached by quaternions, as it was found that Euler angles might suffer from some limitations. However, since the quaternion approach resulted in bending planes that were potentially different compared to the 2D scenario, the switch was made back to Euler angles in the final steps of mapping pressure to bending.

The following section will treat the procedure regarding the step from quaternions to eventual angles regarding the hysteresis plots in more detail. The approach is based on the method used by Lenssen (Lenssen, 2019).

E.1 The Principle of Defining Bending Angle

As is also mentioned in another chapter, the chosen method to define the bending angle is to go from quaternions to rotation matrices, using MATLAB functions. From there, the eigenvalues are defined, which are used to find the angle of vector rotation. Let us start with the following formula:

$$A\mathbf{v} = \lambda\mathbf{v} \tag{1}$$

where A is defined as the rotation matrix, $\mathbf{v}$ is the eigenvector and λ are the eigenvalues. This can be rewritten into

$$A\mathbf{v} = e^{i\theta}\mathbf{v} \tag{2}$$

where θ is the rotation of the vector. Now, the eigenvalues of the rotation matrix will lie on the unitary circle, with real values of the x-axis and imaginary numbers on the y-axis. Decomposing the complex nature of the eigenvalues, these can be used to define the angle:

$$\tan(\theta) = \left(\frac{\mathrm{Im}(e^{i\theta})}{\mathrm{Re}(e^{i\theta})}\right) \tag{3}$$

where θ is the resultant angle of rotation of the vector. There it is! After switching from quaternions to rotation matrices, dividing by the first rotation matrix, and finding the eigenvalues of the remaining rotation matrix, the angle of rotation can be defined based on the relation between the imaginary values and real values of these eigenvalues.

E.2 Post-Processing Angle Data

After figuring out how to find the resultant angle, the angle profile of one of the modules could look like the representation in Figure 13.

Here, it is possible to see that there are three plots, representing the bending behaviour. Interesting to see is that they all add up to zero. This is due to one of the three eigenvalues of the rotation matrix being equal to $\lambda = 1$, meaning that the angle should be at least zero on one of the eigenvalues. The other two are complex conjugates of each other, so they would represent opposite behaviour.

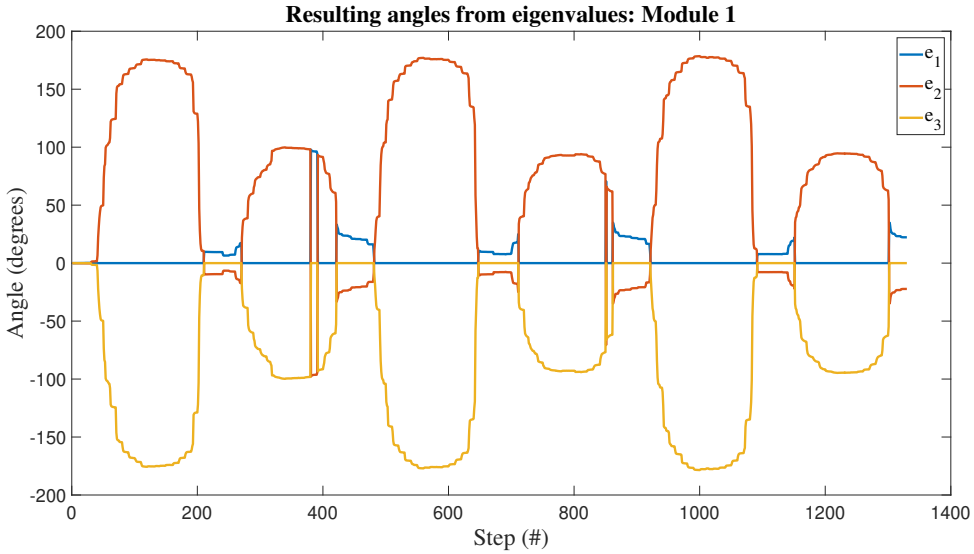

Figure 13: Plot of angles that result from the eigenvalues of the rotation matrix.

After viewing this graph and choosing the bending to the left to be negative bending, for the second peak the yellow graph is chosen. Afterwards, the same repeats. As can be seen, some artefacts still remain where the conjugate suddenly flips.

Appendix F: Hysteresis Results for Inner Sheath Design

To improve the current knowledge regarding the hysteresis behaviour found in the endoscopic design, the alternative design also has been investigated regarding the effects of hysteresis. Two modules that are in accordance with the inner sheath design of Jan Lenssen (Lenssen, 2019) have been used, which are succumbed to a similar tests as with the outer sheath model. The two modules were connected to simulate response in assembly.

Pressure profiles ranging from +0.9 bar up to -0.9 bar were used. The small endoscope was put on the similar plate as the endoscope experiments were held. The pressure profile is repeated three times for both the bottom module and the tip module.

F.1 Results

Figure 14 depicts the bending performance of the tip module and the bottom module of the two-module endoscope.

The bending reached from 8.3 degrees up to -19.4 degrees for the tip module, whereas the bottom module ranged from 6.5 degrees bending towards -4.9 degrees of performance. Interestingly, the tip module shows that bending performance towards the left is higher compared to the right bending.

F.2 Discussion

The bending performance seems rather low compared to the results found in previous work. This could be due to the different environment.

Other reasons could be the difference in applied pressure range or potential differences in construction. The used modules have been tailored using the same fabrication and design procedures, but have not been used for previous studies.

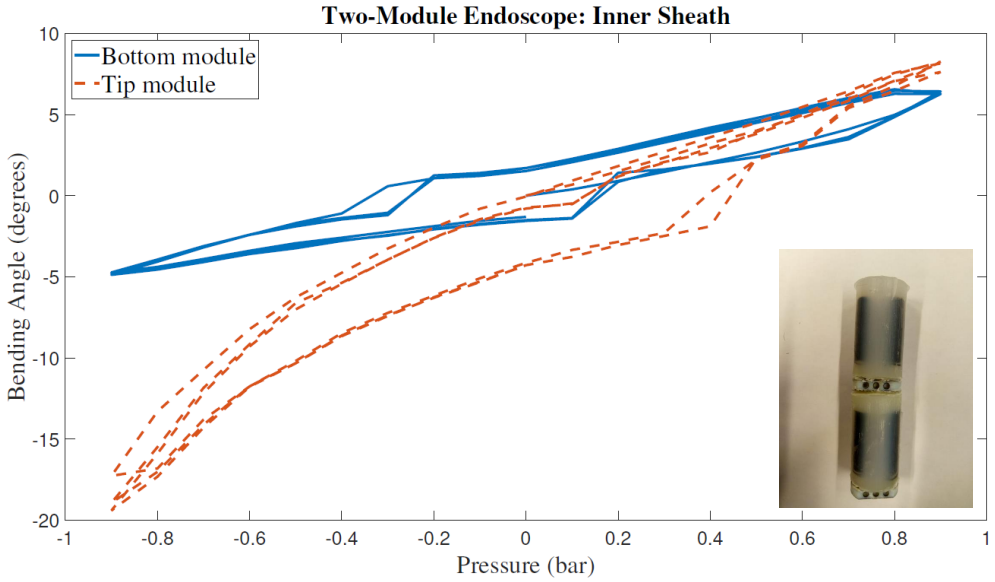

Figure 14: Resulting hysteresis behaviour from the two-module inner sheath endoscope. Both modules have been tested three times.

F.3 Conclusion

After performing similar experiments with the inner sheath module design, it was found that also these modules suffer from hysteresis behaviour. Furthermore, the results indicate a rather limited bending behaviour during performance on the surface.

(a) Endoscope module 2 (Mark 4)

(b) Endoscope module 4 (Mark 3)

Figure 15: Images of the modules ruptured during endoscope characterization. The modules were Mark 4 and 3, which were representing Module 2 and Module 4 of the endoscope. Images show the side with the entrance opening to the pressure chambers, whereas the connector pieces have been removed. The black pressure tubes are only used to emphasize the rupture spot and were not present in the structure before.

Appendix G: Malfunction and Maintenance

The characterization of the endoscope modules in the environment did not occur without problems. During experimental characterization of the second module and fourth module in the endoscope, the actuated module unfortunately ruptured. The accidents happened during actuation of the single chamber and both tears were found to be on the inside of the chamber, connected to the centre hole. Furthermore, both tears occurred in the vicinity of the connector piece, pressurizing the chamber. A potential cause for this problem could be the contact between pressure tube with the chamber wall when the other pressure tubes are actuated. Due to the actuation of both other chambers, the single chamber wall might be pressed into the connector piece pressure tube, causing wear on that specific spot on the chamber wall. However, the exact reason is yet unsure.

Next to this phenomenon, it was examined that the condition of the endoscope modules deteriorated after use. This might not be such a surprise, considering the nature of the consistency of the endoscope, but still could be an interesting point of attention. From the looks of the modules without outer sheathing and by means of inspecting the modules separately, both intact and broken modules, the following deductions could be made:

- Modules feel softer
- Modules change colour

After inspection of the modules, one thing that appears to stand out is the stiffness of the modules. Compared to unused modules, the modules feel much more flexible. The extensive elongation and expansion of the module chambers could result in so-called plastic deformation of the module chambers, causing them to appear less stiff and more flexible. This could point towards deterioration of the chamber quality over time. Furthermore, one could assume the effect of this to further increase bending performance of the module itself, causing a potential shift in properties. This is a very important criterion that could impact performance a lot, which is why it should be examined in the future.

It appears to be the case that, over time, the modules seem to become more green-gray. This could be due to the combination of the glue impacting the material, as well as the outer sheathing leaving filth behind on the modules. Another reason could be the deterioration of the material. Overall, this aspect is assumed to have no real consequences.

Appendix H: Extensive Information Developed RRT*

Initialization The code starts with initializing environment- and obstacle dimensions, start- and target coordinates and initial costs and parents of the path. The obstacle dimensions are utilized to plot the environment, whereas the starting point and target point are also being displayed.

The cost and parent attribute to the nodes are very important components, as they symbolize the connection between nodes and their distance, which eventually help to determine the final path nodes and the total cost in terms of distance.

Random points generation The code runs a loop in which it creates a random point within bounds of the environment for every cycle. This point is plotted. Initially this point was rounded down to an integer, but for scaling reasons this has been adjusted.

A function is added to check whether the target point is reached. The function of Sai Vemprala (Vemprala, 2017) was altered to perform a check upon the specified region, which helps to finish the code earlier. A break function is used to break out of the initial loop when the target region is reached.

Checking nearest neighbor The algorithm of Vemprala (Vemprala, 2017) checks the distance between all the nodes in the tree and the generated random node. The distances are stored in an array, from which the minimal distance is chosen.

The article of Yang et al. (Yang et al., 2014) mentions that the distance array should be in ascending order, as for them also the boundary constraints of the kinematics are taken into account. The current addition to the code does not take this into account. It only verifies whether the condition is met, but does not iterate for the nodes to check if there is a better option.

The check of the angles is done by first determining whether the algorithm is in its initial state (where the q_{near} does not have a parent), after which the cosine rule is implemented to determine the angle between previous parent node, current q_{near} and the q_{rand}. The previous node is found by using the parent formulation of q_{near} as index in the nodes.

The cosine rule makes use of distances between nodes, which are determined by means of Pythagoras theorem. The resulting angle from the cosine rule is converted to degrees.

Propagation After the q_{near} is chosen, some conditions are tested, among others the collision test. Furthermore, the angle is checked, whether it is within desired bounds. This means that the edges cannot make a bend for more than 40 degrees for example.

Once these tests are passed, the code calls the steering function, which steers a line from q_{near} to q_{rand}, using the distance value and the set step value to determine whether this distance can be covered at once (value is within bounds of step) or is further away (value is out of bounds of step), which would imply that the fraction of step of the distance covered in x-direction is added to the q_{near} x-value, as well as for the y-direction. The new x- and y-coordinates are given to q_{new}.

A line is drawn using the q_{near} and q_{new} coordinates, after which the cost of q_{new} is determined as the Pythagorian distance between q_{new} and q_{near} combined with the previous value of q_{near}.

noCollision The function noCollision checks whether the line drawn from q_{near} to q_{rand} (or other combinations) interferes with a defined obstacle.

RRT* property After drawing the line of the tree, the code initiates a search for nearest neighbours. From the current nodes, it is checked whether there is a node that can connect with the

new node without collision and is closer than a radius r to the new node. If this is the case, the node will be added to the selection of nearest neighbours.

After the first for loop, values are set for the cost of the normal branch method and a new variable called q_{min}. The second loop checks again whether the nearest neighbour can make an obstacle-free path to the random node, with the additional criterion to check whether the route from nearest neighbour to the random node has less cost compared to the initial RRT-route. If this is the case, the values of q_{min} and C_{min} are used, which contain the values of position and parent of the nearest neighbour and use the new value of cost in C_{min}. Then a line is drawn in green, following this route.

After this step, the parent of this part is changed from the initial q_{new} parent to the one of the nearest neighbour, by checking whether the coordinates of the q_{min} coincide with the node coordinates. This also works when it turns out the other condition was not met and the initial q_{new} was better. The nodes are stacked together as an array.

Goal Search This part contains the creation of an array containing the distance of node parts to the goal coordinate. The minimum distance is used to start the q_{final} with, as it means that this is the closest node and therefore the final node. The parent of the target receives the same parent as the final node.

H.0.1 Angle Limitation

One can think of several reasons why it is important to limit the necessary amount of bending during operation. One of them is concerning the bending capabilities of the modules themselves. To ensure that the method of path creation is in line with the physical properties of the modules, it should take into account the limitations of these soft robotic modules. Furthermore, the maximum bending of the modules can be seen as another performance criterion that has to be limited in order to improve safety.

To ensure that the path created by the RRT*-planner takes into account these aspects, it was attempted to use an angle limitation on created path branches. This implied that the RRT*-algorithm was only able to expand using branches that made a limited angle with respect to the previous branch. The approach is explained below.

When a new coordinate point is about to be connected to the tree, it is possible to determine the vector that the new point makes with the node that will be connected to it, q_{near}. By means of the stored information regarding the parent node of this q_{near}, we can determine the vector between q_{near} and its parent node. The angle between these vectors should be limited. To determine the angle, the following formula was utilized:

$$\theta_{\text{tree}} = \cos^{-1}\left(\frac{(\mathbf{A}\cdot\mathbf{B})}{||\mathbf{A}||||\mathbf{B}||}\right) \tag{4}$$

Where A and B are respectively the vectors from the q_{near} to the new point and the q_{near} to the previous point. The lengths of these connections are determined using the Pythagoras theorem. A multiplication of these vector lengths serves as the denominator, whereas the numerator is the dot product of the two vectors.

Another script is used to verify whether the condition is met. The script takes into account the path points created, walks through the path and checks every angle. Using this script, it was indeed confirmed that the RRT*-property, which makes for rewiring processes during the operation, disturbs the working principle of the angle limitation. The rewiring action is not penalized by the angle criterion, leaving still some sharp corners. However, next to this action the step towards the target is not always in line with the maximum bending criterion.

Figure 16: A problem occurs when the steps are too big during maximum bending angle limitation: the algorithm cannot find a new way due to the distance criterium of the RRT in combination with the step size and angle limitation.

Both phenomena are now included in the total bending limitation. Simulations show that, when a path can be made, it is indeed following the required maximum bending angle.

However, this technique of confining the bending angle also has some limitations of its own. Due to the tree growing characteristics of the RRT, the algorithm always wants to find a node close to the newly plotted coordinate to connect with. Due to the bending angle limitation, this often cannot be realized effectively. A solution would be to branch out from nodes further away from the randomly spawned point, although this would differ from the normal way of computing in RRT. In effect, this results often in a structure without (much) branching, creating a single path that follows the criterion most often. This also affects the way the algorithm behaves in narrow environments, as often branching is not possible any more and the angle limit prevents any deviation as well. The algorithm thus gets stuck more often. Furthermore, a problem occurs when wanting to scale the angle with respect to the complete module. Currently, steps are made that are smaller than the total size of a module, creating a more detailed path. Since the curvature of both a bending module and this algorithm should be in line to preserve model characteristics, this implies that for smaller steps, the allowed angle should also be smaller. When implementing this into the current algorithm, the algorithm has a much bigger difficulty to complete its tasks, as it cannot find suitable connections that easily in this situation. An optimum has to be searched between maximum bending angle and step size in order to ensure that the path is completely feasible. An example is shown in Figure 16, where too big steps are taken to complete the simulation.

Appendix I: Image Processing of the Experiment Data

During the experiments, the movements of the endoscope throughout the environment have been captured on camera. This is used to determine the deviation between the endoscope and the centerline, as this symbolizes a measure of safety during movement. The centerline is the line furthest away from the obstacles, which means that following this line would correspond to the safest path. By means of determining the error with respect to the centerline, the scenarios for manual insertion and path planned insertion can be compared.

In order to retrieve useful metrics from the created video footage, the video material has to be processed by means of various manipulation steps. The steps taken during this process will transform the current video footage into coordinates of the endoscope skeleton, in combination with the coordinates of the given environment.

I.1 Procedure

In this section, the steps taken from video footage towards eventual information regarding centerline error is presented. This has been realized using image processing techniques. The camera that has been used produced films with approximately 50 frames per second. To limit the amount of data processing, this frame rate will be used as a step size when looping through the total number of frames of the video. This will result in having information based on one frame per second.

After the frame has been selected, the operations start. The image first has been scaled and rotated, to ensure that the orientation of the environment is straight. Furthermore, the images have been cropped to a window which solely contained the environment and the endoscope, reducing the number of false positives detected during image processing. This has been defined for every video individually, and data regarding these procedures have been stored. Next to that, the target point also has been selected and stored beforehand. It has been defined for every participant, how many video files exist. Since one experiment often contains multiple videos, this complicates the procedure. Defining the boundaries and centerline when the endoscope is already far in the environment might influence the quality of defining the obstacles. Therefore, information regarding the environment as well as the centerline data is stored for later rounds, such that these can be used as a reference. Here, it is assumed that the camera has not been moved during the performance of the experiment.

I.1.1 Centerline Definition

After these steps were taken, a section of the algorithm would deal with defining the environment and deriving the centerline from that. By grayscaling the image and using edge detection, the black lines of the obstacle boundaries could be found. Then, using a sequence of operations, the pixels are first expanded to connect the detected points with each other (imclose), after which layers are scraped off (imerode). Eventually a fine line is defined, using the bwmorph function with the thinning setting. Using the bwconncomp function of MATLAB, the now connected obstacle dimensions have been selected as one object and the coordinates are stored.

When the definition of the surrounding obstacle was complete, the middle line y-coordinate was defined. This has been done by averaging the values found for $x = 150$. This is approximately the middle x-value, meaning that it lies in between both corners. The resulting y-value serves as a base y-value for the centerline of the big middle piece. The small sections on the start side and the target side are determined by finding the values that have a difference between 50 and 200 points, since the middle has more than 200 points difference between

them. The average between two consecutive points stands for the middle x-axis value between both lines, and add to the centerline. Based on the $x = 150$ line, the found points are divided into upper section and lower section regarding Scenario 2 and left and right session regarding Scenario 1. The average found x-values for both sides served as a basis x-axis value for those two segments.

Now, the y-value for the middle centerline was found in the bigger segment, as well as the x-axis values for both small sections. However, there is still a gap between the middle line and the other two lines. Therefore, if the difference on the x-axis was found to be more than 200, whereas the y-value deviated a little from the middle line, the found y-value is combined with the defined x-value for the smaller segments, to eventually end up with the representation found in Figure 17. Now, some of the defined centerline points are not corresponding to the exact centerline, since they are laying on the boundary or continue after the target point. These points are filtered out.

I.1.2 Endoscope Skeleton

Finding the endoscope was done by grayscaling the frame, after which specific coordinates were selected that corresponded with the type of grey that is found when previously inspecting the endoscope. A similar approach to defining the environment was used to connect the endoscope elements and create a skeleton line, using the bwmorph function and the thinning option.

Due to the erosion of the expanded endoscope region, the base and tip of the endoscope are also cut of in size. This results in a skeleton, which is mainly situated in the centre of the endoscope. Additional steps were taken to include both the tip and the base in the calculation of the error with respect to the centerline. First of all, the tip of the endoscope was marked using part of a pink dot. This pink dot served as a reference to which the tip position could be defined. Based on inspection of the RGB-values for the pink section under various lighting conditions, a region was defined within the RGB-value spectrum that would eventually capture the dot. With similar procedures as before, the dot was expanded and eroded again, leaving a more compact point. This point serves as a reference, to which the end of the endoscope skeleton was con-

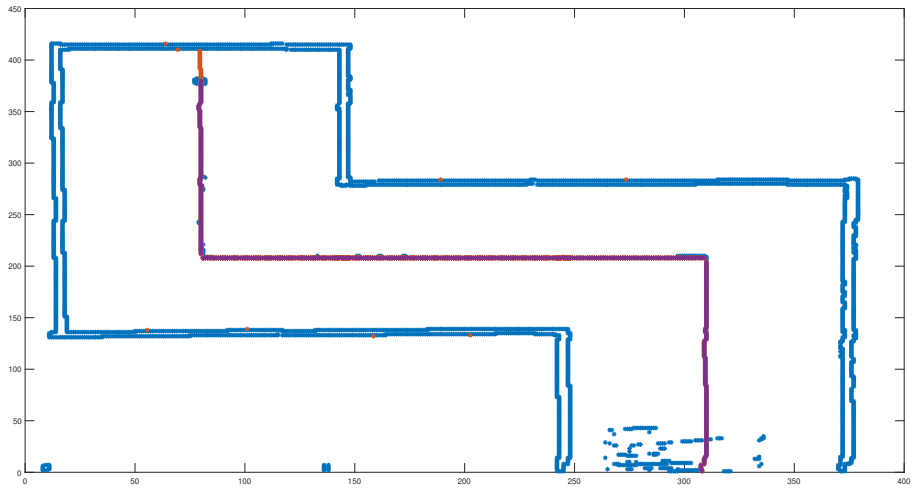

Figure 17: Defined centerline of Scenario 2, after filtering the last points out. The blue points represent the boundaries of the obstacles, whereas the purple line indicates the filtered centerline. The red points define the residue of centerline points of the environment.

nected. Due to the relatively short distance between skeleton and the tip point, a linear line was created, which would spread points between the tip and the skeleton. These points were also included into the calculation of the error.

Furthermore, the base also had to be connected in some way. Using the definition of the x-value for the centerline, this point was eventually connected with the upper side of the tree. Here, also a linear line would be used to define a certain number of points between the base and the endoscope. However, due to finding errors for this method during several occasions, this section is left out of the overall error computation. It is assumed that this section also does not contribute a lot in the overall determination of the error, as the modules that are just getting into the environment are not moved a lot before the first corner.

Combined with the endoscope skeleton points, a comparison can be made between the endoscope coordinates and the centerline coordinates.

I.1.3 Defining distance difference

The difference in distance between the endoscope points and the centerline are determined rather simply. Using the norm of the distance between a point inside the endoscope skeleton and all points on the centerline, a list of distances can be defined. As the ratio of length and width of the frame is not exactly in line with the environment specific ratio and to convert the distance in terms of coordinates into actual lengths, the norm has been altered by incorporating scaling factors for the distances in the x- and y-axis. The minimum value of this distance is selected, and this procedure is done for all points. This eventually creates a summation of the distances, which can be normalized by dividing by the number of points inside the endoscope skeleton. After doing this for every frame, an array of errors is created regarding the behaviour of the endoscope throughout the experiment.

From the experiment, the total error per frame, as well as the weighted error per frame, are stored. To be able to compare the results of the analysis for every participant and with respect to the path planner, the weighted error values are averaged across the complete duration of the experiment.

I.2 Discussion

Although the overall performance of the algorithm works reasonable, there are still some artefacts that occur. A couple of things can be improved regarding the performance of this algorithm, as well as the conditions to which this algorithm has been exposed.

One of the problems in defining the obstacle margins and the boundaries is the presence of the endoscope during the initial frame. This causes disturbances in the initial edge detection, thinking that the module also is part of the obstacle environment. Another aspect that plays an important role in the artefacts occurring inside the module shape and environment is the presence of the pressure tubes, which are also black and hover over part of the endoscopic modules. This causes for disruption in the surface detection of the endoscope shape, making the eventual tree more directed towards the opposite side of the modules. It even sometimes completely disrupts the shape of the endoscope, as due to eroding the thickened surface of the endoscope could create holes on those spots. A difficult phenomenon to tackle for now, was the occurrence of branches inside the created skeleton of the endoscope. These branches cause errors in determining the distance with respect to the centerline. This might be resolvable by defining the distance between points and limiting the number of connected points along the radius of one point. In this way, only maximum two points could be connect to one point. Detecting the start of a branch in combination with finding the branch cost might resolve in choosing the correct longest connection (although the longest connection might not always be the solution). Due to limited time, this has not been implemented yet.

Furthermore, as mentioned before, the use of the connection between base and endoscope skeleton has been put out of use due to several errors that occurred when defining its connection points. Leaving this out causes a gap in the endoscope during the start of the environment, missing data regarding the error with respect to the centerline. However, it is expected that this section might not be of huge interest, as there is often very little deviation in that region and almost nobody actually actuates the lower modules much in the environment. The modules in that position are mainly straight, making other segments far more interesting to compare. However, for completeness, it would be suitable for future work to also include this section in the determination of the overall cost distance. Furthermore, the simulation includes the section as well, so it would benefit the comparison to also include it. Next to that, the point selected from the tip to serve as a connection with the endoscope tree did not always end up to be in the centre, also resulting in some deviations. Furthermore, some errors occurred when no skeleton was present, making the tip connect to the upper left corner. This causes huge errors

A step that really has to be improved in the current algorithm is the selection process for the point inside the endoscope tree, to which the base and tip should be connected. Currently, this has been done by defining the most left point (in the video, the most right) in the endoscope skeleton found in the coordinate plot. Before, the highest and lowest points were selected as connection points. However, with the turning of the endoscope, this did give a lot of errors. There should be an alternative way, optionally by combining the lowest and the most left value together, for resolving this connection problem.

Due to a difference in completion times between participants, as well as with respect to the path planner, this makes the analysis of the behaviour rather difficult. The average weighted error with respect to the centerline only gives limited information regarding the behaviour of the endoscope throughout the experiment. Potential big deviations are possibly masked by rather stable sections throughout the experiment. It is recommended for future work to ensure the equal duration of the experiment, such that procedures can be compared more easily.

Another aspect to consider for future work is the usage of a squared distance cost, as this would penalize the situations in which the endoscope goes further out of bounds. This might help to create a better insight in the overall safety performance.

Appendix J: Results Questionnaire

Table 2: Statements inside the questionnaire

#	Statement	H_0 (1-5)
S1:	The control of the endoscope was rather intuitive	2
S2:	I felt tired after performing the experiment	4
S3:	I needed a lot of guidance from the researcher throughout the experiment	4
S4:	I found it easy to use the four modules to get to my desired configuration	1
S5:	I had to concentrate a lot to stay away from the boundaries	4
S6:	I am satisfied with my performance during the experiment	2
S7:	The duration of the experiment was quite long	5
S8:	I feel confident in controlling the endoscope throughout the environment	2

The results received from the questionnaire have been divided into all participants and participants with flexible endoscope training. The general results are depicted in Figure 18. The results of the participants with flexible endoscope training have been depicted in Figure 19.

Several statements were posed and the participants were asked to rate them from one to five, one being 'Strongly Disagree' and five being 'Strongly Agree'. The statements given plus the expected outcomes are displayed in Table 2.

The participants were also asked to give remarks and future recommendations regarding the current experiment. These are mainly discussed in the Discussion section in the report (Chapter 7).

J.1 Elaboration on Results

In the results of the questionnaire regarding the overall participants, it was found that the general opinion regarding the control of the endoscope was found rather difficult. A majority agreed the statement of with having to concentrate a lot to stay away from the boundaries. This is somewhat in line with what was expected.

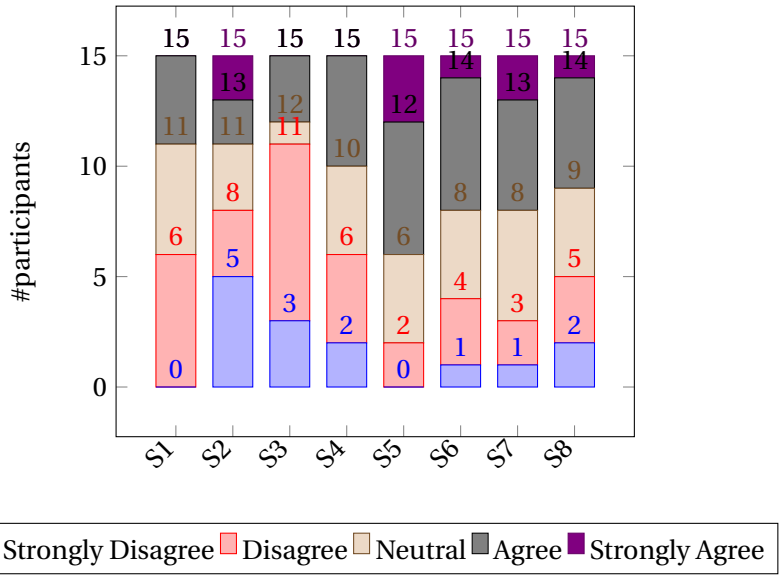

Figure 18: Questionnaire results of all participants during Manual Insertion Experiment. The given answers correspond to the statements, mentioned earlier in this section.

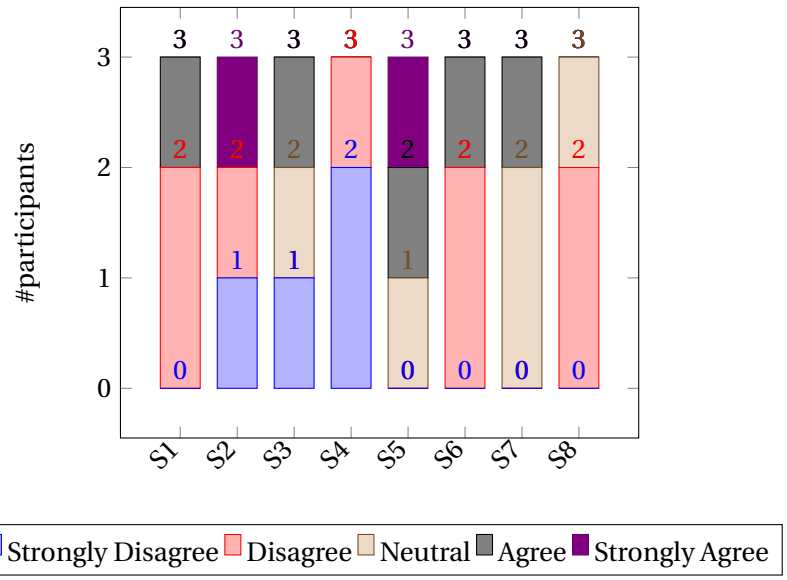

Figure 19: Responses of the participants who had medical training with flexible endoscopes, regarding the questions from the table.

Surprisingly, a majority mentioned not needing a lot of guidance throughout the process. The duration of the experiment was considered rather long.

When considering the results of the participants with medical training regarding flexible endoscopes, the notions of finding the endoscope difficult control were found as well. Here, the results were even more in alignment with the hypothesized results. It must be stressed here that the total amount of medically trained participants was rather low, making it more difficult to draw concrete conclusions. With respect to confidence in control and participant satisfaction, the general opinion was also slightly more negative compared to the overall participant results. The majority of medically trained participants questioned the relevance of their specific application, since the control of this endoscope deviates a lot from the conventional steering of flexible endoscopes. This might also be linked to the notion of overall difficulty in controlling this endoscope.